

---

Theses and Dissertations

---

Fall 2011

# Simulating ingress and egress motion for heavy earthmoving machines

Hyun Jung Kwon  
*University of Iowa*

Copyright 2011 HyunJung Kwon

This dissertation is available at Iowa Research Online: <http://ir.uiowa.edu/etd/2734>

---

## Recommended Citation

Kwon, Hyun Jung. "Simulating ingress and egress motion for heavy earthmoving machines." PhD (Doctor of Philosophy) thesis, University of Iowa, 2011.  
<http://ir.uiowa.edu/etd/2734>.

---

Follow this and additional works at: <http://ir.uiowa.edu/etd>



Part of the [Biomedical Engineering and Bioengineering Commons](#)

SIMULATING INGRESS AND EGRESS MOTION FOR HEAVY EARTHMOVING  
MACHINES

by  
Hyun Jung Kwon

An Abstract

Of a thesis submitted in partial fulfillment  
of the requirements for the Doctor of  
Philosophy degree in Biomedical Engineering  
in the Graduate College of  
The University of Iowa

December 2011

Thesis Supervisor: Professor Karim Abdel-Malek  
Professor Jasbir S. Arora

## ABSTRACT

Design of heavy earthmoving equipment is based primarily on feedback from drivers. Most design studies on ingress and egress focus on the motion itself and rely heavily on experimental data. This process requires physical construction of expensive (in terms of time and money) mockups before any feedback can be obtained. Post-feedback design changes and the analysis of those changes are again expensive processes. Although the design of heavy vehicles requires consideration of human safety and comfort, very little attention has been given to simulating ingress and egress movement for these vehicles. This thesis describes the development of a virtual model to perform ingress and egress motions for heavy equipment and its applications to study the responses of operators with different anthropometries to different cab designs. Different performance measures are suggested and used with predictive dynamics to study human performance since human motion is not governed by a single performance measure. Optimizing multiple performance measures allows the full range of motion for all 55 degrees of freedom to be considered for simulating the task. Once the relevant performance measure was established, case studies were performed on seven different cab designs and digital human models with three different anthropometries. Finally, several different cab design metrics for propensity of injury, comfort, and accessibility were proposed. These design metrics were evaluated for each of the case studies. Finally, each cab design was ranked based on the design metrics to identify the best design for a range of anthropometries. These results help designers make decisions and plan further design changes.

Abstract Approved: \_\_\_\_\_  
Thesis Supervisor

\_\_\_\_\_

Title and Department

\_\_\_\_\_

Date

\_\_\_\_\_

Thesis Supervisor

\_\_\_\_\_

Title and Department

\_\_\_\_\_

Date

SIMULATING INGRESS AND EGRESS MOTION FOR HEAVY EARTHMOVING  
MACHINES

by  
Hyun Jung Kwon

A thesis submitted in partial fulfillment  
of the requirements for the Doctor of  
Philosophy degree in Biomedical Engineering  
in the Graduate College of  
The University of Iowa

December 2011

Thesis Supervisors: Professor Karim Abdel-Malek  
Professor Jasbir S. Arora

Copyright by  
HYUN JUNG KWON  
2011  
All Rights Reserved

Graduate College  
The University of Iowa  
Iowa City, Iowa

CERTIFICATE OF APPROVAL

---

PH.D. THESIS

---

This is to certify that the Ph.D. thesis of

Hyun Jung Kwon

has been approved by the Examining Committee  
for the thesis requirement for the Doctor of Philosophy  
degree in Biomedical Engineering at the December 2011 graduation.

Thesis Committee: 

---

Karim Abdel-Malek, Thesis Supervisor

---

Jasbir S. Arora, Thesis Supervisor

---

Tae-Hong Lim

---

Nicole M. Grosland

---

Timothy Marler

---

Rajan Bhatt

To my parents and Yun  
This work is as much as yours as it is mine.



## ACKNOWLEDGMENTS

Finally, the thesis is complete. I have been working on it all day and all night for over 6 months. I am exhausted! Before I pass out into the sweet coma of REM sleep, my thesis would not be complete if I did not thank everybody who helped me complete it. I want to say something from my heart; this dissertation is made up of liters of tears, cans of beer, tons of coffees and mountains of support.

I am very fortunate to have had a great set of people supporting me in my endeavors over the years. I would like to extend a great amount of thanks to my advisors, Prof. Jasbir Arora and Prof. Karim Abdel-Malek. Their support, encouragement, and expertise have contributed in making this project successful. I am very appreciative of their patience and their challenging- thought provoking questions, all of which have prepared me in my future to become an independent researcher. Thank you for pushing me to be better my research.

I would like to thank the members of my dissertation committee, Dr. Tae-Hong Lim, Dr. Nicole Grosland, Dr. Tim Marler and Dr. Rajan Bhatt who provided critical feedback during my doctoral exams, enabling me to polish and complete my thesis. I was fortunate enough to have them participate in the various committees leading to my PhD.

This work would not have been possible without the support grants from Caterpillar and USCAR. I am grateful to them for generously supporting my research.

I thank all the team at VSR past and present; Dr. Joo Kim and Dr. Yujiang Xiang and Dr. Chung-sunbaenim for always being patient with my questions, even with the stupid ones. Anith who supplied snacks and all the cool information of living in US, and spent countless hours editing documents for me. Jun Choi, my chat buddy, Brian and Rajeev who are patiently listen my awful English. I would like to especially thank Dr. Rajan Bhatt for editing my terrible writing, for believing in me and motivating when I lost hope. Without his wise advice, support, friendship, and teachings; I would have

never finished. Dr. Tim Marler, I will never forget our hour long conversation at the Starbucks, you were a superman! To all other VSR members, to each and every one of them, I would like to say a special “thank you.”

Thanks to my friends in Iowa and Korea; Hawkeye unnis - your friendship has always been a bright light during the last five years. It is impossible to forget all the nights, cocktails and shopping and talking. IDLE; even though you have no clue what I am doing here, you always encourage me to succeed in the US. Special thanks to Jean and Martin for being my family in US.

Finally, I’d like to thank to my parents who constantly reminded me to eat, sleep, and “take care of myself” and call with the most positive words and reassuring tone in their voice at just the right time. Most importantly my husband Yun who never doubted for a minute that I could finish this massive undertaking and gave me the gentle nudging and words of encouragement I needed to keep going.

In conclusion, I would not have made it without you all! OK. Acknowledgement section is done. Sleep.....zzzzzz. Is this “the End”? No, a PhD is just the beginning.

## ABSTRACT

Design of heavy earthmoving equipment is based primarily on feedback from drivers. Most design studies on ingress and egress focus on the motion itself and rely heavily on experimental data. This process requires physical construction of expensive (in terms of time and money) mockups before any feedback can be obtained. Post-feedback design changes and the analysis of those changes are again expensive processes. Although the design of heavy vehicles requires consideration of human safety and comfort, very little attention has been given to simulating ingress and egress movement for these vehicles. This thesis describes the development of a virtual model to perform ingress and egress motions for heavy equipment and its applications to study the responses of operators with different anthropometries to different cab designs. Different performance measures are suggested and used with predictive dynamics to study human performance since human motion is not governed by a single performance measure. Optimizing multiple performance measures allows the full range of motion for all 55 degrees of freedom to be considered for simulating the task. Once the relevant performance measure was established, case studies were performed on seven different cab designs and digital human models with three different anthropometries. Finally, several different cab design metrics for propensity of injury, comfort, and accessibility were proposed. These design metrics were evaluated for each of the case studies. Finally, each cab design was ranked based on the design metrics to identify the best design for a range of anthropometries. These results help designers make decisions and plan further design changes.

## TABLE OF CONTENTS

LIST OF TABLES.....	vii
LIST OF FIGURES.....	ix
CHAPTER 1 INTRODUCTION .....	1
1.1 Motivation.....	1
1.2 Literature Review .....	2
1.2.1 Analysis of Accidents.....	3
1.2.2 Virtual Experimentation .....	4
1.2.3 Generating Human Motion.....	5
1.3 Research Objectives.....	7
CHAPTER 2 PROBLEM DEFINITION.....	8
2.1 Heavy Equipment Environment .....	8
2.2 Ingress/Egress Motion .....	8
2.3 Safety Factors (Regulations).....	9
2.4 Potential Challenges .....	10
CHAPTER 3 INGRESS/EGRESS SIMULATION.....	11
3.1 Video Analysis.....	11
3.1.1 Motion Analysis .....	11
3.1.2 Task Subdivision .....	13
3.1.3 Key Components .....	14
3.2 Target Model .....	15
3.3 Inputs .....	15
3.3.1 Cab geometry.....	16
3.3.2 Hand Inputs .....	19
3.4 Summary of Assumptions.....	20
CHAPTER 4 FORMULATION OF THE PROBLEM .....	21
4.1 Skeletal Model.....	21
4.2 Forward Recursive Kinematics.....	23
4.3 Backward Recursive Dynamics.....	23
4.4 Optimization Problem Definition .....	24
4.4.1 Design Variables .....	24
4.4.2 Objective Function .....	24
4.4.3 Constraints for Ingress and Egress .....	25
CHAPTER 5 SIMULATION RESULTS .....	29
5.1 Joint Angle Profiles .....	29
5.2 Discussion of Results.....	32
5.2.1 Addition of More Constraints.....	33
5.2.2 Task-Specific Joint Angle Limits.....	35
5.2.3 Different Objective Functions.....	37

5.3 Simulation Results with Task-Specific Joint Limits .....	37
5.4 Discussion of Results and Conclusions .....	41
CHAPTER 6 ALTERNATIVE OBJECTIVE FUNCTIONS.....	43
6.1 Dynamic Effort .....	43
6.2 Joint Discomfort .....	44
6.3 Multi-Objective Function Formulation.....	44
6.4 Test Results with Different Objective Functions.....	45
6.4.1 Backward Walking Problem Definition .....	46
6.4.2 Simulation Result with Different Objective Functions .....	47
6.4.3 Objective Function Weighting Coefficients: Case Studies .....	56
6.5 Conclusion.....	64
CHAPTER 7 METRICS FOR CAB DESIGN EVALUATION .....	66
7.1 Propensity to Injury .....	67
7.1.1 Dynamic Effort.....	67
7.1.2 Stability.....	69
7.2 Comfort (Feeling).....	71
7.3 Accessibility .....	73
7.3.1 Ladder to Door .....	73
7.3.2 Door to Seat.....	75
CHAPTER 8 RESULTS FOR CAB EVALUATION .....	77
8.1 Case Study Parameters .....	77
8.2 Anthropometric Study – Digital Human Models.....	80
8.3 Simulation Results.....	83
8.3.1 Results for Ingress.....	86
8.3.2 Results for egress.....	91
8.4 Conclusions.....	96
CHAPTER 9 CONCLUSIONS AND FUTURE RESEARCH .....	98
9.1 Conclusions.....	98
9.2 Future research.....	100
9.2.1 Different Populations.....	100
9.2.2 Different Performance Measures.....	101
9.2.3 Reaction Forces as Design Variables .....	101
9.2.4. Design of Ladder .....	101
REFERENCES .....	103

## LIST OF TABLES

Table 4.1 Constraints for each subtask .....	25
Table 5.1 Applied constraints for upper and lower body.....	35
Table 5.2 Joint angle limits.....	36
Table 6.1 Applied constraints for backward walking.....	47
Table 6.2 Neutral angle - standing.....	48
Table 6.3 Cases for objective function weighting coefficient .....	56
Table 7.1 Metrics for the cab design.....	67
Table 8.1 Geometries for each case .....	80
Table 8.2 Selected avatars.....	81
Table 8.3 Link length (Indexes corresponding Figure 4.1) .....	82
Table 8.4 Values of metrics for ingress (NK: neck joint; KN: knee joint).....	85
Table 8.5 Values of metrics for egress (HP : hip joint) .....	93

## LIST OF FIGURES

Figure 3.1 Task subdivision.....	14
Figure 3.2 Simplified prop models .....	15
Figure 3.3 Inputs.....	16
Figure 3.4 Obstacle inputs .....	17
Figure 3.5 Cab geometry for foot positions.....	18
Figure 3.6 Foot positions for ingress .....	18
Figure 3.7 Foot positions for egress.....	19
Figure 4.1 Digital human model.....	22
Figure 5.1 Joint angle profiles for ingress motion .....	30
Figure 5.2 Joint angle profiles for egress motion .....	31
Figure 5.3 Predicted motion for ingress/egress.....	32
Figure 5.4 Time segmentation for ingress .....	33
Figure 5.5 Joint angle profiles for ingress motion .....	39
Figure 5.6 Joint angle profiles for egress motion .....	40
Figure 5.7 Predicted motion with task-specific joint limits for ingress/egress.....	41
Figure 6.1 Basic foot supporting modes and polygon for backward walking .....	46
Figure 6.2 Predicted motion for backward walking with different objective functions.....	50
Figure 6.3 Joint angles with different objective functions.....	52
Figure 6.4 Joint torques with different objective functions .....	54
Figure 6.5 Joint angles with different weighting coefficients.....	57
Figure 6.6 Joint torques with different weighting coefficients.....	59
Figure 6.7 Objective function values with different weighting coefficients .....	62
Figure 6.8 Pareto optimum curve.....	63
Figure 6.9 Objective function values with different weighting coefficients .....	64
Figure 7.1 Calculation for stability metrics .....	70

Figure 7.2 Shortest distance from point to line.....	70
Figure 7.3 Graph of discomfort joint limit penalty term .....	73
Figure 7.4 Accessibility from ladder to door .....	74
Figure 7.5 Different seat locations.....	75
Figure 8.1 Dimension for default case.....	78
Figure 8.2 Seat position change along x axis (Case 1).....	79
Figure 8.3 Seat position change along z axis (Case 2) .....	79
Figure 8.4 Ceiling height change along y axis (Case 3).....	80
Figure 8.6 Knee torque for ingress with medium avatar .....	87
Figure 8.7 ZMP positions for Table 8.4a by different digital human models .....	88
Figure 8.8 Overall neutral angle difference ranking for ingress.....	89
Figure 8.9 Avatar-wise cab design ranking for ingress .....	90
Figure 8.10 Overall cab design ranks for ingress .....	90
Figure 8.11 Knee torque for egress with medium avatar.....	91
Figure 8.12 ZMP positions for Table 8.5a for different digital human models.....	92
Figure 8.13 Normalized penalty for each joint in Table 8.5a. ....	94
Figure 8.14 Subject-wise cab design ranking for egress.....	95
Figure 8.15 Overall cab design ranks for egress.....	96
Figure 8.16 Overall cab design ranks for ingress and egress.....	97



## CHAPTER 1 INTRODUCTION

### 1.1 Motivation

The design of ingress/egress (enter/exit) systems for heavy vehicles is an area that deserves the attention of designers and ergonomists. Since injuries resulting from the heavy vehicle environment represent a considerable cost to businesses that operate this equipment, a lot of work has been done to analyze the conditions under which accidents happen while performing ingress/egress in the heavy equipment industry. By analyzing those conditions, design changes have been made in ergonomically beneficial and economically viable ways. Hurst and Khalil (1984) exposed a large number of problems related to injury caused by the design of existing vehicles. Lack of or poorly placed side steps, excessive height of steps and other miscellaneous design problems can cause injuries. Therefore, while designing a cab, choosing a functional setup that will allow operators to move without wasting time on unnecessary steps and effort is an important consideration. Because of limited space and limited options for the location of the operating room, heavy vehicles have one of the most constrained environments. They are constraining in the sense that they are geometrically complex environments, with many aspects that define the structure of the cab interior and exterior or provide controls for driving. These elements influence operators' movements and also relate directly to the propensity for injury. In order to achieve all the above-mentioned design objectives, it is important to gather proper feedback from the driver when designing heavy equipment like vehicles specially manufactured for executing construction tasks.

As mentioned earlier, collecting feedback from drivers is important when arranging components inside the heavy vehicle. However, it is costly and time-consuming to organize experiments with various subjects. Moreover, experiments can be performed only if an actual physical model of the cab exists. However, building different

vehicle mock-ups for experiments is also costly and time-consuming. It is even more difficult to change the layout in a physical model significantly in order to test various conceptual designs. If virtual tools are provided that allow the designer to visualize how an operator sees the cab and the surrounding environment once a physical prototype is built, it could be very helpful. In addition, if the virtual tools also allow the designer to get feedback in terms of physics-based data that correspond to how the operator would feel while he ingresses and egresses the cab, it could let designers try various designs to perform a comparative study without building a single prototype. Therefore, this study focuses on simulating ingress and egress motion for a virtual human, especially on a virtual model of heavy equipment. By generating different motions on different models, the designers can integrate the use of virtual human simulation tools into the design of heavy vehicles.

## 1.2 Literature Review

As mentioned earlier, 3-D human motion simulation methods have improved, so attention has now turned to the complicated simulation problem of vehicle ingress/egress. A lot of work has been done to analyze the conditions under which accidents happen while performing ingress/egress in the heavy equipment industry. The wealth of data available from this research can serve as important guidelines for determining metrics for ingress and egress tasks. In addition, it also provides information about what should be avoided and what should be provided in an ideal design. In addition, some work has also been performed in the design and modeling of future cabs using virtual or semi-virtual experimentation. Thus, the following review section is categorized into three parts: analysis of accidents; virtual experimentation, which includes research in designing models for ingress/egress on heavy vehicles; and generating human motion, which includes predictive dynamics.

### 1.2.1 Analysis of Accidents

Due to the characteristics of heavy equipment and its environment, most studies have been focused on analysis of the moment when the accident happens. Gavan *et al.* (1980) reported most of the accidents occurred near the bottom of the ladder. The major dangerous design conditions were identified as excessively flexible supports for lower steps or rungs, inappropriate ground-level-to-first-step distances, poor step designs, and inadequate handrail and guardrail designs. Hirth and Khalil (2002) studied falls from vehicles when entering and exiting, which occur frequently and are very costly. They reviewed the existing standards and guidelines and looked into details about existing problems for drawing attention in order to avoid accidents. Injuries due to falls from equipment in U.S mining operations were studied. Injury databases were utilized to study the injury narrative, nature of injury, body part injured, mine type, and age at injury. Moreover, the impact of those injuries on industry was investigated by Moore *et al.* (2007). Accidents in the trucking industry were well-described by Lin and Cohen (1997). They gathered information about the scope and scale of common injuries and illnesses experienced by workers in the trucking industry. They presented the types of accidents that occurred most frequently as “slips and falls,” “struck by” and “overexertion”. Several recommendations for ergonomic solutions were provided to improve equipment design.

So far, analyses of accidents during ingress/egress for large vehicles have been summarized. Since severe injuries have been mainly caused during the ingress/egress motion, concerns about operators’ health have arisen. Injuries resulting from entering or exiting heavy equipment represent a substantial cost to businesses that operate the equipment. This type of study helps not only as a safety alert to the industry, but also as a guideline for the reduction of injuries and improvement of the work environment.

### 1.2.2 Virtual Experimentation

We learned about the types and causes of accidents in the previous section. In this subsection, attention is turned to safety considerations. Fathallah *et al.* (2000) compared impact forces during various exit methods from commercial equipment such as tractors, a step van, a box trailer, and a cube van. This approach, emphasizing optimal design of entry/exit aids coupled with driver training and education is expected to minimize exit-related injuries. Giguere *et al.* (2005) investigated injuries while stepping down from fire-fighting vehicles and compared the impact forces, the use of upper limbs, and firefighters' perception of danger as they step down from different locations on the fire truck.

The ingress/egress motions were studied for injury aspects before 2001. However, those investigations were concentrated on ingress/egress motion outside of the vehicle such as on the ladder or steps for going up or down. Moreover they just analyzed motions of certain subjects, but did not study improvements of design. Recently, attention has shifted to the ingress/egress motion itself. Reed (2009) presented guidelines for locating steps relative to door openings and seating positions. The motion capture data and reaction force data on a subject were analyzed using two different digital human models. An inverse dynamics analysis was conducted by driving the figure linkage with the measured whole-body kinematics data while applying the reaction forces at the hand and feet. Many vehicles have aids to assist the driver in safely entering/exiting the vehicle. Reed *et al.* (2010) presented foot trajectories on the steps to study suitability of steps for heavy trucks. Monnier *et al.* (2009) measured ingress/egress motion for a truck cabin using a motion capture system. They calculated joint angles and joint loads using inverse kinematics and dynamics methods. Two different methods for evaluating joint loads were presented: a force and moment method and a force-only method. Two different stepping motions were analyzed and validated. However, that study was focused on the stepping up and down motions, and on one specific truck cabin.

So far, Sections 1.2.1 and 1.2.2 have presented state-of-the-art in vehicle ingress and egress design and analysis using virtual or semi-virtual experimentation. To summarize, there are two topics for ingress and egress: study and analysis of the accidents and the optimizing designs to reduce the accidents. Even though studies on ingress and egress have been pursued actively, there are not many studies on ingress and egress of heavy vehicles. Moreover, a greater part of the studies is focused on the outside of the heavy vehicle (on the ladder or on the steps). None of the studies has reported what should be the proper location of the in-cab components. The majority of the ingress/egress studies are based on the motion capture data. Such studies can be costly and time-consuming. The motion either within the different vehicle geometry or with different personal characteristics cannot be predicted.

### 1.2.3 Generating Human Motion

In order to simulate the dynamic motion for ingress and egress effectively with respect to time and cost, some literature is reviewed. The most common approach to generate motions or posture for a certain task is based on the experimental data that are statistically collected from a lot of motion captures. These approaches do not provide enough flexibility to satisfy various needs due to their reliance on motion capture data. Because of this shortcoming, a mathematical approach is required to predict human motion for general tasks. For more natural and realistic simulation, not only should the effects of anthropometry based on kinematics be investigated, but also the effect of dynamics aspects such as force, torque, and/or inertia should be studied.

Lately, the problem of digital human motion simulation for dynamic tasks has been solved using an optimization approach. Optimization-based motion prediction has been widely used in biomechanics to make control strategies, analyze muscle forces, and predict optimal motion. Marler *et al.* (2008) overviewed the computational approaches in digital human modeling. Schiehlen (1997) discussed about the optimal design of a

mechanical system, especially the multicriteria optimization approach. Leboeuf *et al.* (2006) compared the minimum effort and the minimum energy to predict human handstand motion. It was concluded that the minimum effort is apt to generate more natural motion and the minimum energy made a smoother motion. Although many performance measures have been investigated for human motion prediction, there is limited work on developing constraints for a human motion using the optimization formulation. Xiang *et al.* (2009) proposed an approach based on an optimization formulation that minimizes the dynamic effort of people during walking while considering physical and kinematical constraints. This approach, along with the implemented constraints and performance measures performed well and was validated for different tasks. Therefore, we will use this optimization approach for generating ingress/egress motion.

Xiang *et al.* (2009) mentioned that range of motion at certain joints, such as the spine and shoulder, is artificially restricted to control the walking motion. However, restricted motion could be used to predict motion for subjects with certain medical conditions like injuries or minor pain. However, the use of such artificial constraints can also restrict the motion that can be predicted and may make otherwise valid motion impossible to predict. Therefore, it is necessary to be able to generate natural-looking motion without the use of artificial constraints.

From now on, this study will predict ingress/egress motion for heavy vehicles using above mentioned optimization-based digital human modeling approach. The predicted motion will then be used to study operator performance for different cab designs such as the effect of the controller, handle, and seat on the driver's safety, health, and efficiency. Moreover, case studies will be performed for different input parameters and different-sized digital human models with the multi-objective optimization approach. After the simulations, in order to help designers decide whether one design is better than the other, several different design metrics will be proposed for injury, comfort, and

accessibility considerations. Finally, each cab design will be graded based on the metrics to eliminate the relatively bad designs and select a few designs for prototype development and further experimental analysis.

### 1.3 Research Objectives

The primary objective of this study is to evaluate ingress/egress characteristics of heavy equipment using digital human modeling and simulation. By simulating human motion in a virtual environment, the interaction between human and environments can be studied. For this study, attention is paid to four objectives. The first objective is to generate ingress and egress motion separately in the operating room using the predictive dynamics approach. In order to use the predictive dynamics approach, it is important to understand the difference between a simple task such as walking and a complex one such as ingress/egress. By understanding the characteristics of ingress/egress, dynamic human motion prediction for ingress/egress can be improved using multi-objective optimization. In this study, a backward walking task will be used as a simple task to test different performance measures with multi-objective optimization. This test will give us clues about the driving factors of human motion for ingress/egress. The second objective is to allow the user to test different vehicle designs. Case studies will be performed with different parameters and different-sized digital human models (anthropometric variations). In order to help designers make a decision about whether one design is better than the other, several critical design metrics will be set up. By creating design metrics, the designer will receive reliable feedback on the effect of design changes and differently sized humans. This will help designers make decisions and plan further design changes. The final goal of this study is to investigate proper location of cab components such as the controller, steering wheel (handle), and seat.

## CHAPTER 2

### PROBLEM DEFINITION

#### 2.1 Heavy Equipment Environment

Unlike passenger cars, heavy equipment vehicles connect components, transmit loads, and have attachment points for different components. In addition, the heavy equipment vehicle is designed to travel over uneven ground. The operating room of the vehicle is located high off the ground and is accessible through a ladder. This high position of the operating room is to both protect the operator from the harsh construction environment and provide a wider view of the construction area. While the driver's seat is located proximally to an entrance door for a passenger car, in heavy equipment vehicles the operator's seat is located in the center of the room.

As a result, the operating room has more space for the driver to move in and out. In addition, the operating room ceiling is placed at a higher level, making it easy for the operator to walk upright and reach the operator's seat. The machine's frame, articulation (control panel), and steering for wheeled equipment are the major parts of the heavy equipment. Once the operator steps off the access ladder, the operator has to avoid those items to get in or out. Since it is off the ground and has limited space, the locations of those components become important. The location and placement of these components should guarantee the operator's safety.

#### 2.2 Ingress/Egress Motion

Ingress and egress movements are complex, as almost the whole body is involved in the motion within a highly constrained environment. These motions are affected by not only the physical capability of the operator, but also by the dimensions and anthropometry of the operator's body. The size, layout, width, and shape of the door influence the motion as well. A detailed motion analysis must be carried out in order to be able to generate different movements for predicting the entire motion. Initially the



movement is divided into two logical phases: ingress and egress. The motion is defined based on the structure of the object (vehicle). Stepping up or climbing a ladder is included in ingress motion for the heavy equipment vehicle; conversely, exiting the cab and climbing down the ladder is included in egress. But for some larger vehicles (like the wheel loader) that have large operating rooms, entering into the operating room and sitting could be also a part of ingress; conversely, egress would include exiting the room. In general, ingress is the act of entering, which can include walking to the ladder, climbing the ladder, entering the operating room, and sitting. Egress, on the other hand, is the act of exiting, which involves getting up and moving out of the operating room and then descending the ladder.

### 2.3 Safety Factors (Regulations)

Heavy equipment operators are prone to fall frequently both on and off the work zone premises, and for many different reasons (Flatow, 2000). Conventional or cab-over-truck cabs can be several feet off the ground, and a driver can sustain serious injuries if he/she falls while entering or exiting the truck. Transitioning out of the cab onto slippery, greasy, or oily surfaces can also cause slips and falls. In winter weather, snow and ice can accumulate on the truck deck that leads in/out of the cab. Oil and grease can accumulate on yard surfaces and be transferred to the driver's shoes. Another factor in falls is that the driver's legs may "fall asleep" during long periods of driving. Use of foot and handholds, as well as non-skid coating on the deck, can help prevent falls. In addition, drivers are expected to maintain a "three-point stance" during truck ingress and egress. That is, they are expected to have two feet on the steps and one hand on the handhold at all times. This stance should also be used when climbing up and down or between the cab and trailer to connect brake and light lines. Furthermore, the driver must be aware that jumping from cabs and trailers is dangerous.

## 2.4 Potential Challenges

To sum up previous sections, understanding the characteristics of ingress/egress is important for this study. The biggest difference between ingress/egress with a simple task like walking is that ingress/egress motion interacts with geometries. While a person could walk without any geometry, ingress/egress motion needs to have an object to get in and out of. During ingress/egress motion, a person cannot strike the objects. Each frame and individual component of the object would be an obstacle to avoid. Therefore, collision avoidance should be imposed at the proper time on the proper object.

When the design changes, the locations of the obstacles also change. This is going to make the motion different. Moreover, the subject normally does not carry a heavy load to get in and out, so it is quite different than dynamic-type tasks. It is more like a kinematic task dealing with geometries. The motion for walking does not change much, except in the lower body, and it could be a continuous motion. However, ingress/egress motion keeps changing over time depending on the location of the object. Therefore, a typical predictive dynamics approach using dynamic effort as an objective function may not fit this type of task. Investigation of the most appropriate performance measure for ingress/egress will be a challenge.

In this study, understanding the industries is also important. Since ingress/egress is directly related to the injuries, understanding when and why accidents occur, when the subjects feel uncomfortable, and where they get injuries is critical and should be imposed on the design. Therefore, development of a guideline for deciding a better design will be another challenge.

## CHAPTER 3

### INGRESS/EGRESS SIMULATION

Since ingress and egress is a complex task, it is difficult to deal with one large task. In order to simplify the process of modeling and simulating motion, it is divided into two smaller independent tasks: ingress and egress. There are a couple of things that need be considered for generating the ingress/egress motion. The current design considerations for ingress and egress are as follows: design features should be comfortable, design and placement should be safe, important controllers and components should be reachable and displays should be visible to the user, there should be no obstructions while getting in and out, and they should be usable by a wide range of the population. In this chapter, progress on modeling the ingress/egress task is presented.

#### 3.1 Video Analysis

##### 3.1.1 Motion Analysis

Video analysis was carried out in order to determine the main interactions between the driver and the cab. The model used for video analysis was the Caterpillar Wheel Loader 950. The wheel loader is normally used to move mounds of earth from one place to another at building and construction sites. The wheel loader has four wheels and a square bucket attached to the front. These machines come in a variety of configurations based on their desired purpose.

Experienced drivers were asked to get in and out of a wheel loader. Two runs were performed, the first time with the door closed and the second time with the door opened. These two door configurations were tested in order to identify the possible influence of door handling on the motion strategy. However, only the open door motion strategy is studied as a pilot study in this thesis. The observation is mostly focused on how to move from or to the interior of the cab while avoiding obstacles.

Key components are determined as obstacles to avoid. The movement of the body and direction of the foot are tracked in the cab geometry. Ingress and egress are analyzed in chronological phases. The observed motion phases that can be used for characterizing ingress/egress movement are as follows:

**Ingress:**

The ingress movement begins with walking to the ladder followed by the operator climbing up the ladder. Once the operator reaches the cab level, he/she then grabs the steering wheel with his/her left hand while simultaneously stepping in. The second step of ingress involves the left foot taking a step forward and the right hand moving to the controls located on the right side of the seat. During the stepping-in phase, the door frame on either side of the operator and the ceiling frame above the operator are considered obstacles to avoid. Since the operating cab is not at the same level as the ladder and is actually raised a step above the ladder, the edge of the step is considered another obstacle. In the final step of the ingress, the right foot swings in front of the seat, and the operator sits down and places the right hand on the armrest.

**Egress:**

Egress movement starts from the sitting position. The first step is the driver placing his/her left hand on the outer safety bar while stepping sideways along the seat toward the outside. During the second step of egress, the right hand is moving on the door frame while the whole body is off the seat. The final step of egress is the left foot exiting the cab, then the right foot swings outside the cab to face the body toward the cab for safety and the right hand is placed on the outer safety bar. During the final step, the operator needs to step down, and the whole body turns (rotates). Then the operator descends the ladder and walks away from the cab.

### 3.1.2 Task Subdivision

Ingress consists of three distinct motion phases called subtasks: walking forward (to approach the Caterpillar cab), ladder climbing, and the ingress maneuver. The ingress maneuver is again divided into two subtasks: entering the cab and sitting. Egress also consists of three distinct motions: egress maneuver, ladder descending, and walking from the ladder (to be away from the cab). The egress maneuver is again divided into two subtasks: rising and exiting the cab as shown in Figure 3.1. For continuity of the motion for ingress, the ending position of each subtask should be identical to the next starting position. The key frames for each subtask are summarized below.

#### Subtask 1 – Entering

Since ladder climbing and opening the door will not be considered in this subtask, the starting position should be the standing posture. Therefore, Subtask 1 starts from a standing posture and ends in a sit-ready position in the cab.

#### Subtask 2 – Sitting

This is the position in which an operator fits his/her body in a narrow area between the dashboard and seat. The hip should be located in the proper area of the seat.

#### Subtask 3 – Rising

This is the position in which the operator gets up and prepares to move out. The hip should be off the seat while grasping the safety bar.

#### Subtask 4 – Exiting

This is the position in which the operator steps down from the operating room while exiting the cab. The operator rotates his/her body to face the cab.

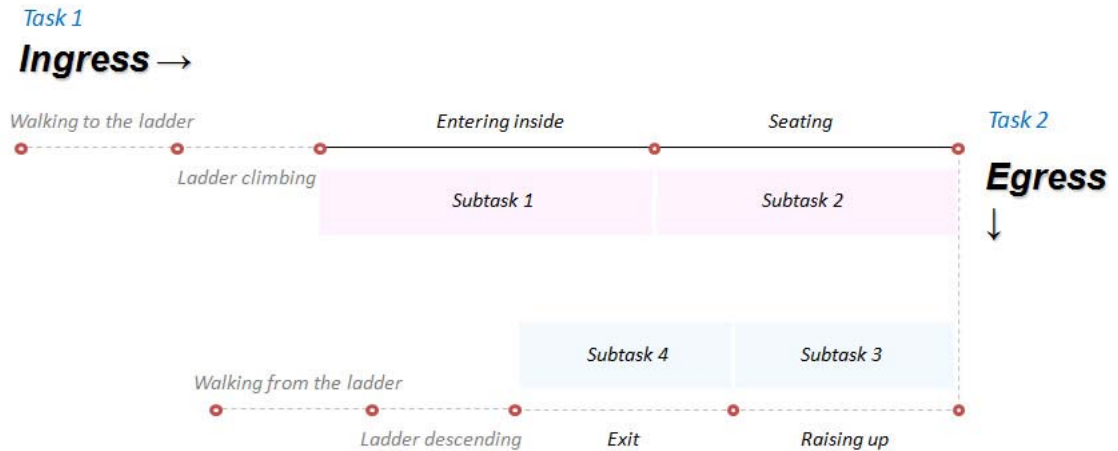


Figure 3.1 Task subdivision

### 3.1.3 Key Components

In order to improve computational efficiency, not all components of the cab are included. Key components are determined by video analysis. When the operator gets in through the door frame, it becomes a key component to avoid. The arms cannot penetrate the frames and the foot cannot go through the step; the operator has to bend to avoid hitting his head on the top side of the frame. While moving in and out of the narrow seat area, the lower body should avoid the seat. Therefore, the seat is defined as another key component. The key components are provided to the ingress and egress model in the form of simple primitives that represent the complicated cab geometry.

### 3.2 Target Model

A CAD model of the cab is redefined and reduced to a primitive model. This “prop” model consists of key components, giving users the ability to test and interact with between these components easily and study the resulting motion. It also simplifies the model, allowing the user to easily define the necessary parameters for a given task. This model takes on the size and shape of a generic model that can be used in the simulation process. The user can scale this prop model to size, orientation, and position as required for the task. The properties defined by the model are then passed to the digital human modeling evaluator, and task analysis can be performed. It is imperative that the user has the ability to easily define the parameters. It is also important for the user to be able to expand the ingress and egress models to different cab models. For these reasons, it has been determined that the best way to give the user both ease of use and flexibility is to use a simpler prop model than the complex CAD model.

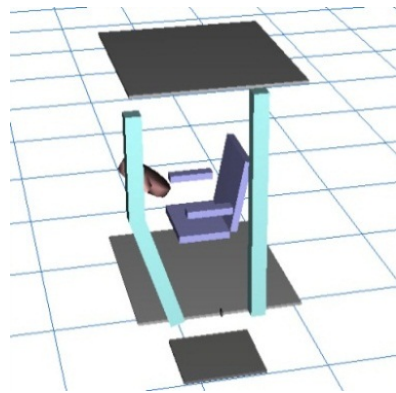


Figure 3.2 Simplified prop models

### 3.3 Inputs

If there were many things to be defined by the user, it would be quite inconvenient. Inputs can be categorized into two parts: cab geometry and grab positions for hands as shown in Figure 3.5. These create obstacles and foot positions internally.

While imposing those inputs, the body automatically follows the direction of the foot avoiding the obstacles.

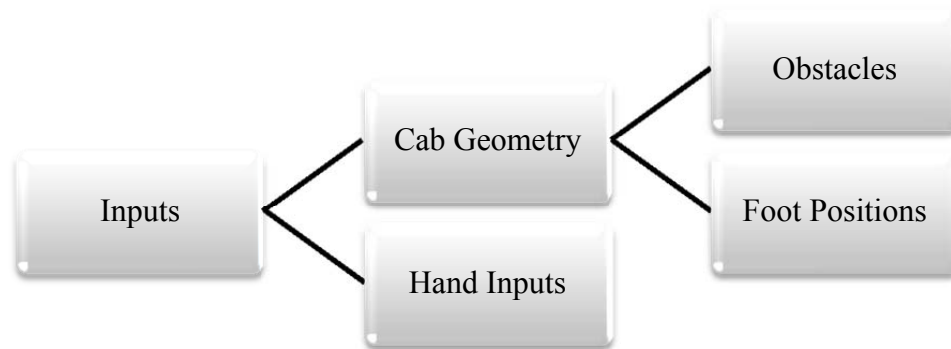


Figure 3.3 Inputs

How the cab geometry acts as obstacles and foot positions are presented in Section 3.5.1, and Section 3.5.2 describes how hand positions are assigned by users.

### 3.3.1 Cab geometry

#### 3.3.1.1 Obstacle Input

The first type of input needed from the user is information about the particular cab model. This is provided for the ingress motion in the form of simple primitives that represent the complex cab geometry that Santos<sup>TM</sup> will encounter while entering and exiting the cab. This task accepts two types of primitives, cylinders and planes. The cylinders and planes can be defined as either finite or infinite. For finite cases, the cylinder is defined by two end points and a radius, while a plane is defined by three points and a thickness. These primitives can then be used to approximate geometry with which Santos will come into contact during ingress and egress. Figure 3.4 demonstrates



how these obstacles could be placed by a user to define the seat, cab frame, and cab ceiling.

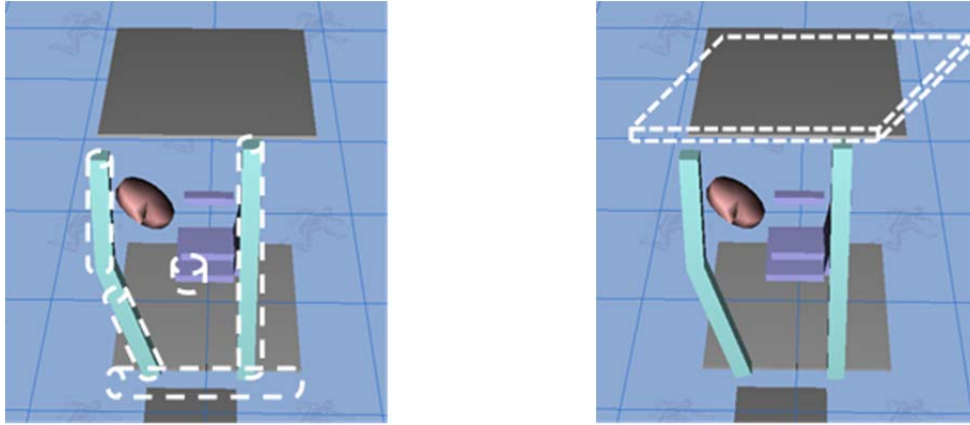


Figure 3.4 Obstacle inputs

### 3.3.1.2 Foot Position Inputs

Foot position is defined the size of the seat cushion (which is assumed to be a square) and the location of the door, used as a criterion to recognize the entry point for Santos.  $w_{\text{Seat}}$  is the width of the seat cushion, which is assumed to be square in shape (Figure 3.5).  $m_{\text{Door}}$  is the middle point of the door, which is located on the floor of the operating room. It is used as a criterion to recognize the door location for Santos so that he knows where to enter or exit. Foot position is also defined by the available room area that Santos can walk in.  $w_{\text{Room}}$  is the width of the space in which Santos can walk. If  $w_{\text{Room}}$  is large (as available area in the room gets larger), larger step sizes are needed. The seat position point is located in the middle of the seat cushion. This point has  $x, y, z$  coordinates. All the point information, such as  $m_{\text{Door}}$  and seat position, is measured from Santos's global frame A for ingress (Figure 3.6) and B (Figure 3.7) for egress. Stair

height is the height (y direction) from the tip of ladder (called the deck) to the operating room floor.

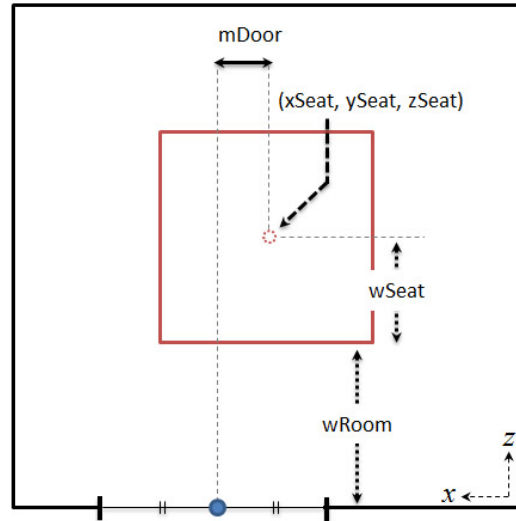


Figure 3.5 Cab geometry for foot positions

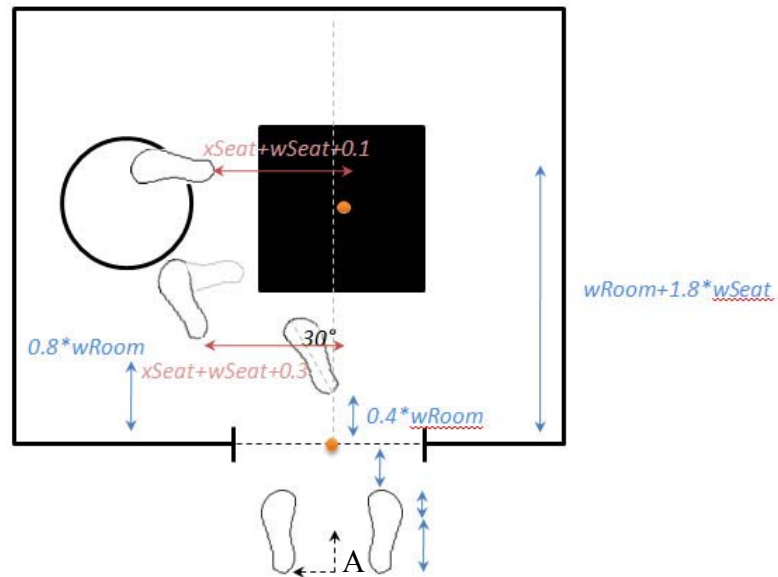


Figure 3.6 Foot positions for ingress

Therefore, once the user makes changes to the cab geometry, the step will be automatically adjusted. In other words, foot position itself is not predicted; it is given by the user indirectly when he/she stipulates the cab geometries. Figures 3.6 and 3.7 depict how foot position is defined according to the cab geometry.

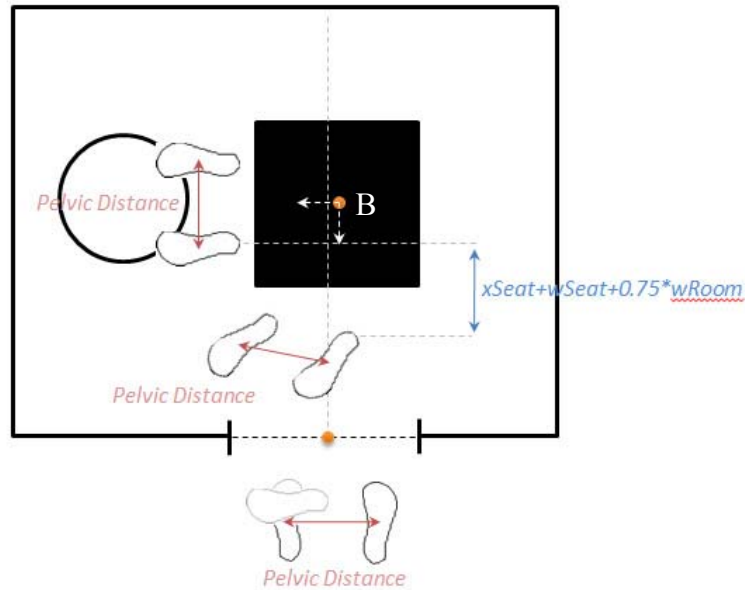


Figure 3.7 Foot positions for egress

### 3.3.2 Hand Inputs

#### 3.3.2.1 Hand Position

To adhere to the three points of contact safety regulations in Section 2.3, the operator must grab something for his/her safety while moving into the cab. In order to satisfy this condition, the user has to specify hand location as an input. Hand position is measured in Cartesian coordinate space from the global axis of Santos. The user can choose either the right hand or the left hand.

### 3.3.2.2 External Force on the Hands

Reaction forces at the points of contact play an important role during ingress and egress and must be considered for the final tool to produce acceptable results. In order to consider external forces when the hand is positioned on the object, external forces are imposed as inputs. Therefore, if there is reliable data, the user could use those data. Reed *et al.* (2010) studied right hand force generated on handhold during the initial phase of the ingress. They concluded that hand force exceeded 35% of the body weight. Schultz *et al.* (1992) investigated force on the armrests at lift-off of rising from a chair. In their study, approximately 150 N at an angle of approximately 50 degrees with respect to the horizontal force is used. In this study, approximate forces, which are 5 to 10% of the body weight in one direction (pushing when sitting and getting up, pulling when moving in and out), are applied.

### 3.4 Summary of Assumptions

For this study, several assumptions are made. Walking to the ladder, ladder climbing, and ladder descending are not considered. Instead of connected motion between ladder climbing and entering, it is assumed that Santos is standing on the deck area for his starting position. The door of the operating room is open so the driver does not need to open and close it during the motion. The operator's movable range is limited to a minimum of three steps. The adjustable area for the objects should not interrupt the stepping area. Vision effects and friction effects are not considered.

## CHAPTER 4

### FORMULATION OF THE PROBLEM

A predictive dynamics approach is used to predict the ingress and egress motion of the operator in the cab. This approach solves a nonlinear optimization problem to determine the joint angle profiles of various joints of a human to predict a motion for a given task. The approach also calculates the actuation torques required to achieve that motion while satisfying various constraints. A dynamic-effort-based human performance measure is minimized subject to the available information about the human model as well as the task. In this chapter, we will describe the digital human model and formulate the optimization problem that will be used to predict the ingress and egress motion. Some details of the basic predictive dynamics approach are omitted as they are presented by Xiang *et al.* (2009).

#### 4.1 Skeletal Model

The human body is modeled as a series of links connected by revolute joints to represent musculoskeletal joints. A generalized coordinate,  $q_i$ , represents the rotational displacement of each joint. In this study, a 55-DOF three-dimensional digital human skeletal model is considered as shown in Figure 4.1. In this model, the six global DOFs, three translations and three rotations between the origin of the fixed inertial coordinate and the current pelvic position, allow the global movement of the digital human model. The spine section consists of four joints, each with three rotational DOFs. The legs and arms are assumed to be symmetric. Each leg consists of a thigh, a shin, a rear foot, and a fore foot. The hip joint has three rotational DOFs, the knee joint has one DOF, the ankle joint has two rotational DOFs, and the ball of foot has one rotational DOF. Each arm consists of a clavicle, an upper arm, a lower arm, and a hand. The clavicle joint has two

DOFs, the shoulder joint has three DOFs, the elbow joint has two DOFs, and the wrist has two DOFs. In addition, there are five DOFs for the head.

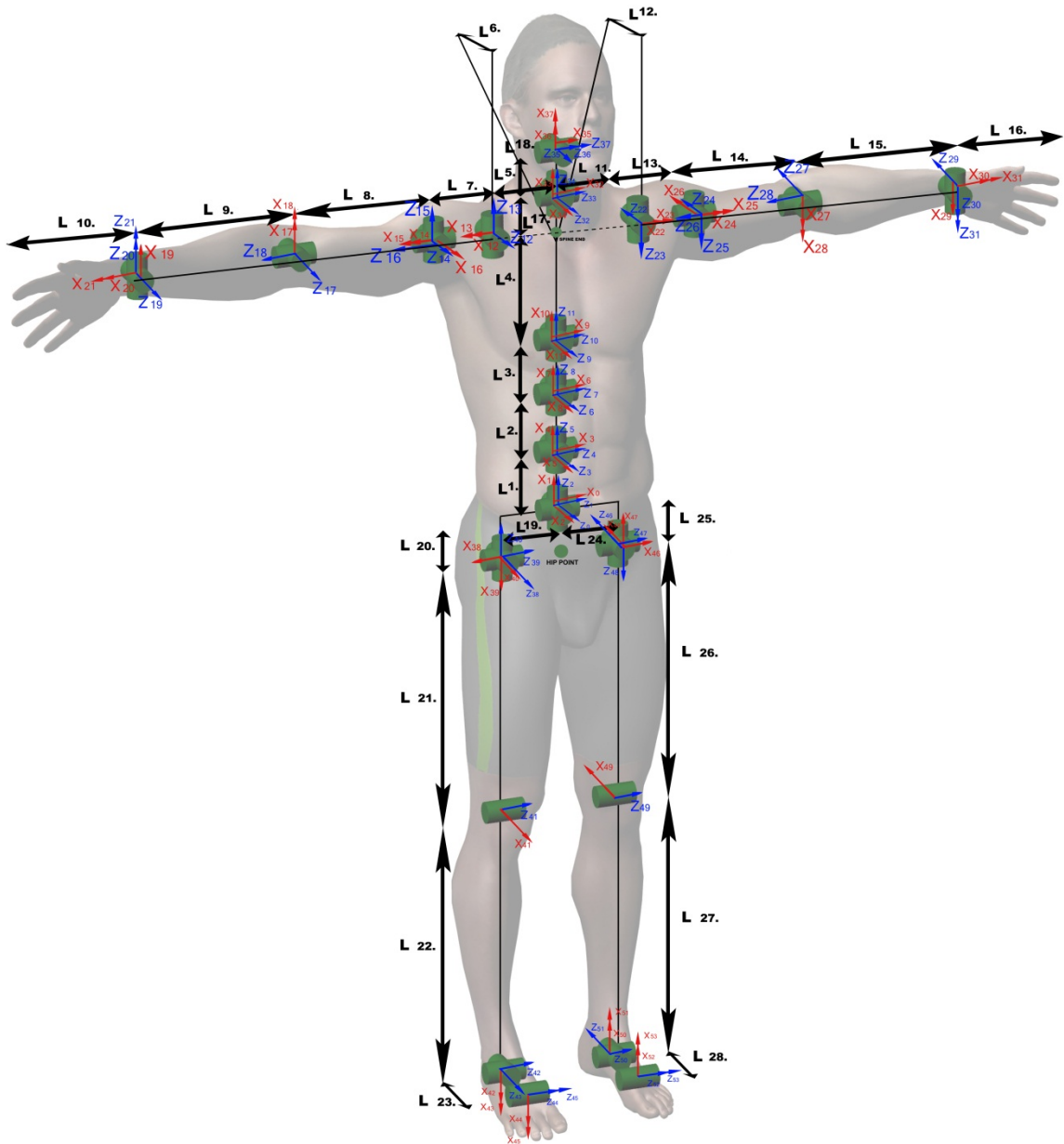


Figure 4.1 Digital human model

### 4.2 Forward Recursive Kinematics

In this process,  $4 \times 4$  transformation matrices  $\mathbf{A}_j$ ,  $\mathbf{B}_j$  and  $\mathbf{C}_j$  are defined to represent the recursive position, velocity, and acceleration, respectively, for the  $j^{\text{th}}$  joint. Given the link transformation matrix ( $\mathbf{T}_j$ ) and the kinematics state variables for each joint ( $q_j, \dot{q}_j, \ddot{q}_j$ ), then for  $j = 1$  to 55 we have:

$$\mathbf{A}_j = \mathbf{T}_1 \mathbf{T}_2 \mathbf{T}_3 \cdots \mathbf{T}_j = \mathbf{A}_{j-1} \mathbf{T}_j \quad (4.1)$$

$$\mathbf{B}_j = \dot{\mathbf{A}}_j = \mathbf{B}_{j-1} \mathbf{T}_j + \mathbf{A}_{j-1} \frac{\partial \mathbf{T}_j}{\partial q_j} \dot{q}_j \quad (4.2)$$

$$\mathbf{C}_j = \dot{\mathbf{B}}_j = \ddot{\mathbf{A}}_j = \mathbf{C}_{j-1} \mathbf{T}_j + 2\mathbf{B}_{j-1} \frac{\partial \mathbf{T}_j}{\partial q_j} \dot{q}_j + \mathbf{A}_{j-1} \frac{\partial^2 \mathbf{T}_j}{\partial q_j^2} \dot{q}_j^2 + \mathbf{A}_{j-1} \frac{\partial \mathbf{T}_j}{\partial q_j} \ddot{q}_j \quad (4.3)$$

$$\mathbf{A}_0 = [0] \text{ and } \mathbf{B}_0, \mathbf{C}_0 = [0]$$

After obtaining all transformation matrices  $\mathbf{A}_j$ ,  $\mathbf{B}_j$ , and  $\mathbf{C}_j$ , the global position  ${}^0\mathbf{r}_n$ , velocity  ${}^0\dot{\mathbf{r}}_n$ , and acceleration  ${}^0\ddot{\mathbf{r}}_n$  of a point in the Cartesian coordinate system can be calculated using the following formulas:

$${}^0\mathbf{r}_n = \mathbf{A}_n \mathbf{r}_n; \quad {}^0\dot{\mathbf{r}}_n = \mathbf{B}_n \mathbf{r}_n; \quad {}^0\ddot{\mathbf{r}}_n = \mathbf{C}_n \mathbf{r}_n \quad (4.4)$$

where  $\mathbf{r}_n$  represents the augmented local coordinates of the point in the  $n^{\text{th}}$  coordinate system.

### 4.3 Backward Recursive Dynamics

Based on forward recursive kinematics, the backward recursion for the dynamic analysis is accomplished by defining a  $4 \times 4$  transformation matrix  $\mathbf{D}_i$  and  $4 \times 1$  transformation matrices  $\mathbf{E}_i$ ,  $\mathbf{F}_i$ ,  $\mathbf{G}_i$ , as follows. Given the mass and inertia properties of each link, the external force  $\mathbf{f}_k^T = [f_x \ f_y \ f_z \ 0]$ , and the moment  $\mathbf{h}_k^T = [h_x \ h_y \ h_z \ 0]$  for link  $k$  ( $1 \leq k \leq n$ ) defined in the global coordinate system, the joint actuation torques  $\boldsymbol{\tau}_i$  for  $i = n$  to 1 are computed as follows (Xiang *et al.*, 2009):

$$\boldsymbol{\tau}_i = tr \left[ \frac{\partial \mathbf{A}_i}{\partial q_i} \mathbf{D}_i \right] \quad (4.5)$$

$$\boldsymbol{\tau}_i = tr \left[ \frac{\partial \mathbf{A}_i}{\partial q_i} \mathbf{D}_i \right] + \mathbf{g}^T \frac{\partial \mathbf{A}_i}{\partial q_i} \mathbf{E}_i + \mathbf{f}_k^T \frac{\partial \mathbf{A}_i}{\partial q_i} \mathbf{F}_i + \mathbf{G}_i^T \mathbf{A}_{i-1} \mathbf{z}_0 \quad (4.6)$$

$$\mathbf{D}_i = \mathbf{J}_i \mathbf{C}_i^T + \mathbf{T}_{i+1} \mathbf{D}_{i+1} \quad (4.7)$$

$$\mathbf{E}_i = m_i {}^i \mathbf{r}_i + \mathbf{T}_{i+1} \mathbf{E}_{i+1} \quad (4.8)$$

$$\mathbf{F}_i = {}^k \mathbf{r}_f \delta_{ik} + \mathbf{T}_{i+1} \mathbf{F}_{i+1} \quad (4.9)$$

$$\mathbf{G}_i = \mathbf{h}_k \delta_{ik} + \mathbf{G}_{i+1} \quad (4.10)$$

where  $\mathbf{D}_{n+1} = \mathbf{E}_{n+1} = \mathbf{F}_{n+1} = \mathbf{G}_{n+1} = [0]$ ;  $\mathbf{J}_i$  is the inertia matrix for link  $i$ ;  $m_i$  is the mass of link  $i$ ;  $\mathbf{g}$  is the gravity vector;  ${}^i \mathbf{r}_i$  is the location of center of mass of link  $i$  in the local frame  $i$ ;  ${}^k \mathbf{r}_f$  is the position of the external force in the local frame  $k$ ;  $\mathbf{z}_0 = [0 \ 0 \ 1 \ 0]^T$ , and  $\delta_{ik}$  is Kronecker delta. The first term in the torque expression is the inertia and Coriolis torque, the second term is the torque due to gravity, the third term is the torque due to external force, and the fourth term represents the torque due to the external moment.

#### 4.4 Optimization Problem Definition

##### 4.4.1 Design Variables

The design variables are the joint angle profiles  $q_i(t)$  for ingress and egress motion where  $i$  is 55 DOF.

##### 4.4.2 Objective Function

The dynamic effort (the integral of the squares of all joint torques) is used as the objective function for the ingress and egress motion prediction that is defined as:

$$\text{Minimize } f(\mathbf{q}) = \int_{t=0}^T \left( \frac{\boldsymbol{\tau}(\mathbf{q}, t)}{|\boldsymbol{\tau}|_{\max}} \right)^T \left( \frac{\boldsymbol{\tau}(\mathbf{q}, t)}{|\boldsymbol{\tau}|_{\max}} \right) dt \quad (4.11)$$



where  $T$  is the total time for one step, and  $|\boldsymbol{\tau}|_{\max}$  is the maximum absolute value of each joint torque limit.

#### 4.4.3 Constraints for Ingress and Egress

Several constraints are proposed and implemented in this work to satisfy the laws of physics and boundary conditions throughout the ingress and egress process. These constraints include joint angle limits, ground penetration, foot contacting positions, ZMP location, hand position, obstacle avoidance, and continuity conditions (Kwon *et al.*, 2011). Applied constraint names for each subtask are presented in Table 4.1.

Table 4.1 Constraints for each subtask

Task \ Constraints	Ingress		Egress	
	Subtask 1	Subtask 2	Subtask 3	Subtask 4
Joint angle limits	o	o	o	o
Ground penetration	o	o	o	o
ZMP constraint	o	o	o	o
Contacting position	o	o	o	o
Hand position	o	o	o	o
Continuity conditions	x	o	x	o
Obstacle avoidance	o	o	o	o
Joint torque limits	o	o	o	o

where “o” means it is applied, “x” means it is not applied.

##### 4.4.3.1 Joint Angle Limits

The joint angle limits accounting for the physical range of motion are obtained from experiments:

$$\mathbf{q}^L \leq \mathbf{q}(t) \leq \mathbf{q}^U, \quad 0 \leq t \leq T \quad (4.12)$$

where  $\mathbf{q}^L$  is the lower limit and  $\mathbf{q}^U$  is the upper limit on the joint angles.

#### 4.4.3.2 Ground Penetration

While the foot is in contact with the ground, the height of the contacting points is zero. The other points should be above the ground and the height greater than zero. When the foot contacts the ground, the velocity of the contacting points also should be zero.

#### 4.4.3.3 ZMP Constraint

The stability is achieved by constraining the ZMP to be in the foot supporting region.

$$z_{zmp}(t) \in FSR, \quad x_{zmp}(t) \in FSR, \quad 0 \leq t \leq T \quad (4.13)$$

where  $z_{zmp}$  and  $x_{zmp}$  are the coordinates of calculated ZMP.

#### 4.4.3.4 Foot Contacting Position

Since the step length  $L$  is given, the foot contacting position is known and specified at each time:

$$\mathbf{P}_{actual}(t) = \mathbf{P}_{target}(t) \quad (4.14)$$

where  $\mathbf{P}$  is the point position at the contacting time  $t$ . Therefore, to step on the specified points (target points); the difference of actual foot points and target points should be zero.

#### 4.4.3.5 Hand Position

The tip of the hand is chosen for the hand point. Since position information for the object comes from input, the object position is known. Hand position should be identical to object position at a certain time  $t$ .

$$\mathbf{P}_{hand}(t) = \mathbf{P}_{object}(t) \quad (4.15)$$

where  $\mathbf{P}$  is the point position at the contacting time  $t$ . Therefore, to grab the specified points (object points); the difference of hand points and object points should be zero.

#### 4.4.3.6 Continuity Conditions

All the ingress and egress tasks are divided into separate subtasks for the convenience of calculation. To combine subtasks, continuity constraints are imposed. The basic idea is that the final posture of the previous subtask and the initial posture of the subsequent subtask should be identical. These conditions are expressed as

$$\begin{aligned} \mathbf{q}_{pre}(T) &= \mathbf{q}_{post}(0) \\ \dot{\mathbf{q}}_{pre}(T) &= \dot{\mathbf{q}}_{post}(0) \end{aligned} \quad (4.16)$$

where  $\mathbf{q}_{pre}$ ,  $\mathbf{q}_{post}$  and  $\dot{\mathbf{q}}_{pre}$ ,  $\dot{\mathbf{q}}_{post}$  represent the angle and velocity of each DOF at time  $t$ .  $T$  is the final time and  $0$  is the initial time at each subtask. Therefore, the joint angles and velocities of the previous subtask at the final time should be the same as the joint angles and velocities of the next subtask at the initial time. The continuity condition is imposed on subtask 2 and subtask 4.

#### 4.4.3.7 Obstacle Avoidance

The avatar must avoid the collision of its body segments with other non-adjacent body segments as well as with objects in the environment while performing a task. The body segments are represented by using one or more spheres rigidly attached to a local reference frame, such that these spheres move with the body segments. The objects in the environment are modeled using one or more of the five primitive geometries: spheres, infinite cylinders, infinite planes, finite cylinders, and finite planes. A generic collision avoidance strategy is developed to avoid spheres with all five primitive geometries used for representing obstacles. Therefore, when the arm is swinging near the hip joint, it cannot go into the body. This constraint is related to the simulation environment, expressed as

$$\mathbf{P}_{object}(t) - \mathbf{P}_{body}(t) \geq 0, \quad 0 \leq t \leq T \quad (4.17)$$

The distance from the position of the object and the position of the body segment should be greater than zero.

#### 4.4.3.8 Joint Torque Limits

The joint torque limits accounting for the physical range of motion are obtained from experiments:

$$\boldsymbol{\tau}^L \leq \boldsymbol{\tau}(t) \leq \boldsymbol{\tau}^U, \quad 0 \leq t \leq T \quad (4.18)$$

where  $\boldsymbol{\tau}^L$  is the lower limit and  $\boldsymbol{\tau}^U$  is the upper limit on the joint torques.

## CHAPTER 5

### SIMULATION RESULTS

#### 5.1 Joint Angle Profiles

The formulation given in Chapter 4 is implemented in the Santos environment. The ingress/egress motion is simulated with the formulated objective function (dynamic effort) and constraints. A few joint angle profiles for the ingress/egress simulation are plotted in Figure 5.1. In Figure 5.1, extension motion is observed at the neck and shoulder joints. Spine flexion is expected to avoid the ceiling while moving inside; however, simulation results show spine extension. For the right shoulder joints, a lot of internal and external rotational movement is observed during the motion. For the lower neck joint, left and right bending is observed at 4.5 s, which is the end of motion. These motions are shown in Figure 5.3a. Left and right bending for the neck joint and internal and external rotation for the shoulder joint are compared with the neutral angle, which is selected as a relatively comfortable posture in Figure 5.1.

For egress, a lot of clavicle and shoulder motions are observed in Figure 5.2. This is also shown in Figure 5.3b. Compared to the neutral angle, which is relatively comfortable, both clavicle motions, which are Retraction-Protraction and Elevation-Depression-Shrug, are far from the neutral angle. To satisfy hand-grab constraint, clavicle motion is needed; however, even the starting posture, which has to be comfortable, is far from the neutral angle. This caused the shoulder to move awkwardly as shown in last frame of Figure 5.3b.

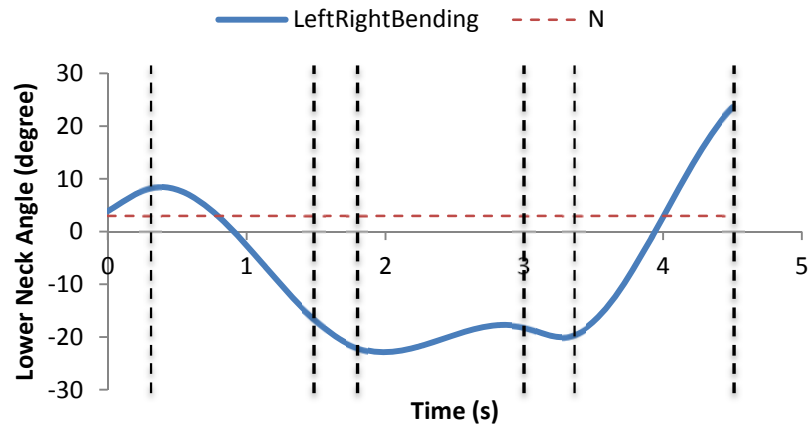
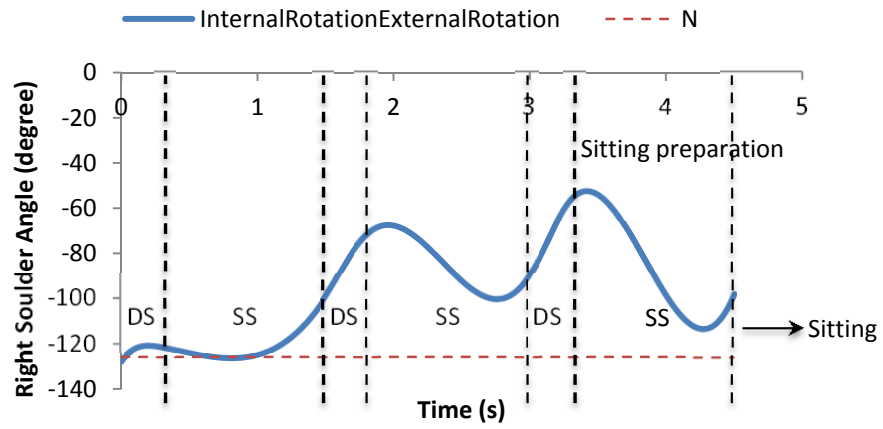
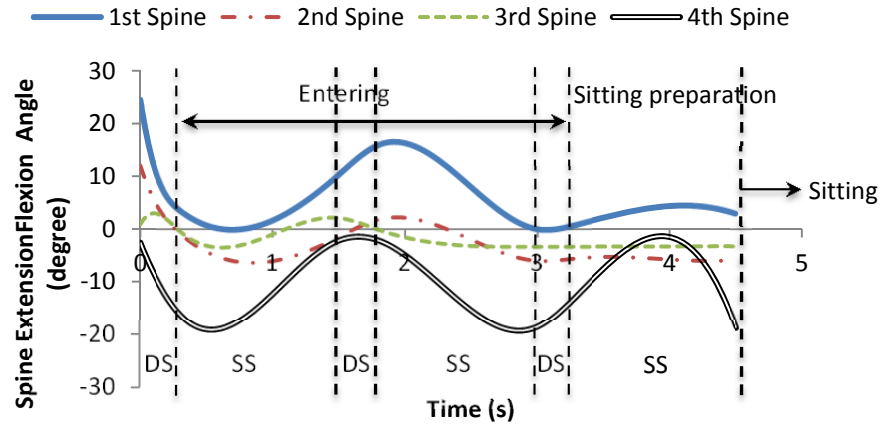


Figure 5.1 Joint angle profiles for ingress motion

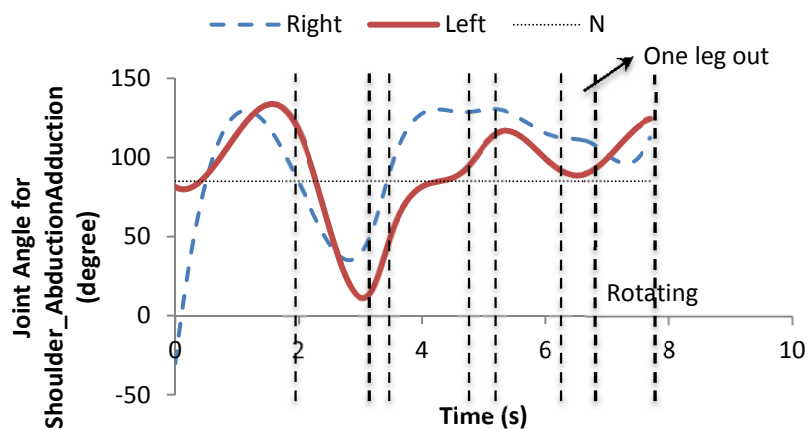
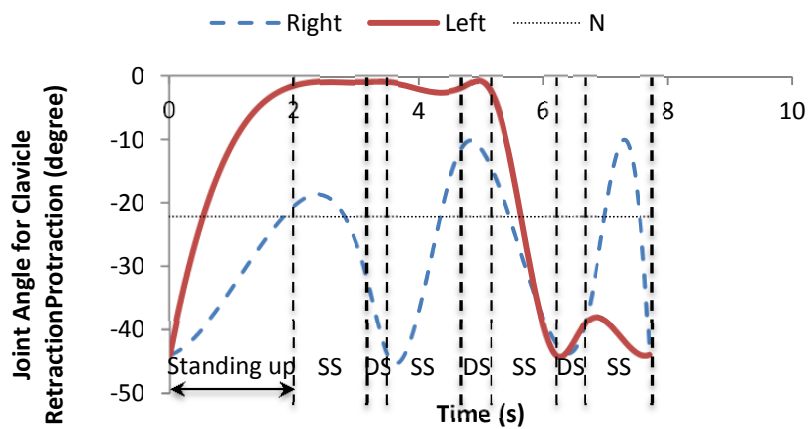
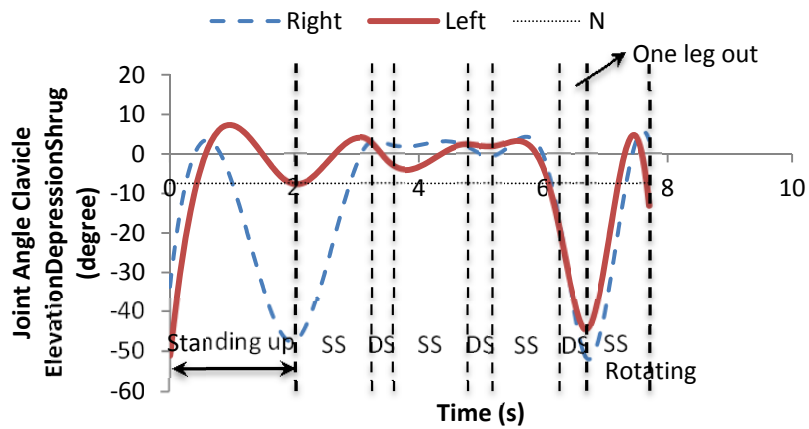


Figure 5.2 Joint angle profiles for egress motion

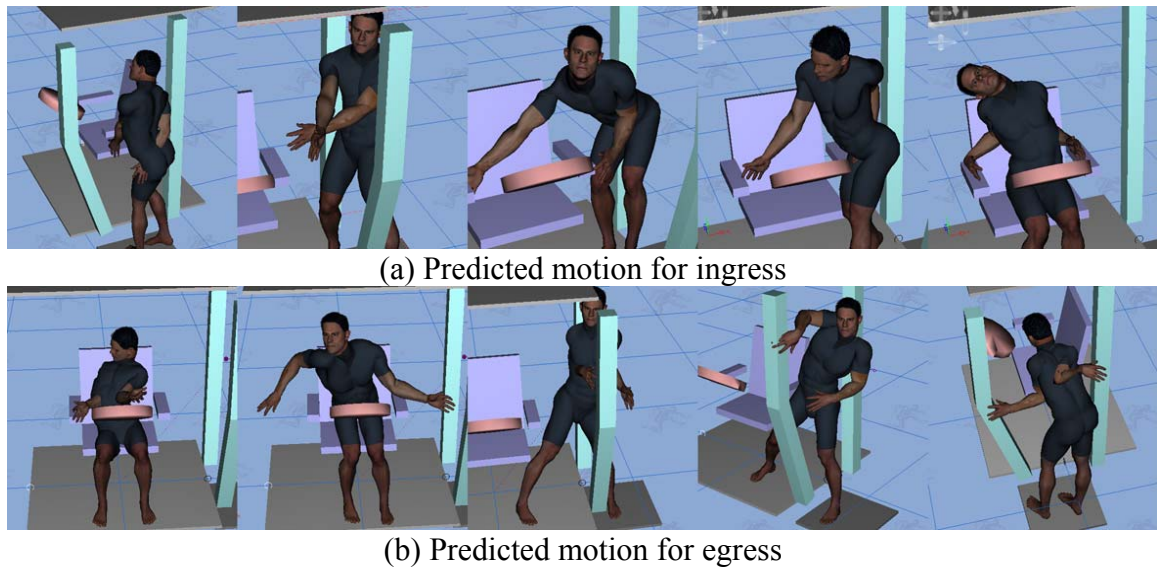


Figure 5.3 Predicted motion for ingress/egress

## 5.2 Discussion of Results

In Section 5.1, unnecessary motions at the spine, shoulder, and neck joints are observed for ingress (Figure 5.1), and excessive motion at the clavicle and shoulder joints for egress are observed in Figure 5.2. Unnecessary motion is observed for both ingress/egress motions, especially for the upper body. To avoid those unrealistic motions, three formulation strategies are discussed. Firstly, some artificial constraints can be added in the formulation. This can be done in two different ways. Either the existing constraints can be evaluated at more time instances or more constraints can be added. Secondly, the range of motion for certain joints that show excessive motion can be restricted. Thirdly, alternate performance measures that drive the motion can be considered. In the following sections, those options are discussed in more detail.



### 5.2.1 Addition of More Constraints

Since we use an optimization-based framework to predict/simulate the motions, one of the easiest ways to make a model behave as desired is by restricting the space of feasible solutions. Therefore, to obtain desired motions, some artificial constraints could be added in the formulation. This can be obtained in two different ways: (i) increasing the number of time instances where the constraints are evaluated, and (ii) introducing additional constraints on the joint angles to avoid unrealistic motions.

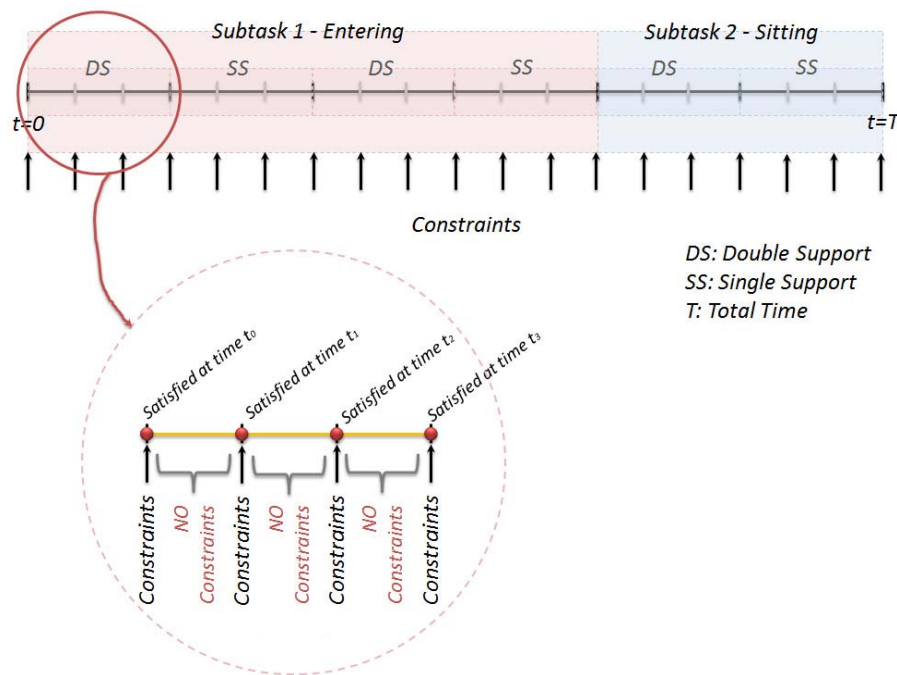


Figure 5.4 Time segmentation for ingress

As seen in Figure 5.4, the constraints and objective functions are evaluated at discrete instances of time  $t_0, t_1, \dots, T$ . Constraints are implemented at discrete time  $t_0, t_1, t_2, t_3, \dots, T$  (marked as a red dot), but not at the time on the orange line. The motion of the avatar between these instances of times is obtained by interpolating the values at these times. Therefore, even if the constraints are maintained at these time points, they

may be violated during the interpolated motion. In order to avoid this, the time between each evaluation can be reduced by adding more points where the constraint and objective functions are evaluated. However, this would increase the total number of constraints and thus the optimization problem size.

Another method is to add different types of artificial constraints to achieve desired behavior. While looking at the whole-body motion and comparing upper-body motion with lower-body motion, most of the unnecessary motion occurs in the upper body. Such a behavior may be caused due to larger feasible space created by a smaller number of constraints. The lower body has more constraints than the upper body, so that is controlled relatively easily. Implemented constraints are listed in Table 5.1. Therefore, if the upper body is constrained further, a better solution may be obtained. However, ingress and egress are very complex tasks. They need the virtual human model's interaction with obstacles over time. Therefore, this kind of constraint would limit the range of motion of various joints, resulting in the inability of the human to interact with the obstacles. Ingress has 2688 constraints and egress has 3605 constraints, compared to 1734 constraints in the regular walking task. If more constraints are added, this would make calculation time longer. It could also make it harder to find a feasible solution. In addition, the solution obtained by adding more artificial constraints may not be realistic and may severely restrict the ability to perform various what-if studies with different cab configurations. Therefore, this option of adding more constraints is not pursued any further.

Table 5.1 Applied constraints for upper and lower body

Constraints	Upper Body	Lower Body
Joint angle limits	o	o
Ground penetration	x	o
ZMP constraint	x	o
Contacting position	x	o
Hand position	o	x
Continuity conditions	o	o
Obstacle avoidance	o	o
Joint torque limits	o	o

where “o” means it is applied, “x” means it is not applied.

### 5.2.2 Task-Specific Joint Angle Limits

One way to reduce unnecessary motion while keeping the current formulation is to add task-specific joint angle limits. In the constraint set, there are joint angle limits. Those limits (called general limits) are read from a joint angle limit set. Instead of reading from general limits, they could be read from task-specific joint angle limits listed in Table 5.2. General joint angle limits represent the range that humans can actually generate. Task-specific joint limits have smaller ranges than general joint angle limits. By reducing these limits for some joints, unnecessary motion could be removed at certain joints. Most of the limits are reduced for the upper body; reduced limits are marked in bold type in Table 5.2. Therefore, adding task-specific joint limits is selected first, and new simulation results are generated that are presented later.

Table 5.2 Joint angle limits

Joint Names	Joint Angles	General Limits (degree)		Task Specific Limits (degree)	
		Lower Limits	Upper Limits	Lower Limits	Upper Limits
GlobalTranslation_Progress		-50.00(m)	50.00(m)	<b>-5.00(m)</b>	<b>5.00(m)</b>
GlobalTranslation_Transverse		-50.00(m)	50.00(m)	<b>-5.00(m)</b>	<b>5.00(m)</b>
GlobalTranslation_Pitch		-50.00(m)	50.00(m)	-50.00(m)	50.00(m)
GlobalRotation_Tilt		-180.00	180.00	<b>-10.00</b>	<b>10.00</b>
GlobalRotation_Bend		-180.00	180.00	-180.00	180.00
GlobalRotation_Rotate		-180.00	180.00	-180.00	180.00
SpineLow_LeftRightBend		-2.00	2.00	<b>-10.00</b>	<b>10.00</b>
SpineLow_ExtensionFlexion		-0.12	26.56	-0.12	26.56
SpineLow_RightLeftRotation		-1.50	1.50	-1.50	1.50
SpineMidLow_LeftRightBend		-9.00	9.00	<b>-1.00</b>	<b>1.00</b>
SpineMidLow_ExtensionFlexion		-6.00	30.02	-6.00	30.02
SpineMidLow_RightLeftRotation		-2.00	2.00	-2.00	2.00
SpineMidHigh_LeftRightBend		-4.50	4.50	<b>-1.00</b>	<b>1.00</b>
SpineMidHigh_ExtensionFlexion		-3.33	8.00	-3.33	8.00
SpineMidHigh_RightLeftRotation		-3.00	3.00	-3.00	3.00
SpineHigh_LeftRightBend		-18.01	18.01	<b>-1.00</b>	<b>1.00</b>
SpineHigh_ExtensionFlexion		-18.63	3.05	-18.63	3.05
SpineHigh_RightLeftRotation		-38.02	38.02	<b>-10.00</b>	<b>10.00</b>
RightClavicle_ElevationDepressionShrug		-51.77	3.26	<b>-10.00</b>	<b>-4.00</b>
RightClavicle_RetractionProtraction		-44.04	-0.91	<b>-23.00</b>	<b>-20.00</b>
RightShoulder_AbductionAdduction		-34.68	130.40	<b>70.00</b>	<b>90.00</b>
RightShoulder_ExtensionForwardFlexion		-48.45	143.55	<b>-5.00</b>	<b>90.00</b>
RightShoulder_InternalRotationExternalRotation		-157.55	2.53	<b>-127.00</b>	<b>-124.00</b>
RightElbow_FlexionExtension		-156.29	-10.90	-156.29	-10.90
RightElbow_PronationSupination		-77.01	85.79	<b>-15.38</b>	<b>-14.23</b>
RightWrist_RadialUlnarDeviation		-20.51	35.56	-20.51	35.56
RightWrist_ExtensionFlexion		-67.35	82.33	<b>-30.00</b>	<b>30.00</b>
LeftClavicle_ElevationDepressionShrug		-51.77	3.26	<b>-10.00</b>	<b>-4.00</b>
LeftClavicle_RetractionProtraction		-44.04	-0.91	<b>-23.00</b>	<b>-20.00</b>
LeftShoulder_AbductionAdduction		-34.68	129.90	<b>70.00</b>	<b>90.00</b>
LeftShoulder_ExtensionForwardFlexion		-48.40	138.69	<b>-5.00</b>	<b>90.00</b>
LeftShoulder_InternalRotationExternalRotation		-157.55	2.35	<b>-127.00</b>	<b>-124.00</b>
LeftElbow_FlexionExtension		-156.29	-15.90	-156.29	-15.90
LeftElbow_PronationSupination		-77.01	82.79	<b>-15.38</b>	<b>-14.23</b>
LeftWrist_RadialUlnarDeviation		-18.51	35.56	-18.51	35.56
LeftWrist_ExtensionFlexion		-67.35	80.85	<b>-30.00</b>	<b>30.00</b>

Table 5.2 continued

Joint Names	Joint Angles	General Limits (degree)		Task Specific Limits (degree)	
		Lower Limits	Upper Limits	Lower Limits	Upper Limits
LowerNeck_LeftRightBending		-22.11	23.59	<b>-15.00</b>	<b>15.00</b>
LowerNeck_ExtensionFlexion		-13.61	43.42	<b>-10.00</b>	<b>10.00</b>
LowerNeck_RightLeftRotation		-52.56	50.89	<b>-15.00</b>	<b>15.00</b>
UpperNeck_LeftRightBending		-20.09	17.75	<b>-10.00</b>	<b>10.00</b>
UpperNeck_ExtensionFlexion		-50.37	21.67	<b>-15.00</b>	<b>15.00</b>
RightHip_AbductionAdduction		-42.64	29.52	-42.64	29.52
RightHip_FlexionExtension		-123.40	8.75	-123.40	8.75
RightHip_ExternalRotationInternalRotation		-45.08	41.74	-45.08	41.74
RightKnee_HyperextensionFlexion		13.77	149.82	13.77	149.82
RightAnkle_DorsiPlantarFlexion		7.35	71.65	7.35	71.65
RightAnkle_EversionInversion		-18.34	35.85	-18.34	35.85
RightMidFootLateral_ExtensionFlexion		-65.63	-5.60	-65.63	-5.60
LeftHip_AbductionAdduction		-42.64	29.52	-42.64	29.52
LeftHip_FlexionExtension		-123.40	8.75	-123.40	8.75
LeftHip_ExternalRotationInternalRotation		-45.08	41.74	-45.08	41.74
LeftKnee_HyperextensionFlexion		13.77	149.82	13.77	149.82
LeftAnkle_DorsiPlantarFlexion		7.35	71.65	7.35	71.65
LeftAnkle_EversionInversion		-18.34	35.85	-18.34	35.85
LeftMidFootLateral_ExtensionFlexion		-65.63	-5.60	-65.63	-5.60

### 5.2.3 Different Objective Functions

Even though all the constraints are satisfied and give a feasible solution, it still shows uncomfortable motion. Between the time points where constraints are imposed, objective function governs the motion; however, the current objective function (dynamic effort) may not have enough control over the motion. Instead of using dynamic effort as an objective function, other objective functions need to be considered. This will be discussed in the next chapter.

### 5.3 Simulation Results with Task-Specific Joint Limits

Among the options in Section 5.2, option 5.2.2 is chosen to test first. With the given formulation in Chapter 4 using task-specific joint limits, a few joint angle profiles

are presented in Figure 5.5. Previously, in Section 5.1, excessive motion was observed at the right shoulder and lower neck joints for ingress. To impose reduced joint angle limits at certain joints, ranges of motion for the right shoulder (Extension/Flexion) and the lower neck (LeftRight\_Bending) have been reduced. These angles follow neutral angles and slightly change after 3 s when the sitting motion occurs within the range of task-specific joint angle limits. Even though the range for the Extension/Flexion spine joint remains the same, compared to Figures 5.1 and 5.5, motions are changed. This is because other spine joints having reduced range of motion affected this motion. The spine motion is stiff when entering (0 s to 3 s), in that spine motion has barely changed; the spine tends to bend for sitting after 3 s. Predicted motion with task-specific joint limits is shown in Figure 5.7a.

As before, a few joint angles are displayed in Figure 5.6. Compared to Figure 5.1, both clavicle motion and shoulder abduction/adduction motion are reduced as a result of using task-specific joint angle limits. Predicted motion with task-specific joint limits, as shown in Figure 5.7b, is a better motion than that in Figure 5.2b. However, from 0 s to 3.5 s when getting up from the seated position and moving to the next step, clavicle motion is very stiff. This motion is shown in the second frame of Figure 5.7b.

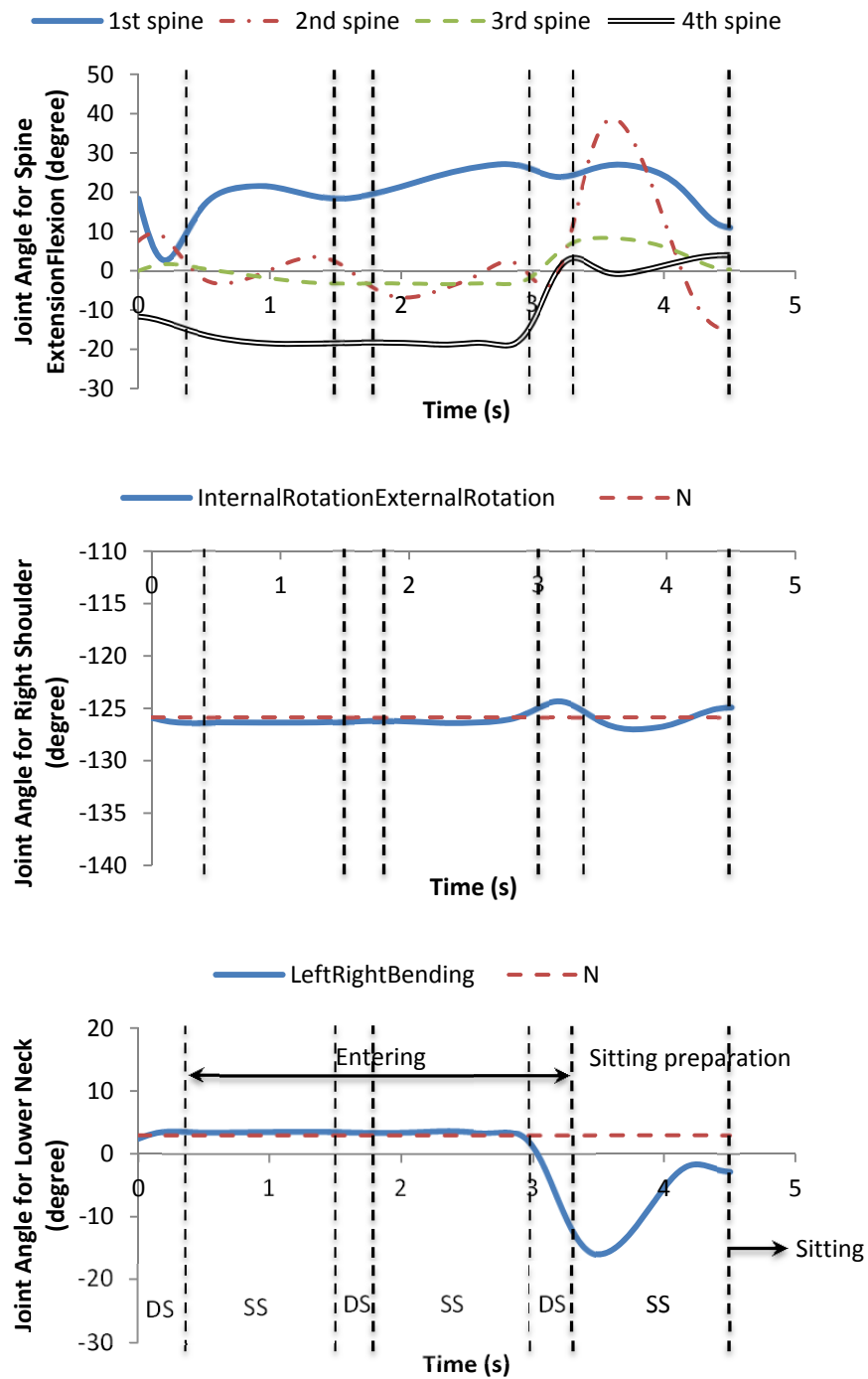


Figure 5.5 Joint angle profiles for ingress motion

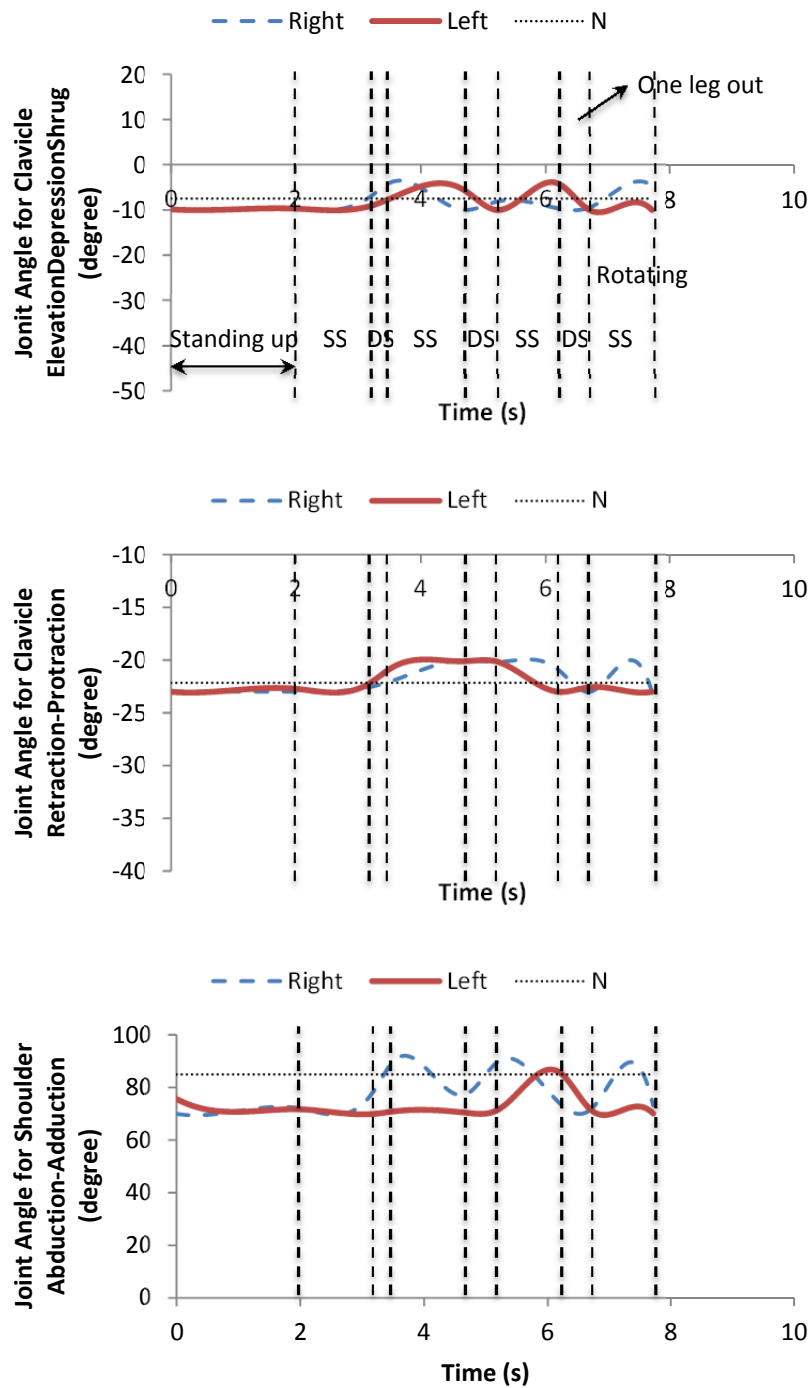
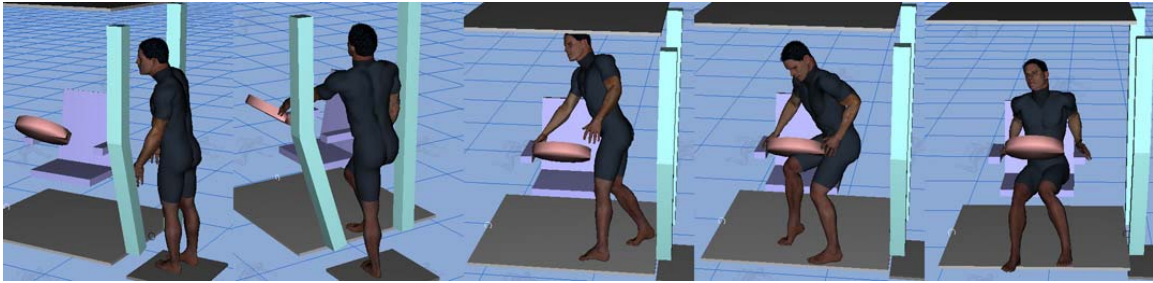
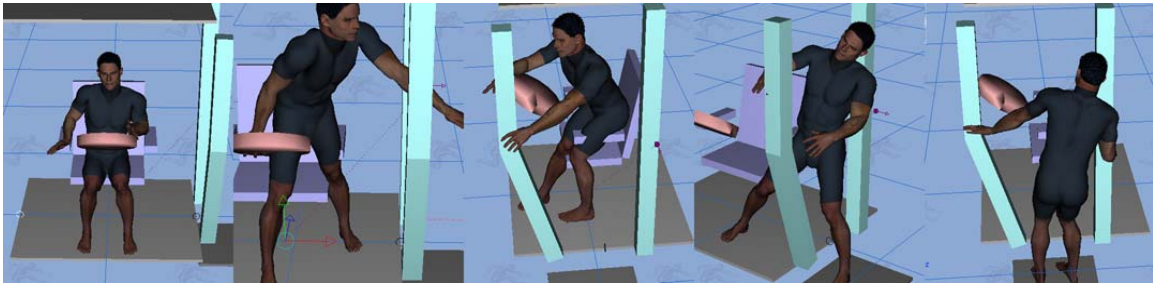


Figure 5.6 Joint angle profiles for egress motion





(a) Ingress with task-specific joint limits



(b) Egress with task-specific joint limits

Figure 5.7 Predicted motion with task-specific joint limits for ingress/egress

#### 5.4 Discussion of Results and Conclusions

By imposing reduced joint angle limits at a certain joint to avoid excessive motion, a better motion has been predicted than the motion with general limits. However, there are several problems to be discussed. First of all, the range of motion for 27 DOFs are reduced as listed in Table 5.2. These are called artificial constraints. This means that only 28 DOFs move in the range that humans can actually generate. Even though a 55-DOF digital human model is presented, only 28 DOFs act freely. Therefore, we cannot say we have used a 55-DOF model. Moreover, actual motion at the joint that had a reduced range of motion could not be observed properly.

Secondly, the task-specific joint limits can be applied for one specific cab model. Ingress/egress is a complex task compared to a simple task like walking. It interacts with obstacles and cab geometry. For the walking task, task-specific joint limits might work

with different avatars because motion does not change much and nothing interacts with walking. However, motion for ingress/egress varies a lot depending on geometries or obstacles or inputs. Hence, task-specific joint limits are appropriate for this kind of complex task. If geometries or inputs are changed, the solution would be infeasible with restricted limits. Eventually, we would not be able to obtain right motion. Therefore, using task-specific joint limits (option 5.2.2) should be excluded. In the next chapter, use of alternate objective functions (option 5.2.3) is explained.

## CHAPTER 6

### ALTERNATIVE OBJECTIVE FUNCTIONS

In the simulations of the previous chapter, uncomfortable motions were produced even though all the constraints were satisfied and the solutions were feasible. This means that the physics that is being modeled needs to be improved. Again, one of the ways to improve the physics is by adding constraints that correspond to some physics-based behavior. Another way could be to study why humans move in the particular way they do. In other words, we need to determine answers to the question “what drives their motion?” In this chapter, we try to answer that question by using various objective functions.

#### 6.1 Dynamic Effort

The term “dynamic effort” is inspired by a desire to model the energy consumption for a manipulator. Energy consumption varies greatly depending on the specific design of the system, as well as the types of actuators. It is difficult to get the exact formula for the energy consumption without details of the specific machine and its physical characteristics. For this reason, simplified forms of energy consumption generally are used as a performance measure in the optimization process. Usually, the energy consumption is modeled to be proportional to the actuator forces or torques. Hence, the first term of the objective function represents dynamic effort.

$$\int_{t=0}^T \boldsymbol{\tau}(\mathbf{q}, t)^T \boldsymbol{\tau}(\mathbf{q}, t) dt \quad (6.1)$$

where  $T$  is the total time for a task. The use of energy consumption as a cost function implies several important points. First of all, minimum energy consumption indicates minimum fuel usage. Secondly, for smooth movement of each joint, the second derivative of the joint variables in the energy cost function naturally ensures the smooth

movement of each joint without unnecessary fluctuation in the joint angle profiles. However, dynamic effort does not control the ingress/egress motion effectively, as seen in Chapter 5. The torque profiles are calculated from joint profiles using the recursive Lagrangian dynamics equations. Therefore, we need a more direct way to control the motion.

### 6.2 Joint Discomfort

The joint comfort objective function represents joint displacement and deviation from the neutral position at each joint. The neutral position is selected as a relatively comfortable posture, typically a standing position with arms at one's side. In equation (6.2),  $\mathbf{q}_N$  is the neutral position of a joint, which represents overall posture. The summation of these values is called a discomfort function and is given as follows:

$$\int_{t=0}^T (\mathbf{q}(t) - \mathbf{q}_N)^T (\mathbf{q}(t) - \mathbf{q}_N) dt \quad (6.2)$$

This objective function is to force joint angles to move in a comfortable way to reduce joint discomfort.

### 6.3 Multi-Objective Function Formulation

It is useful with multi-objective optimization (MOO) to transform the objective functions such that they all have similar units and orders of magnitude. Summation of the dynamic effort (the integral of the squares of all joint torques) and the joint discomfort (the integral of the squares of all joint discomforts) is used as the objective function and is defined as:

$$\text{Minimize } F = c_{de} f_{de}^{norm}(\mathbf{q}) + c_{jd} f_{jd}^{norm}(\mathbf{q}) \quad (6.3)$$

where  $f_{de}^{norm}(\mathbf{q})$  is normalized dynamic effort, and  $f_{jd}^{norm}(\mathbf{q})$  is normalized joint discomfort.

The two objective functions are summed with the weighting coefficients  $c_{de}$  and  $c_{jd}$ . Using different values for weighting coefficients, different objective functions can be generated. For instance, when  $c_{de} = 0$  and  $c_{jd} = 1$ , it means that only joint discomfort is used as an objective function. On the other hand, when  $c_{de} = 1$  and  $c_{jd} = 0$ , dynamic effort is the objective function.

As suggested by Marler (2005), normalizing objective functions is advantageous with a MOO problem. Consequently, the two objective functions are normalized using the following approach:

$$f^{norm} = \frac{f(\mathbf{x}) - f_{min}}{f_{max} - f_{min}} \quad (6.4)$$

where  $f_{max}$  is a maximum and  $f_{min}$  is a minimum value for the objective function  $f(\mathbf{x})$ . Often, weights are used to indicate the relative significance of the different objectives and thus provide a single solution that incorporates the designer's preferences. Hence, each objective function is presented in normalized forms as in equations (6.5) and (6.6):

$$f_{de}^{norm}(\mathbf{q}) = \sum_{i=1}^{ndof} \int_{t=0}^T \left( w_i^{de} \frac{\tau_i(\mathbf{q}, t)}{\tau_i^{up} - \tau_i^{low}} \right)^2 dt \quad (6.5)$$

$$f_{jd}^{norm}(\mathbf{q}) = \sum_{i=1}^{ndof} \int_{t=0}^T \left( w_i^{jd} \frac{q_i(t) - q_i^N(t)}{q_i^{up} - q_i^{low}} \right)^2 dt \quad (6.6)$$

where  $\tau^{up}$  is a maximum and  $\tau^{low}$  a minimum torque value, and  $q^{up}$  is a maximum and  $q^{low}$  a minimum angle value for each joint.  $w^{de}$  and  $w^{jd}$  are weights for each joint that can be manipulated. Since some joints' articulation is more important than others', weights  $w^{de}$  and  $w^{jd}$  are introduced to stress the relative stiffness of a joint.

#### 6.4 Test Results with Different Objective Functions

To test with different objective functions, a relatively simple task such as backward walking is used. Backward walking itself does not interact with geometries, so it has fewer constraints than ingress/egress motion.

### 6.4.1 Backward Walking Problem Definition

The backward walking problem uses a 55-DOF three-dimensional digital human skeletal model identical to the one in Section 4.1. A backward walking step is defined as two phases: the single support (SS) phase and the double support (DS) phase. The double support phase is when both feet contact the ground, and the single support phase is when one foot contacts the ground while the other leg is swinging. In this study, the gait cycle starts with the right foot leading (backward) and striking the ground.

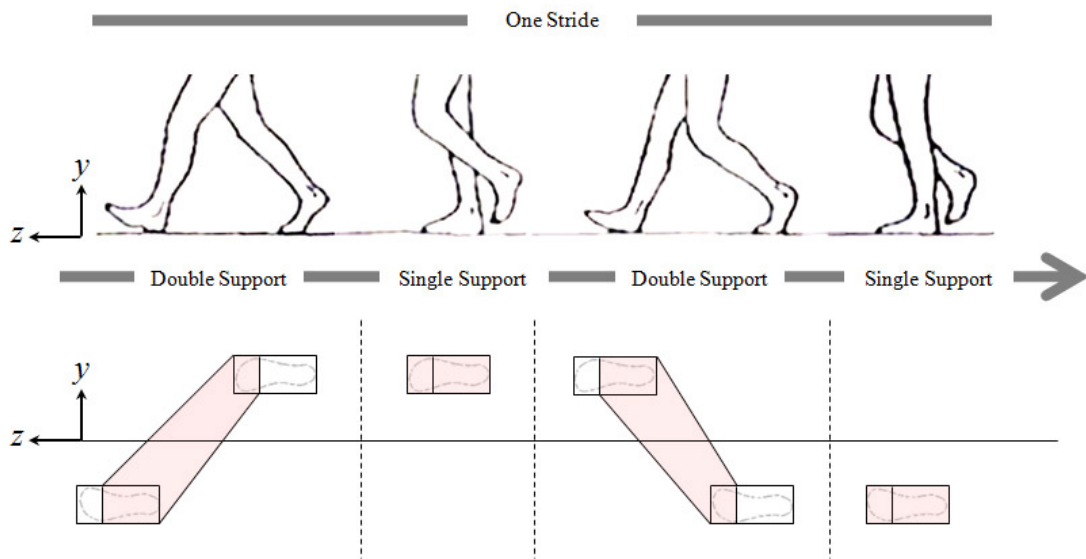


Figure 6.1 Basic foot supporting modes and polygon for backward walking

The design variables are the joint profiles  $q_i(t)$  for a symmetric and cyclic gait motion. Besides the joint profiles, the initial posture is also optimized rather than specifying it from the experiment. The final posture should satisfy the symmetry condition with the initial posture so that continuous joint profiles are generated. Meanwhile, the torque profiles are calculated from joint profiles using recursive Lagrangian dynamics equations. The constraints include joint angle limits, ground

penetration, foot-contacting positions, ZMP location, knee flexion at mid-swing, symmetry conditions, arm-leg coupling, and self-collision avoidance.

#### 6.4.2 Simulation Result with Different Objective Functions

To solve for a backward walking simulation, the inputs used are step size 0.55 m, velocity -0.75 m/s, and double support duration time ratio 0.115. Three different simulation results are presented and compared: (i) results with the dynamic effort as an objective function, (ii) results without task-specific joint angle limits, and (iii) results by imposing joint discomfort as an objective function without task-specific joint limits.

The three resultant cases of predicted motion for backward walking are shown in Figure 6.2. Figure 6.2(a) shows the motion using dynamic effort as an objective function. As discussed in Section 5.2.1, fewer constraints are applied to the upper body than the lower body; as a result, a lot of unnecessary and excessive upper-body motion is observed. The constraints applied for backward walking are listed in Table 6.1. Applied neutral angles are the standing postures listed in Table 6.2. The neutral position is selected as a relatively comfortable posture, typically a standing position with arms at one's side. Motion for walking backward is close to the standing posture.

Table 6.1 Applied constraints for backward walking

Constraints	Upper Body	Lower Body
Joint angle limits	o	o
Ground penetration	x	o
ZMP constraint	x	o
Contacting position	x	o
Knee flexion at mid-swing	x	o
Symmetry condition	o	o
Arm-leg coupling	o	o
Self-collision avoidance	o	o
Joint torque limits	o	o

where “o” means it is applied, “x” means it is not applied.

Table 6.2 Neutral angle - standing

Joint Name	Joint Angle (degree)	Standing
GlobalTranslation_Progress	0	
GlobalTranslation_Transverse	0	
GlobalTranslation_Pitch	0	
GlobalRotation_Tilt	0	
GlobalRotation_Bend	0	
GlobalRotation_Rotate	0	
SpineLow_LeftRightBend	0	
SpineLow_ExtensionFlexion	0	
SpineLow_RightLeftRotation	0	
SpineMidLow_LeftRightBend	0	
SpineMidLow_ExtensionFlexion	0	
SpineMidLow_RightLeftRotation	0	
SpineMidHigh_LeftRightBend	0	
SpineMidHigh_ExtensionFlexion	0	
SpineMidHigh_RightLeftRotation	0	
SpineHigh_LeftRightBend	0	
SpineHigh_ExtensionFlexion	0	
SpineHigh_RightLeftRotation	0	
RightClavicle_ElevationDepressionShrug	-7.5	
RightClavicle_RetractionProtraction	-22.2	
RightShoulder_AbductionAdduction	85	
RightShoulder_ExtensionForwardFlexion	-4.8	
RightShoulder_InternalRotationExternalRotation	-125.9	
RightElbow_FlexionExtension	-34.4	
RightElbow_PronationSupination	-14.8	
RightWrist_RadialUlnarDeviation	1.6	
RightWrist_ExtensionFlexion	17.6	
LeftClavicle_ElevationDepressionShrug	-7.5	
LeftClavicle_RetractionProtraction	-22.2	
LeftShoulder_AbductionAdduction	85	
LeftShoulder_ExtensionForwardFlexion	-4.8	
LeftShoulder_InternalRotationExternalRotation	-125.9	
LeftElbow_FlexionExtension	-34.4	
LeftElbow_PronationSupination	-14.8	
LeftWrist_RadialUlnarDeviation	1.6	
LeftWrist_ExtensionFlexion	17.6	





Table 6.2 continued


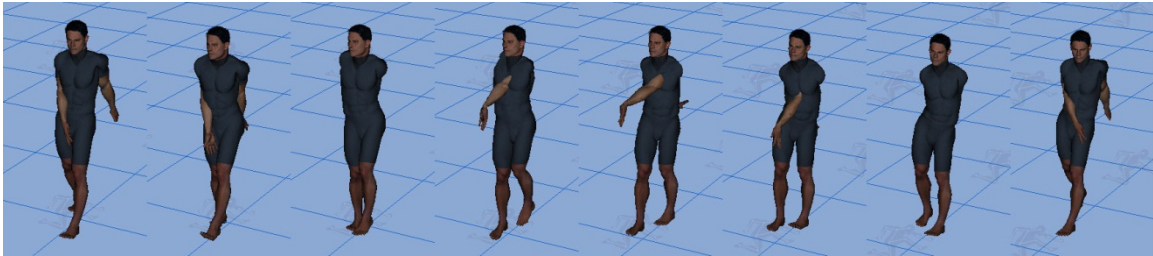
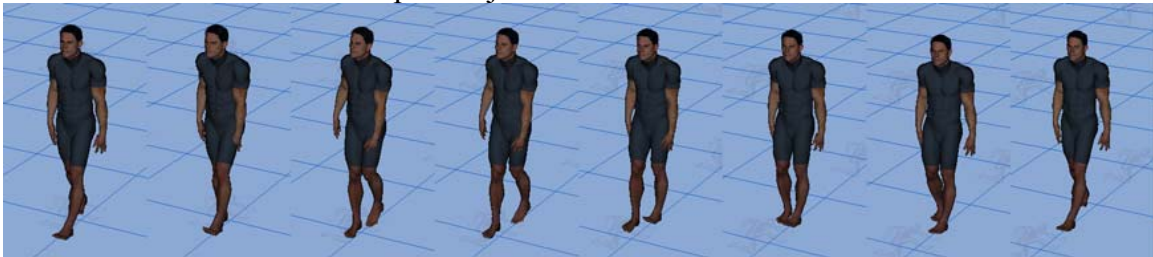
Joint Name	Joint Angle (degree)	Standing
LowerNeck_LeftRightBending	3	
LowerNeck_ExtensionFlexion	19.1	
LowerNeck_RightLeftRotation	2.6	
UpperNeck_LeftRightBending	-4.7	
UpperNeck_ExtensionFlexion	-35	
RightHip_AbductionAdduction	0	
RightHip_FlexionExtension	0	
RightHip_ExternalRotationInternalRotation	0	
RightKnee_HyperextensionFlexion	16	
RightAnkle_DorsiPlantarFlexion	17.5	
RightAnkle_EversionInversion	0	
RightMidFootLateral_ExtensionFlexion	-25	
LeftHip_AbductionAdduction	0	
LeftHip_FlexionExtension	0	
LeftHip_ExternalRotationInternalRotation	0	
LeftKnee_HyperextensionFlexion	16	
LeftAnkle_DorsiPlantarFlexion	17.5	
LeftAnkle_EversionInversion	0	
LeftMidFootLateral_ExtensionFlexion	-25	

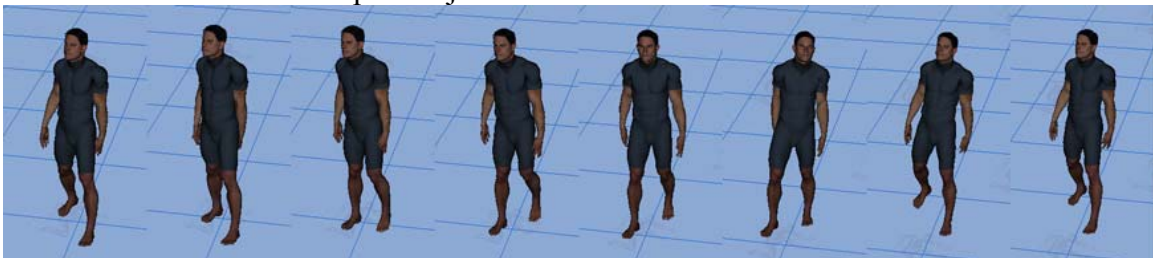
Figure 6.2b shows improved results from the previous case (Figure 6.2a) after adding task-specific joint limits (TSJ). The restricted limits for walking backward are mostly applied to the upper body. Therefore, only 14 DOFs are fully considered for the problem. Figure 6.2c represents the motion using joint discomfort as an objective function. Although Figure 6.2c does not use task-specific joint limits, by minimizing the joint angle difference between the current angle and the neutral angle, unnecessary upper-body motion is reduced. However, since motion tends to follow the neutral angles, the resulting simulation gives a very stiff motion of Santos.



(a) Predicted motion for backward walking using dynamic effort as an objective function without task-specific joint limits



(b) Predicted motion for backward walking using dynamic effort as an objective function with task-specific joint limits



(c) Predicted motion for backward walking using joint discomfort as an objective function without task-specific joint limits

Figure 6.2 Predicted motion for backward walking with different objective functions

A sample of joint angles and torques for the right shoulder, right knee, right clavicle, right hip, and 4<sup>th</sup> spine, which generated uncomfortable motion, are presented and compared in Figure 6.3 and Figure 6.4. For the joint angle in Figure 6.3, simulation results using joint discomfort and dynamic effort (with TSJ) as objective functions follow a similar trend only for the upper body. For the lower body, all three cases follow a similar trend. Again, since the lower body is constrained more than the upper body, it is well-controlled regardless of any objective function. For the upper body, the result using

dynamic effort shows a lot of movement compared to other cases. This is why excessive motion is observed in Figure 6.2a.

Figure 6.3 presents torques for the set of joints in Figure 6.2. In most cases, results using dynamic effort as an objective function generate less torque due to the characteristics of the objective function, which minimizes summation of the joint torques. However, the result using joint discomfort as an objective function generates more torques at the start of the motion.

In conclusion, neither using dynamic effort nor using joint discomfort alone, without task-specific joint limits, produces a natural walking motion. Using dynamic effort alone generates less torque but also creates unnecessary motion. On the other hand, using joint discomfort alone generates a more natural motion but also generates more torques. Therefore, using two objective functions simultaneously—a multi-objective function—is suggested.

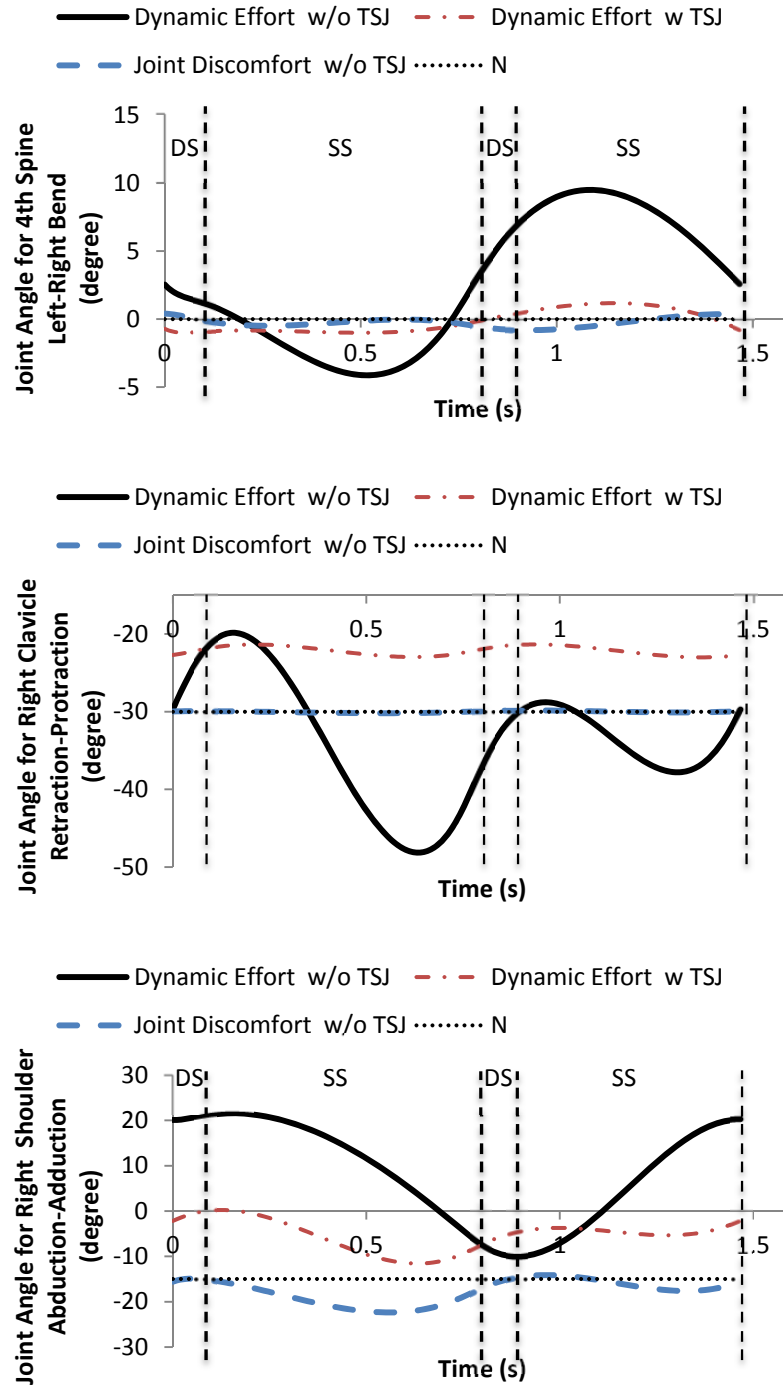


Figure 6.3 Joint angles with different objective functions

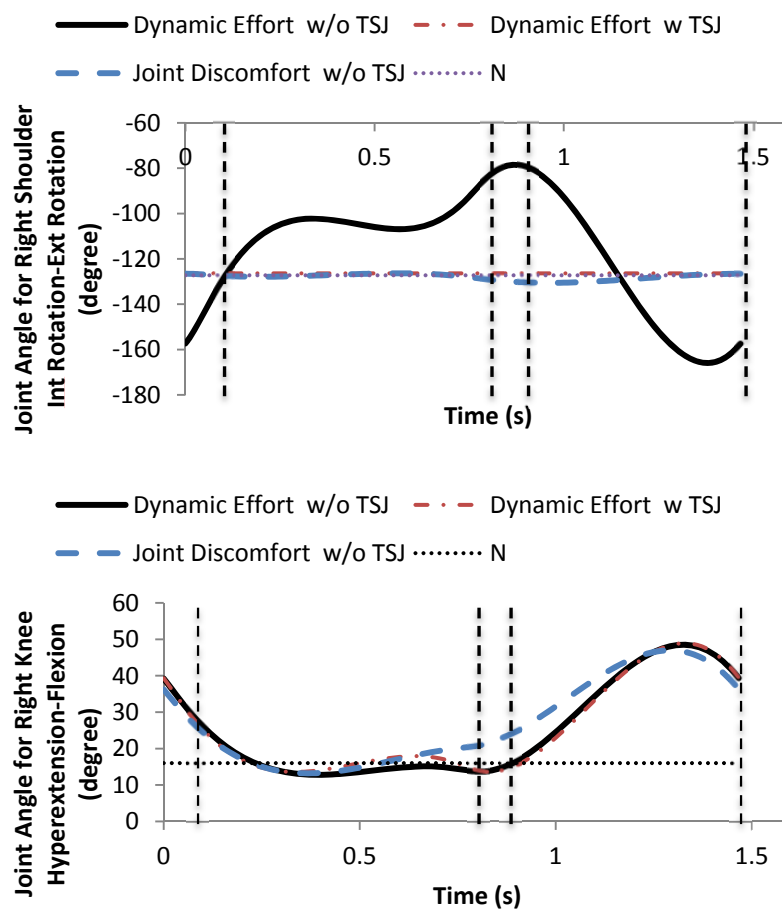


Figure 6.3 continued

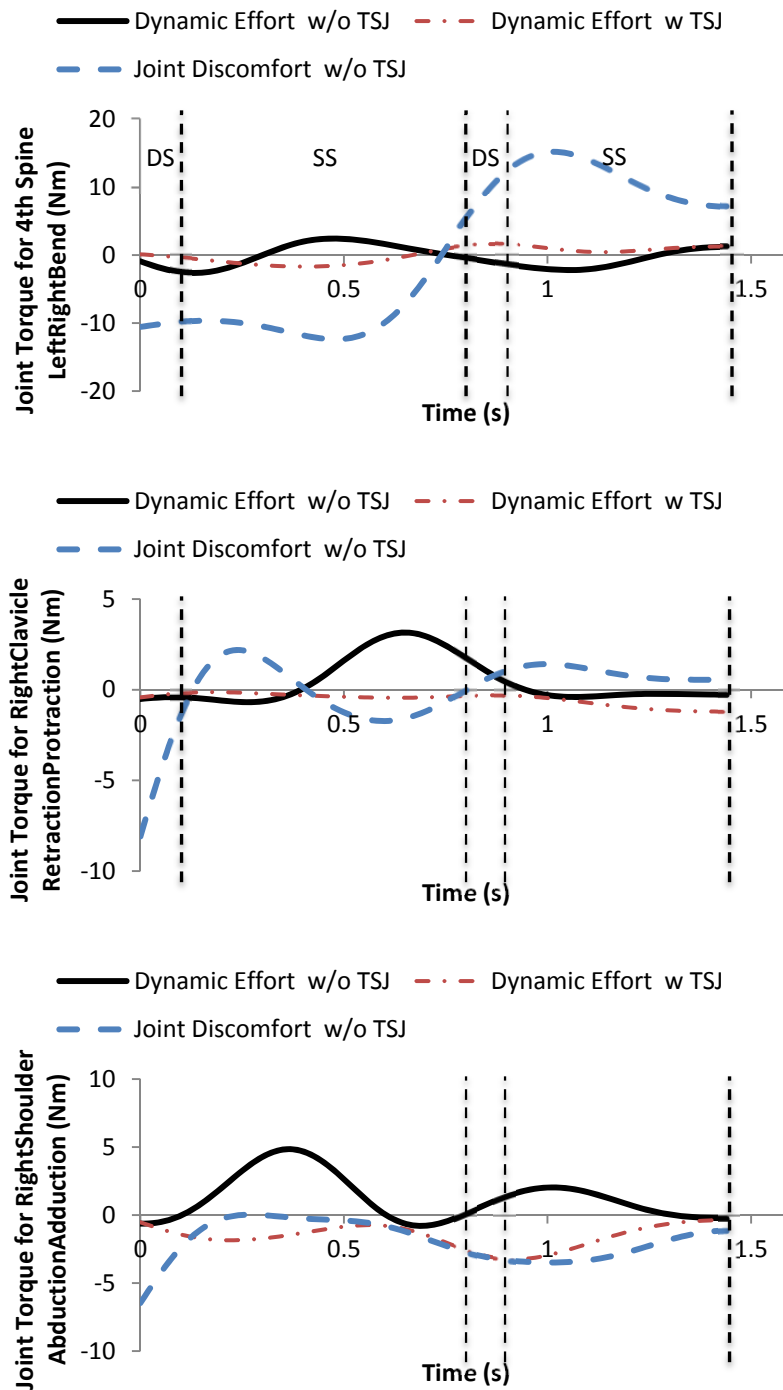


Figure 6.4 Joint torques with different objective functions

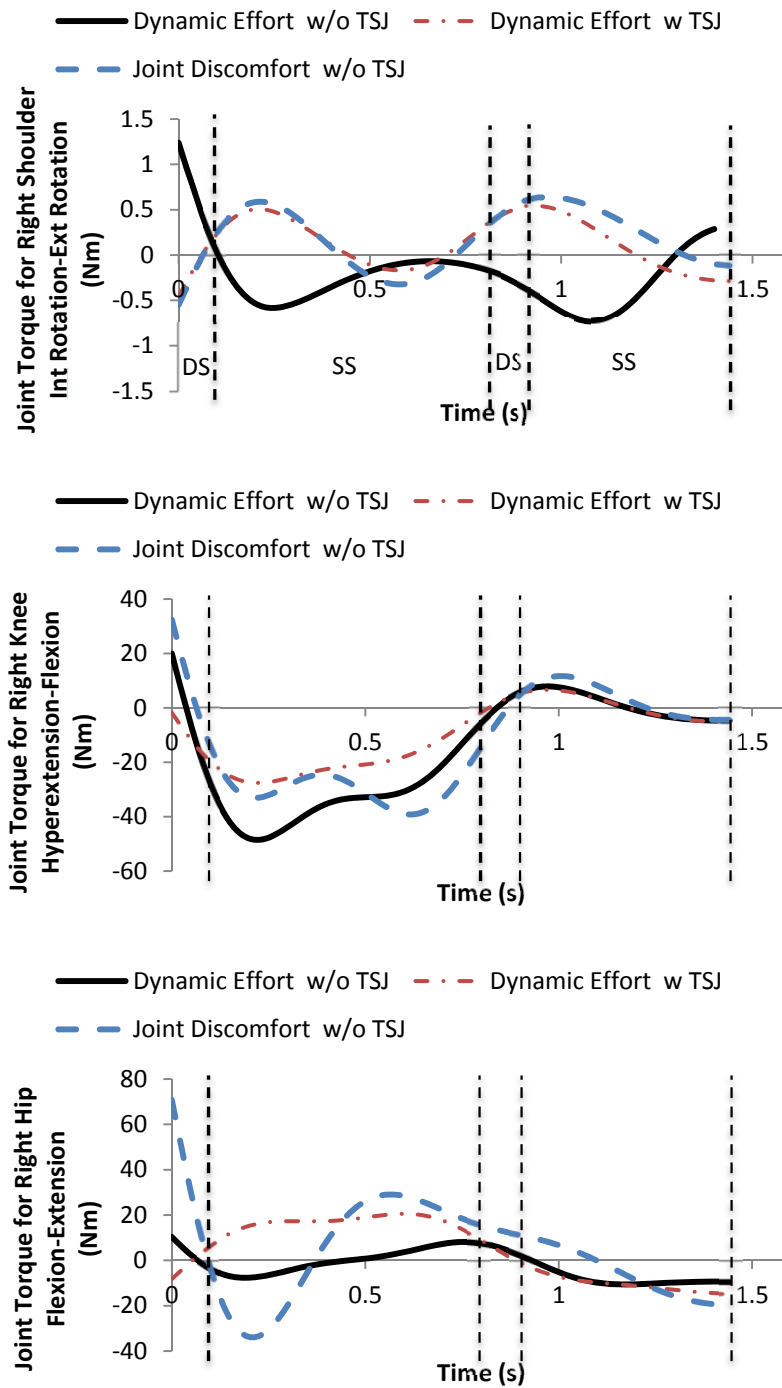


Figure 6.4 continued

### 6.4.3 Objective Function Weighting Coefficients:

#### Case Studies

In the previous section, a multi-objective function is suggested; however, which objective function governs motion has to be studied using the weighting coefficients for the objective functions. Weighting coefficients are sorted in five different cases listed in Table 6.3.

Table 6.3 Cases for objective function weighting coefficient

	$c_{de}$	$c_{jd}$
Case1	0.0	1.0
Case2	0.3	0.7
Case3	0.5	0.5
Case4	0.7	0.3
Case5	1.0	0.0

( $c_{de}$  : coefficient for dynamic effort,  $c_{jd}$  : coefficient for joint discomfort)

Joint angles and torques for the different cases are presented at the same set of joints in Figure 6.5 and Figure 6.6 to investigate which objective function controls the motion. Using dynamic effort as an objective function with task-specific joint limits is also investigated at the same time since it showed natural motion in Figure 6.1(b). Therefore, without task-specific joint limits, we expect the motion to follow the same trend as dynamic effort as an objective function with TSJ (the red blank line) while generating little torque.



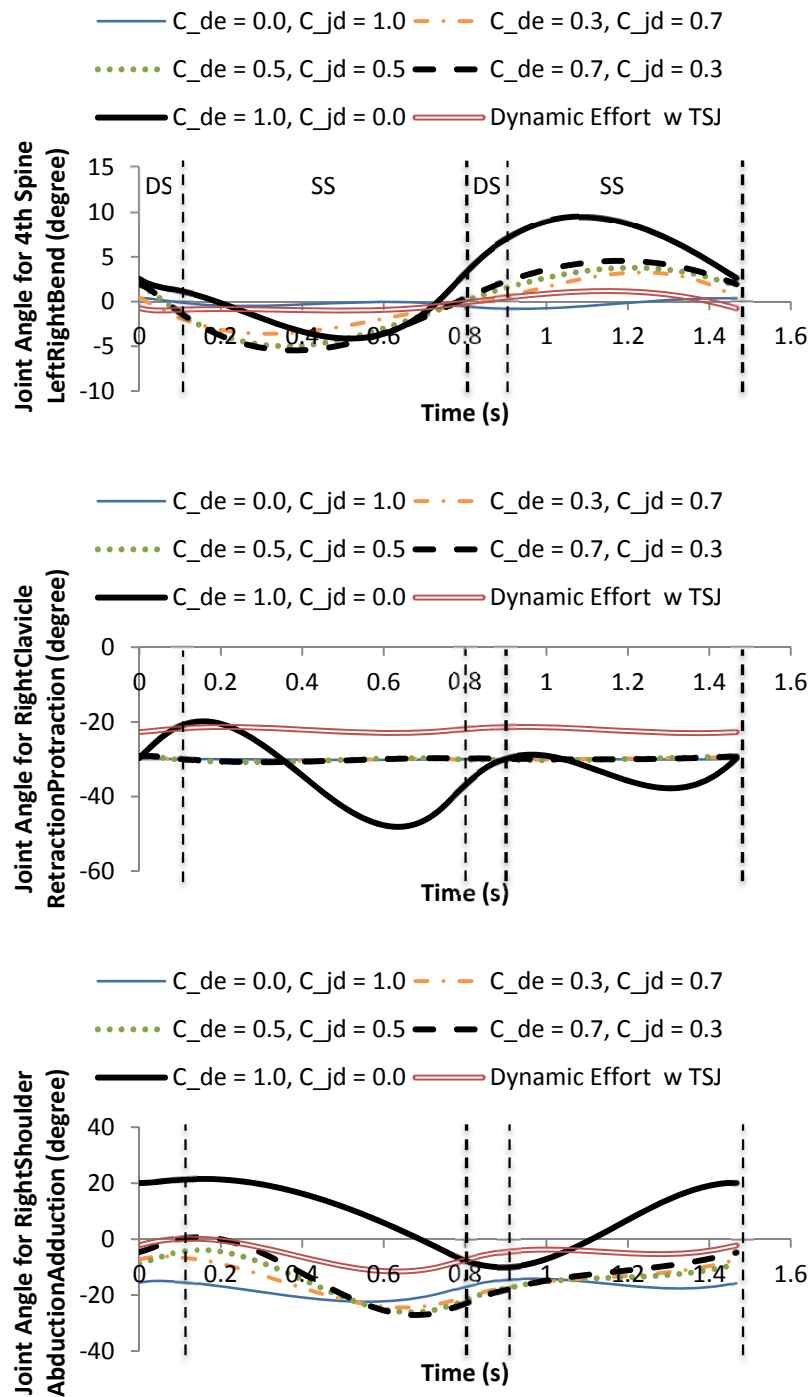


Figure 6.5 Joint angles with different weighting coefficients

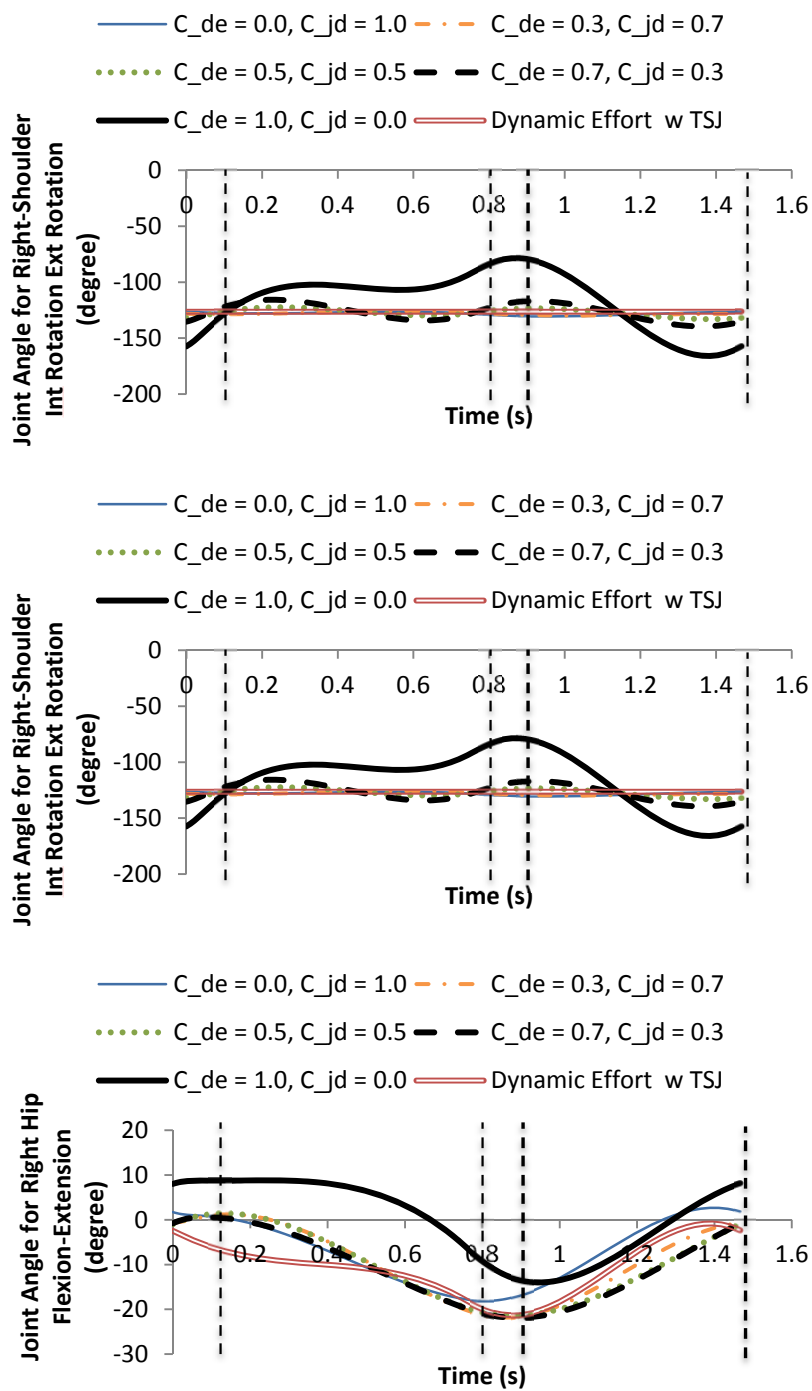


Figure 6.5 continued

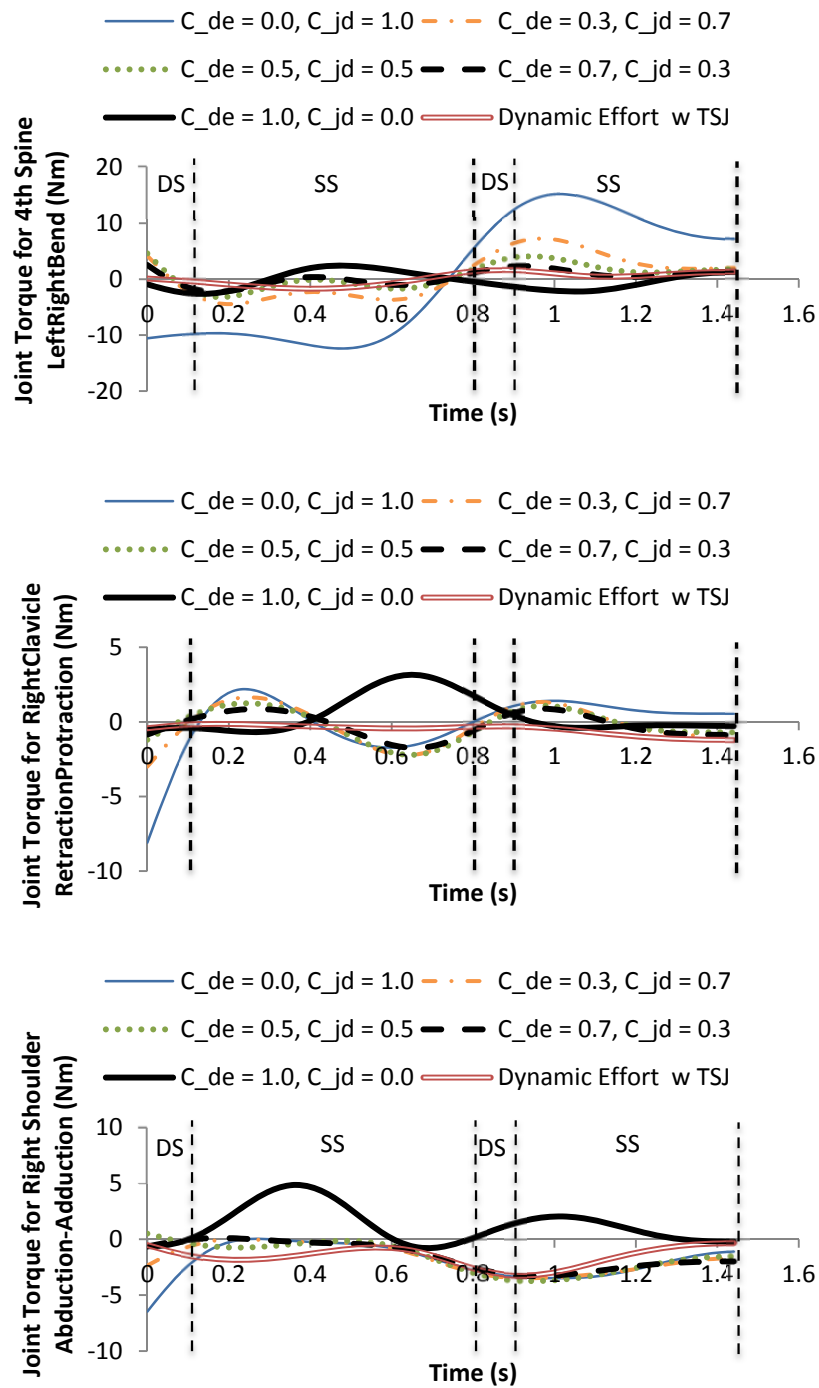


Figure 6.6 Joint torques with different weighting coefficients

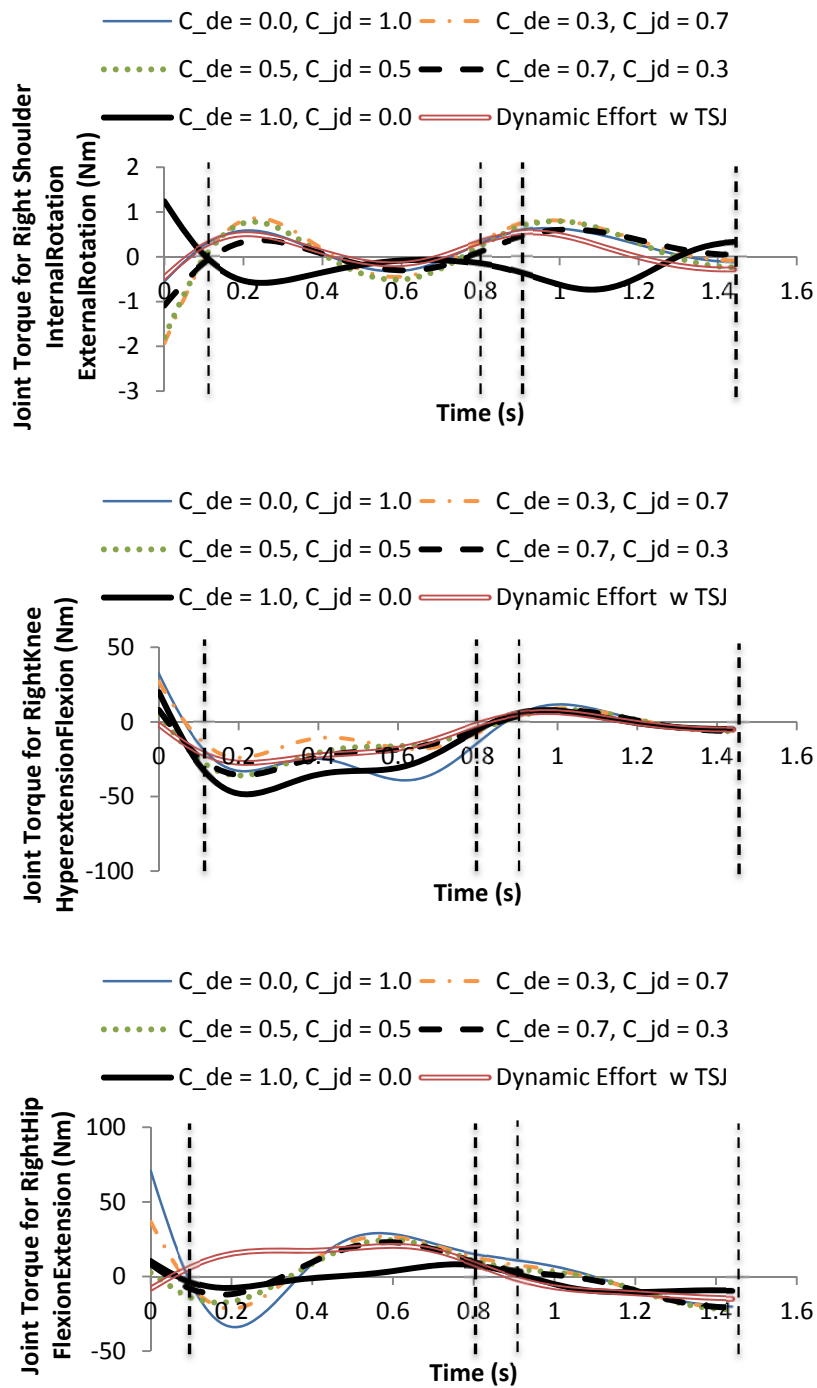


Figure 6.6 continued

For the joint angles in Figure 6.5, most of the cases show similar trends, except the case using a single objective function (dynamic effort without TSJ, the black thick solid line). However, the joint torque profiles in Figure 6.6 (the black dotted line that has  $c_{de} = 0.7, c_{jd} = 0.3$ ) generates less torque than the other cases.

In order to further investigate the effect of the weighting coefficient combination, objective function values are plotted for each combination in Figure 6.7. Each set of graphs plots the multi-objective (MO) function value with the given set of the weighting coefficient. In addition, to observe the effects of individual objective function values, two more function values, joint discomfort (JD) and dynamic effort (DE), are also plotted on the same graph. Therefore, the three different curves correspond to the values for MO, JD, and DE in each graph. First of all, the set of  $c_{de} = 0, c_{jd} = 1$  is observed. Because of the dynamic effort coefficient,  $c_{de} = 0$ , the MO function value follows the JD objective function value. However, the DE value is still high, and the motion looks very stiff, as shown in Figure 6.2c. Therefore,  $c_{de} = 0, c_{jd} = 1$  is not a good combination. Next, for  $c_{de} = 1, c_{jd} = 0$ , the JD objective function values are significantly higher than the DE values. In this case, the motion looks too flexible, as shown in Figure 6.2a. When either coefficient is zero, the motion gives extreme results: it is either rigid or too flexible. For the case when  $c_{de} = 0.3, c_{jd} = 0.7$ ,  $c_{de} = 0.5, c_{jd} = 0.5$  and  $c_{de} = 0.7, c_{jd} = 0.3$ , the objective function values are smaller than in the previous cases. In order to find the best combination, motion is analyzed visually. We determined that when the JD objective function is larger, the motion looks flexible. Conversely, when the JD value is smaller, the motion looks stiffer (and follows the neutral position closely).

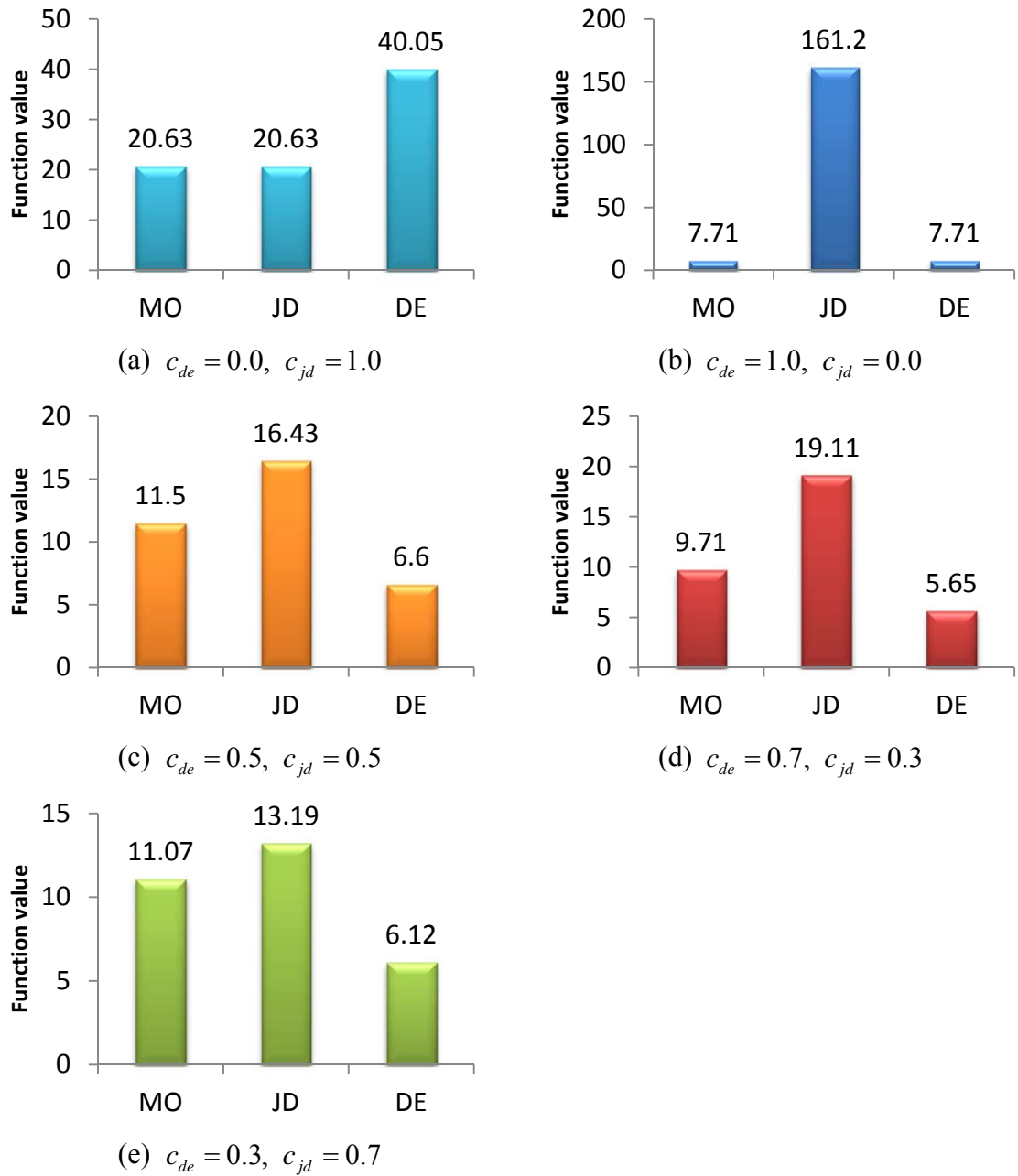


Figure 6.7 Objective function values with different weighting coefficients

Therefore, when  $c_{de}$  gets larger, the motion becomes smoother, but it is not good enough to be classified as a natural motion until  $c_{de} = 0.7, c_{jd} = 0.3$ . In the simulation, this

combination generated the most natural motion so far. Therefore, the set of  $c_{de} = 0.7$ ,  $c_{jd} = 0.3$  is the best combination of weighing coefficients.

Once again, to prove that the quality of a selected weighting coefficient is useful, a Pareto optimal curve is generated in Figure 6.8. The set of ( $c_{de} = 0.7$ ,  $c_{jd} = 0.3$ ) is located in the area that minimizes both DE and JD.

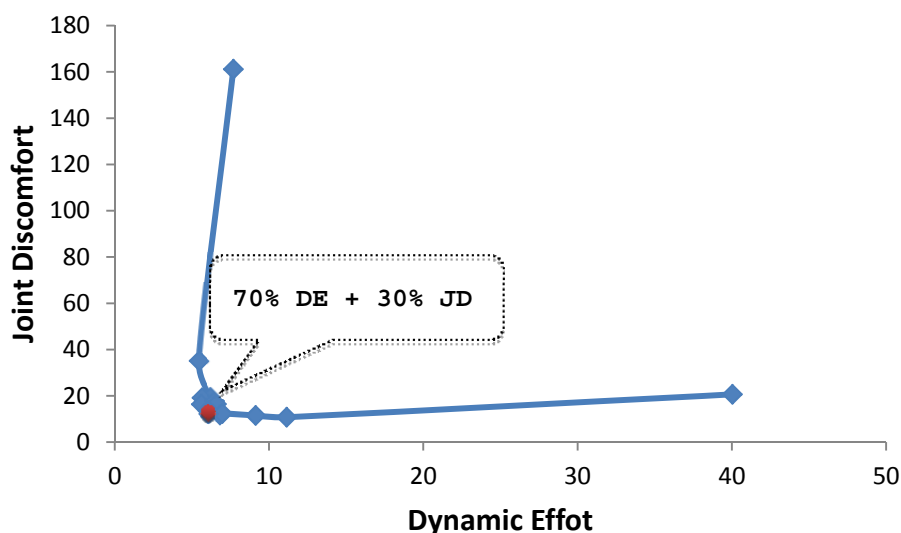


Figure 6.8 Pareto optimum curve

In Figure 6.7, we learned that the single objective function - either DE or JD - does not govern the human motion. Moreover, in order to prove that the typical predictive dynamics approach - using DE as an objective function with task-specific joint limits - is not always the most appropriate, Figure 6.9 is presented. This graph includes two blocks, which are the DE values in the MO with the best combination of weighting coefficients, and the DE values in a single objective (SO) function using DE as an objective function with task-specific joint limits (TSJ). The simulation results show similar natural motion. However, the MO values with  $c_{de} = 0.7$ ,  $c_{jd} = 0.3$  are smaller than the SO function with TSJ. Compared to the DE values, the MO values are also smaller than the SO values (SO

itself is DE). Therefore, an MO function with  $c_{de} = 0.7$ ,  $c_{jd} = 0.3$  generates natural motion using less effort than using an SO function with TSJ. Moreover, using this combination of MO functions, artificial constraints such as TSJ can be eliminated. Thus, the full range of motion for all 55 DOFs can be considered.

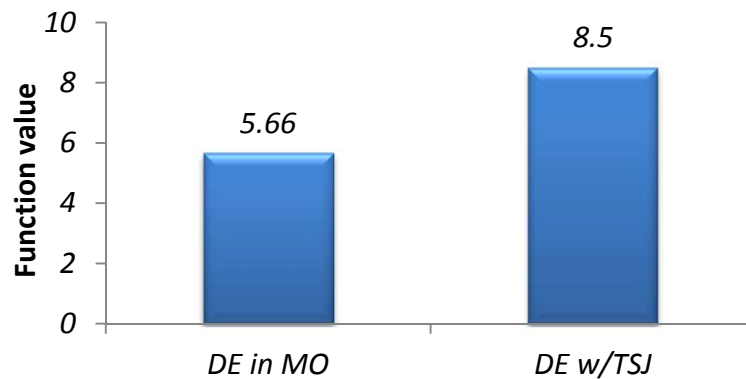


Figure 6.9 Objective function values with different weighting coefficients

### 6.5 Conclusion

In this chapter, two different objective functions were introduced. A multi-objective function with  $c_{de} = 0.7$ ,  $c_{jd} = 0.3$  generates natural motion using less effort than using a single objective function with task-specific joint limits. Moreover, using this combination of multi-objective functions, artificial constraints such as task-specific joint limits can be eliminated. Thus, the full range of motion for all 55 DOFs can be considered. To prove that the quality of a selected weighting coefficient is useful, a Pareto optimal curve is generated in Figure 6.8. This also shows that the set ( $c_{de} = 0.7$ ,  $c_{jd} = 0.3$ ) is the best combination, giving smaller values for both dynamic effort and joint discomfort. Since the function of the brain to control the movement is so complicated, it is difficult to understand how the brain governs different motions and decides on the final



motion from infinite possible solutions. However, based on earlier studies (Marler *et al.*, 2005) the motion may not be governed by one objective. By comparing different weighing coefficients, we proved that the human tries to move by minimizing both effort and discomfort.

## CHAPTER 7

### METRICS FOR CAB DESIGN EVALUATION

Designers always strive to develop new designs that are better than an existing design. This is a challenging and time-consuming activity for designers. Usually, the decision of whether one design is better than another is made by setting up different design metrics and comparing them for the two designs. Therefore, we need to be able to provide accurate information about these design metrics to designers to help them make decisions and plan further design changes. Design metrics are, thus, necessary to identify what factors are important for the design; they are a crucial source of information for decision-making. A few key metrics must be selected. The choice of key design metrics should be based on the quality drivers. This choice will vary by designers' purposes, as there is no single right answer independent of context. However, it is not easy to define useful metrics with which design quality can be measured.

Metrics are a well-known concept in the software engineering field. IEEE Standard 1061 (IEEE, 1998) lays out a methodology for developing metrics for software quality attributes. The standard defines an *attribute* as "a measurable physical or abstract property of an entity." A metric is a measurement function, and a software quality metric is "a function whose inputs are software data and whose output is a single numerical value that can be interpreted as the degree to which software possesses a given attribute that affects its quality." To develop a set of metrics for cab design, we borrowed this concept and then created a list of quality factors that are important for it. A *quality factor* is a type of attribute, "a management-oriented attribute of design that contributes to its quality."

- What attribute are we trying to measure?
- What is the relationship of the attribute to the metric value?

- If we change circumstances or behavior in order to improve the measured results, what impact are we going to have on the attribute?

Based on the quality factors, design metrics to evaluate a heavy equipment cab design are created as listed in Table 7.1. A detailed explanation of the metrics will be given in the following sections.

Table 7.1 Metrics for the cab design

Attribute	Selected Metric
Propensity to get injured	Overall torque Maximum torque at key joints Stability at the deck
Comfort (Feeling)	Joint which reaches the limits Overall neutral difference for key joints
Accessible	Seat – door position Door – ladder position

### 7.1 Propensity to Injury

This section explains metrics which express the tendency to get injured. This attribute – propensity to get injured is categorized into overall torque, maximum torque at the key joints, and stability at the deck area. Details are explained in the following sections.

#### 7.1.1 Dynamic Effort

Lin and Cohen (1997) studied types of accidents in truck industries. Overexertion is one of the most frequent and severe types of accidents reported in the truck industry. This type of injury uniquely has a long-term effect on the injured person even years after treatment. The torque output contains artifacts that are associated with how much effort the operator spends while performing a particular task. The amount of dynamics effort can be expressed as a function of torque exerted by each joint. Exerted torque can be

calculated in two different ways; one is by calculating total torque and another is by identifying the maximum torque at key joints.

When designers simply want to check the overall value of dynamic effort, they could use the average torque over all joints. The torque exerted by each joint can be obtained by integrating the normalized torque values over the duration of the task. Since each joint exerts the values within its own limits, joint torque value should be normalized before summing all the torque values. Therefore, normalized torque values are now used to sum over time. The metric, propensity to get injured, based on dynamic effort,  $M_{Overall\_torque}^{Injury}$ , can be defined as;

$$M_{Overall\_torque}^{Injury} = \frac{1}{ndof \times T} \sum_{i=1}^{ndof} \int_{t=0}^T (\tau_i^{norm}(\mathbf{q}, t)) dt \quad (7.1)$$

$$\tau_i^{norm}(\mathbf{q}, t) = \begin{cases} \frac{\tau_i(\mathbf{q}, t)}{\tau_i^{up}}, & \text{if } \tau_i(\mathbf{q}, t) \geq 0 \\ \frac{\tau_i(\mathbf{q}, t)}{\tau_i^{low}}, & \text{if } \tau_i(\mathbf{q}, t) < 0 \end{cases} \quad (7.2)$$

where  $\tau_i^{up} > 0$  is the maximum and  $\tau_i^{low} < 0$  is the minimum torque value for each joint.  $t$  is the time parameter as  $0 \leq t \leq T$ .  $ndof$  is the number of degrees of freedom, and  $T$  is total time.

Another way to express the metric is by evaluating the maximum torque at some key joints. Maximum torque also represents risk to get injured. By observing maximum torque value at some key joints during the execution of a task, the designer could predict the potential for injury to the operator, such as bone fracture or strain *etc.*, based on hypothesis that higher torque values may correspond to higher potential for injury. Since the operator can get injured by exerting smaller torque if its limit is smaller, the absolute value cannot tell its magnitude. Thus, maximum torque is calculated as its normalized value and represented in Equation (7.3).

$$M_{Max\_torque}^{Injury} = \max_{0 < t < T} \{ \tau_i^{norm}(\mathbf{q}, t) \} \quad (7.3)$$

where the index  $i$  corresponds to the joint of interest.

### 7.1.2 Stability

Falling when entering and exiting heavy vehicles is a major problem that merits serious consideration by designers. Hurst and Khalil (1984) drew attention to this problem and provided several guidelines based on the fundamentals of ergonomics and safety engineering. In 1990, 1767 claims in Ohio alone were filed for worker's compensation due to falling from elevated vehicles (Woodson *et al.*, 1992). These falls can lead to costly claims and lost workdays.

The step-handhold relationship should be arranged so that the worker is balanced as he/she mounts the steps to the cab. Balance can be achieved by using the three-point system, meaning that the worker always has three limbs in contact with the vehicle or ground. If the operator is not balanced when he/she climbs up the ladder and stands on the deck area to get in the operating room, it can cause an accident. The stability can be calculated using the location of the zero moment point (ZMP). It is important where ZMP is located in the foot support region (FSR) shown in Figure 7.1a. Use of ZMP is explained in Section 4.3. If ZMP location is relatively biased, it infers the potential to fall. Therefore, metrics for stability can be represented as the ratio of maximum ( $d_{max}$ ) and minimum ( $d_{min}$ ) distance from the boundary line to the ZMP and is shown in Figure 7.2 b and expressed in Equation (7.4).

$$M_{Stability}^{Injury} = \frac{d_{min}}{d_{max}} \quad (7.4)$$

An ideal result for this metrics is having same distances through  $d_1$  to  $d_6$ ; therefore, the best result would be 1.

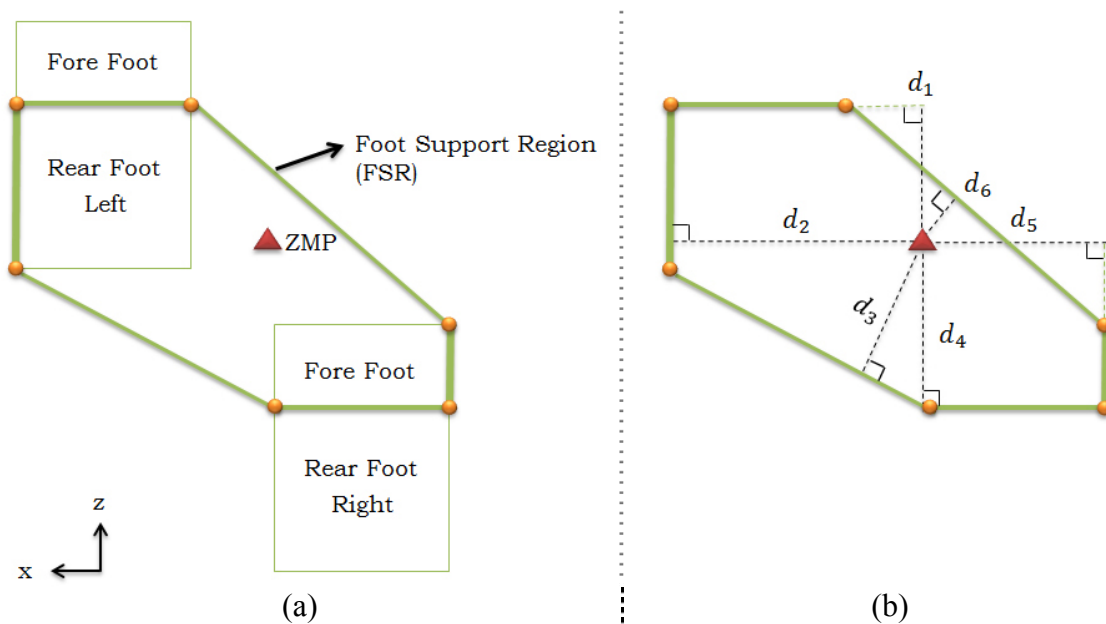


Figure 7.1 Calculation for stability metrics

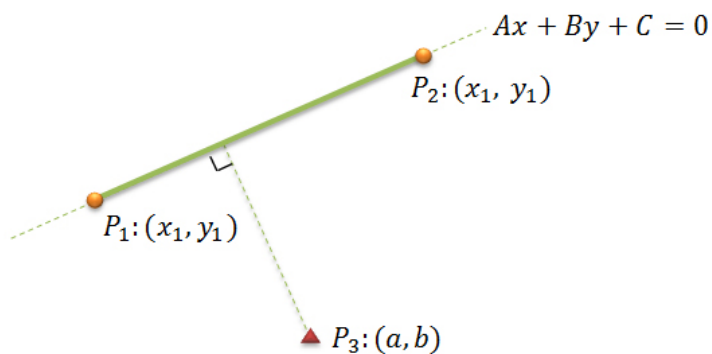


Figure 7.2 Shortest distance from point to line

This paragraph describes the technique for calculating stability. It also gives the procedure to compute the shortest distance from a point to a line or line segment. The equation of a line (of FSR) defined through two points  $P_1(x_1, y_1)$  and  $P_2(x_2, y_2)$  in Figure 7.2 is

$$y - y_1 = \frac{y_2 - y_1}{x_2 - x_1} \cdot (x - x_1) \quad (7.5)$$

Comparing this equation with the equation of the line  $Ax + By + C = 0$  gives the value of  $A$ ,  $B$ , and  $C$

$$\begin{aligned} A &= -\frac{y_2 - y_1}{x_2 - x_1} \\ B &= 1 \\ C &= -\left( \frac{(y_1 - y_2)x_1}{x_2 - x_1} + y_1 \right) \end{aligned} \quad (7.6)$$

The point  $P_3: (a, b)$  is closest to the line at the tangent to the line, which passes through  $P_3$ . The shortest distance from the point  $P_3: (a, b)$  to the line  $Ax + By + C = 0$  is

$$\frac{|Aa + Bb + C|}{\sqrt{A^2 + B^2}} \quad (7.7)$$

Therefore, the distance between the point  $P_3$  and the line can be calculated by substituting Equation (7.6) into Equation (7.7).

### 7.2 Comfort (Feeling)

In order to justify the costs of using an ergonomically designed cab, it is necessary to relate improved design to improved performance. Lesser discomfort in a cab can improve operator performance, reducing injuries and thus downtime. There are two different ways to present discomfort; one is deviations from neutral postures (Yang *et al.*, 2004) to the joint angle history that occur due to variety of body movements around different joints. Designers can observe the overall discomfort as we did in Section 6.3. To calculate overall discomfort for the deviation from neutral angle to the joint angle history, the deviation from the neutral angle should be normalized. It is then integrated over time and its average is taken. The complete equation is given as

$$M_{Overall}^{Discomfort} = \frac{1}{ndof \times T} \sum_{i=1}^{ndof} \int_{t=0}^T \left( \frac{|q_i(\mathbf{q}, t) - q_i^N|}{q_i^{up} - q_i^{low}} \right) dt \quad (7.8)$$

where  $ndof$  is number of DOF,  $T$  is the total time,  $q_i^{up}$  is the upper limit and  $q_i^{low}$  the lower limit for each joint angle, and  $q_i^N$  is the neutral angle.

Because poor design is associated with increased discomfort, how much the joint angle approaches the limits could be a criterion for discomfort. Such knowledge is needed to better understand potentially adverse effects of poor working postures in the industrial population. Therefore, designers can predict the possible discomfort using this metric. Eventually they could use this to rearrange the objects to avoid excessive use of joint range of motion. Yang *et al.* (2004) proposed a new discomfort function presented in Equation (7.9). This includes the normalized discomfort term in Equation (7.10) and the penalty term in Equation (7.11).

$$M_{ROM}^{Discomfort} = \frac{1}{G} \left[ (\Delta q_i^{norm})^2 + G \times QU_i + G \times QL_i \right] \quad (7.9)$$

$$\Delta q_i^{norm} = \frac{q_i - q_i^N}{q_i^{up} - q_i^{low}} \quad (7.10)$$

$$QU_i = \left( 0.5 \text{Sin} \left( \frac{5.0(q_i^{up} - q_i)}{q_i^{up} - q_i^{low}} + 1.571 \right) + 1 \right)^{30} \quad (7.11)$$

$$QL_i = \left( 0.5 \text{Sin} \left( \frac{5.0(q_i - q_i^{low})}{q_i^{up} - q_i^{low}} + 1.571 \right) + 1 \right)^{30}$$

where  $G \times QU$  is a penalty term associated with joint values that approach their upper limits, and  $G \times QL$  is a penalty term associated with joint values that approach their lower limits.



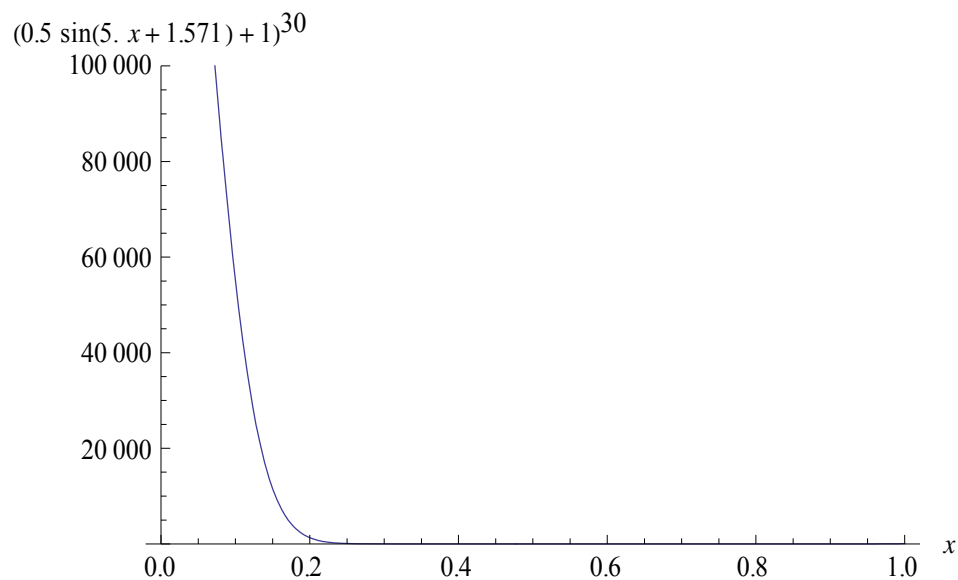


Figure 7.3 Graph of discomfort joint limit penalty term

Figure 7.3 illustrates the basic structure of the penalty terms, which has a value of zero until the joint value reaches the upper or lower 20% of its range. Thus, when it reaches the upper or lower 20% of its range, it is assumed that the operator feels more uncomfortable. For some joints that mostly move toward one way, such as knee bending or elbow bending, the penalty terms are considered only for its range of motion.

### 7.3 Accessibility

To build a criterion of accessibility evaluation based on the kinematics of the performed movement, the pathways from ladder to door to seat are considered. The door should be located properly to avoid falling after climbing the ladder, and the seat should be placed at the right position to get seated in a comfortable way.

#### 7.3.1 Ladder to Door

The deck area (Figure 7.4) where the operator steps up right after climbing the ladder is a limited space and is off the ground. If the door is located far from the ladder, the operator has to move to reach to the ladder or to the door in the limited space, which

may be dangerous for the operator. However, in this thesis, we assume that the operator takes one step to get in the operating room from the deck. Thus, the door could be at three different locations: sideways (left and right) from the ladder or forward from the ladder. If the door is biased sideways, the operator has to rotate his/her body to take the first step in. Even though ladder design has not been considered in this thesis; the accessibility from ladder to the door can be considered. In order to observe how the door location affects the joints, the rotation angle of the trunk is measured at the time when the first step goes in the cab. The metric for accessibility from ladder to door is obtained using the summation of the spine angles in the rotational direction.

$$\begin{aligned}
 M_{LadderDoor}^{Accessibility} &= ave(q_{trunk\_rotation}^{norm}(\mathbf{q}, 0)) \\
 &= \frac{1}{4} \sum_{i=1}^4 q_{i^{th} spine\_rotation}^{norm}(\mathbf{q}, 0)
 \end{aligned}
 \tag{7.12}$$

where  $q_{trunk\_rotation}^{norm}(\mathbf{q}, 0)$  is the summation of the normalized spine in rotation from 1<sup>st</sup> spine to 4<sup>th</sup> spine at the time 0.

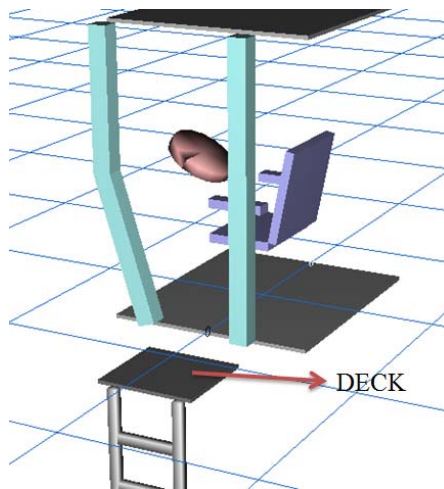


Figure 7.4 Accessibility from ladder to door

### 7.3.2 Door to Seat

Another accessibility to be measured is the pathway from door to seat. The seat location should be reachable from the door. There are three possible ways for positioning seat location as shown in Figure 7.5. Cases like those in Figures 7.5b and 7.5c make it relatively easy to reach the seat; however, as the seat is located toward windshield, the movable area gets narrow. In this case, the simulation result shows a lot of knee and hip bending motion to avoid the seat. This is because an obstacle avoidance constraint is imposed when the operator passes the seat area, and the seat is considered an obstacle. Consequently, the right leg tends to go over the seat. In order to create the metrics for accessibility from door to seat, knee and hip bending motions are measured to judge accessibility to the seat area. If the accessibility value for door to seat is higher than a comparable design, it means the movable area near the seat is smaller and the operator needs to lift up the legs to pass the corner of the seat.

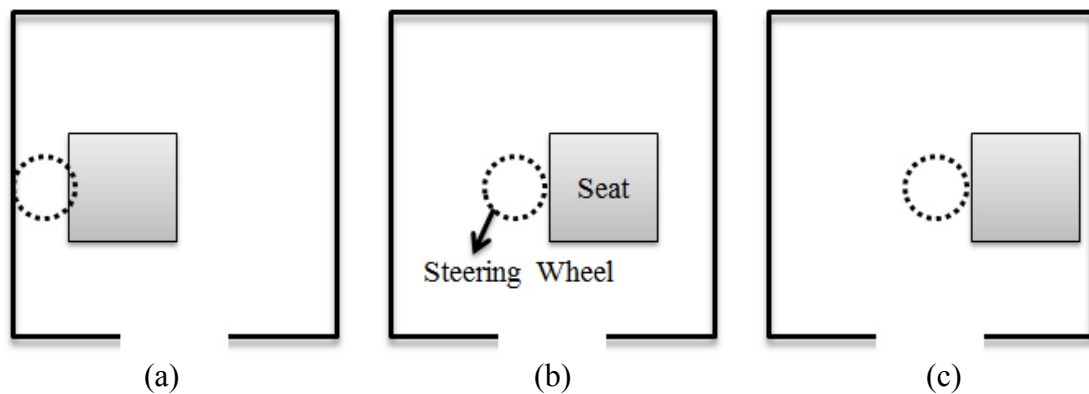


Figure 7.5 Different seat locations

The metric is defined as the deviation between the value of knee bending and hip bending angle for the operator, while performing ingress/egress, and the maximum knee and hip bending values obtained from normal walking. The knee and hip joint angles for

the operator were obtained from the normal and comfortable walk motion the operator performed while he accessed the seat. We track the joint angles of the hip and knee over the walking motion and check the difference with their maximum values. The complete description is represented in Equation (7.13). Again, since two different joints, the knee and the hip are being used, and the values need to be summed, both joint angle values are first normalized and averaged before adding them.

$$\begin{aligned}
 M_{DoorSeat}^{Accessibility} &= ave(DV_{knee} + DV_{hip})_t \\
 \text{if } q_{knee\_bending} &> q_{knee\_bending(walking)}^{\max} \\
 q_{hip\_bending} &> q_{hip\_bending(walking)}^{\max} \\
 DV_{knee} &= \frac{|q_{knee\_bending} - q_{knee\_bending(walking)}^{\max}|}{q_{knee\_bending(walking)}^{\max}} \\
 DV_{hip} &= \frac{|q_{hip\_bending} - q_{hip\_bending(walking)}^{\max}|}{q_{hip\_bending(walking)}^{\max}}
 \end{aligned} \tag{7.13}$$

where  $t$  is the time at right foot mid-swing around seat,  $q_{knee\_bending(walking)}^{\max}$  is 65 degrees and  $q_{hip\_bending(walking)}^{\max}$  is 22.5 degrees at normal speed (1.2 m/s) and 0.6 m step length (Xiang *et al.*, 2011).

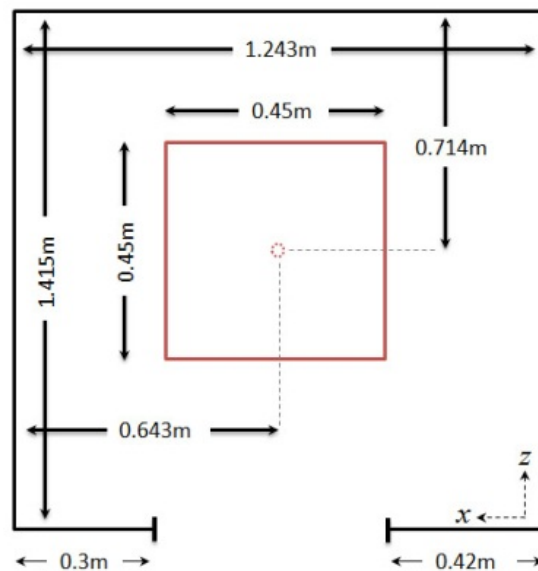
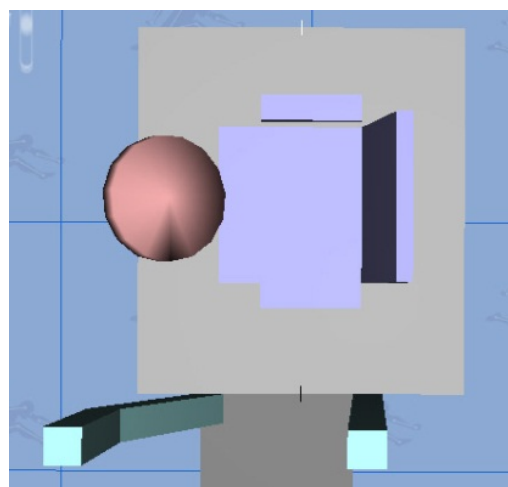
## CHAPTER 8

### RESULTS FOR CAB EVALUATION

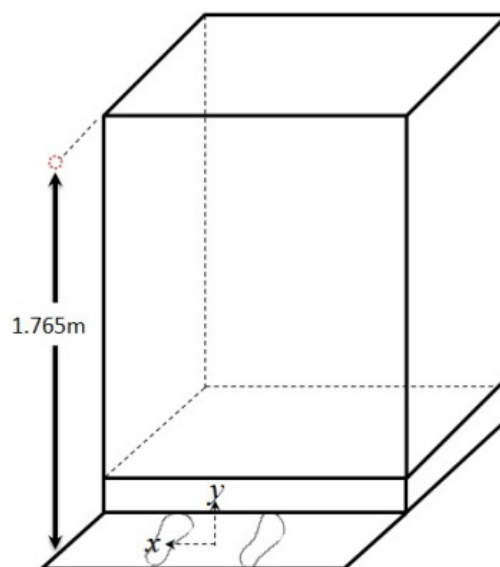
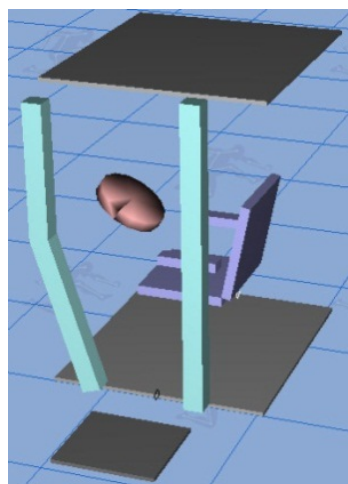
Several different heavy earthmoving equipment cab designs are presented to study the effect of layout on human ingress and egress motion. Since there are many components in a typical cab, many variables could be considered for design changes, for instance, entrance location, seat location, and ceiling height. In this study, only one variable is selected at a time to study the cause and effect of changing that parameter on the motion as well as the actuation torques requirement while simulating ingress and egress motion. Seven different cases are simulated to investigate the effects of the location of key components with regard to the movement of the digital human. In all cases, the operating room area is kept constant. Two more digital human models are presented to study the anthropometric effect. For this case study, a multi-objective optimization formulation is used with the weighting coefficient as  $c_{de} = 0.7$ ,  $c_{jd} = 0.3$ .

#### 8.1 Case Study Parameters

In this subsection, seven different design cases are introduced. First of all, assuming that the operating room area does not change, seat position is selected in three different locations, each along the x axis as shown in Figure 8.2. Maximum movable points are marked as Points 1 and 3 in Figure. 8.2. Point 2, which is on the line joining Points 1 and 3, is the default case. The default case is a current design for the Caterpillar wheel loader 950 model, which is marked as a red solid line in Figure 8.1. Movable seat area is measured excluding the least amount of area for the foot rest. Geometries for each case are presented in Table 8.1. The marked area is the smallest area that should exist.



(a) Top view



(b) Side view

Figure 8.1 Dimension for default case

Similar to the previous case, seat position is selected in three different locations along the z axis as shown in Figure 8.3. Maximum movable points are marked as Points 1 and 3 in Figure. 8.3. Point 2, which is on the line joining Points 1 and 3, is the default case. The movable seat area is measured excluding the least amount area for the foot rest

and the control panel area. Ceiling height along the y axis is a variable in Case 3 (Figure 8.4). Point 3 is selected based on the sitting height of the digital human, and Point 1 is the standing height on the floor of the operating room. The default location of the actual model is Point 2 in Figure 8.4.

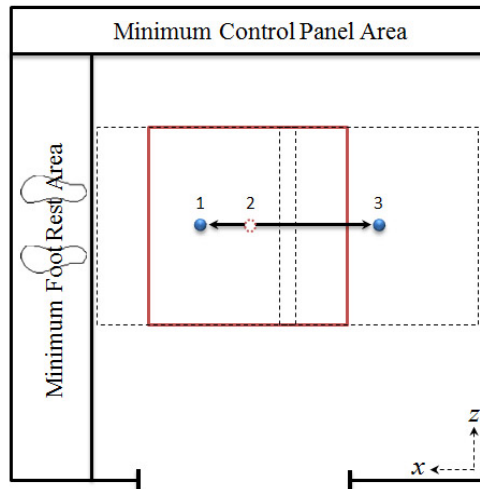


Figure 8.2 Seat position change along x axis (Case 1)

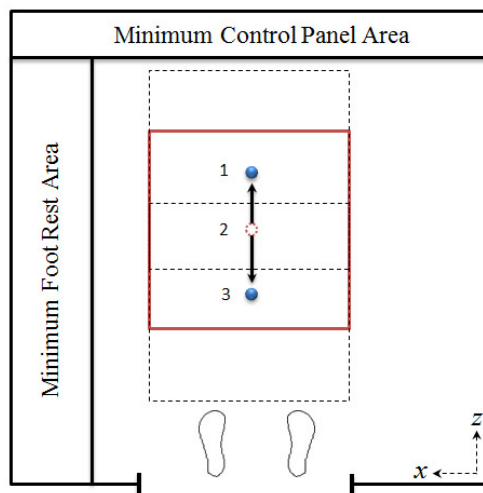


Figure 8.3 Seat position change along z axis (Case 2)

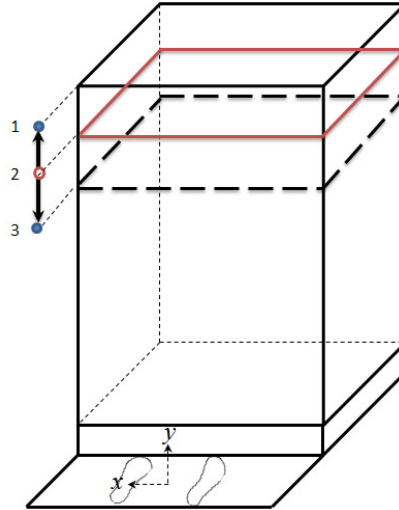


Figure 8.4 Ceiling height change along y axis (Case 3)

Table 8.1 Geometries for each case

		x	y	z
Case1 (Seat center position)	Point 1	+0.15m	default	default
	Point 2	default	default	default
	Point 3	- 0.25m	default	default
Case2 (Seat center position)	Point 1	default	default	+0.32m
	Point 2	default	default	default
	Point 3	default	default	-0.17m
Case3 (Ceiling height)	Point 1	default	+0.24m	default
	Point 2	default	default	default
	Point 3	default	-0.18m	default

## 8.2 Anthropometric Study – Digital Human Models

In this world of a global economy, a heavy vehicle designed in one part of the world could be used in a different part. The anthropometry of the people who will operate the vehicle may be very different from the anthropometry of the people where the vehicle was designed. Hence, when the designer creates a new model, he/she should carry out the anthropometric study to investigate how the design affects the operator who has different body dimensions and anthropometry. Cab design has to be an important



parameter of this study since most of the candidate operators can operate the vehicle without much difficulty. If the door is not big enough for a group of tall and heavy people, they probably would spend more effort to get in and out. On the other hand, if the seat position is far away from the door, a group of short people would take more steps or spend more effort to reach the seat. Therefore the location of the object should be defined with respect to one's anthropometry and reach capacity. The motion for ingress and egress is affected by not only the physical capability of the operator, but also by the dimensions and anthropometry of the operator's body. Thus the anthropometric study should be carried out to investigate the proper design for a wider range.

Table 8.2 Selected avatars




Index	Tall-Heavy	Medium	Short-Lean
Avatar			
Height (m)	1.91	1.80	1.59
Weight (kg)	105.4	78	53.6

Table 8.3 Link length (Indexes corresponding Figure 4.1)

Link Index	Index Name	Tall-Heavy	Medium	Short-Lean
L01	Spine Low	0.068053	0.064751	0.056282
L02	Spine Mid-Low	0.065829	0.062634	0.054442
L03	Spine Middle	0.072564	0.069042	0.077691
L04	Spine Up	0.21931	0.208666	0.190689
L05	Spine to Clavicle Right	0.020658	0.019655	0.017084
L06	Right Clavicle Offset	0.067464	0.06419	0.044466
L07	Right Clavicle	0.226743	0.173272	0.120278
L08	Right Upper Arm	0.26824	0.297634	0.284627
L09	Right Lower Arm	0.284171	0.284673	0.246902
L10	Right Hand	0.206191	0.206191	0.206191
L11	Spine to Clavicle Left	0.021471	0.020429	0.017757
L12	Left Clavicle Offset	0.067478	0.064203	0.040928
L13	Left Clavicle	0.229293	0.163123	0.115993
L14	Left Upper Arm	0.276489	0.298275	0.284279
L15	Left Lower Arm	0.256367	0.284796	0.225854
L16	Left Hand	0.213612	0.213612	0.213612
L17	Spine to Neck	0.055723	0.053018	0.029499
L18	Neck	0.108853	0.10357	0.090024
L19	Right Pelvic Width	0.102977	0.09798	0.085165
L20	Right Pelvic Height	0.14884	0.10357	0.090024
L21	Right Upper Leg	0.462763	0.440304	0.363275
L22	Right Lower Leg	0.43587	0.454126	0.39473
L23	Right Back Foot	0.13632	0.103759	0.090188
L24	Left Pelvic Width	0.102977	0.09798	0.085165
L25	Left Pelvic Height	0.14884	0.10357	0.090024
L26	Left Upper Leg	0.462763	0.440305	0.363028
L27	Left Lower Leg	0.435805	0.454125	0.39473
L28	Left Back Foot	0.132525	0.10376	0.090189
L29	Right Fore Foot	0.124889	0.124889	0.124889
L30	Left Fore Foot	0.124889	0.124889	0.124889
L31	Head	0.249779	0.249779	0.249779

Three different digital human models are selected - tall-heavy, normal, and short-lean – as given in Table 8.2. Two of the models – the tall-heavy and short-lean models are provided by United States Army Soldier Systems Center (SSC). The tall-heavy model is in the 99<sup>th</sup> percentile for weight and the 99<sup>th</sup> percentile for height. The short-lean model is in the 2<sup>nd</sup> percentile for weight and the 2<sup>nd</sup> percentile for height based on GEBOD (Generator of Body Data). The link lengths of the three body-types are compared and listed in Table 8.3. In this thesis, we assume that every human generates the torque and angles in the same limits.

### 8.3 Simulation Results

In order to investigate the effects of digital human models with different anthropometry and design changes to the motion, ingress and egress motions are simulated with different avatars for each design case. Individual results are presented in Table 8.4. Obtained numbers are scaled as 0 to 10; 0 indicates good design, and 10 indicates bad design based on the selected metric. In the case of the metric for stability at the deck, 10 was originally the most stable status; however, in order to match other metrics, we subtracted it from 10.

In summary, the first attribute in Table 8.4 is the metric related to the propensity to get injured as discussed in detail in Section 7.1. The overall torque exerted by each joint can be obtained by integrating the normalized torque values over the duration of the task. The torques for key joints are normalized, and the maximum torque value among the key joints is presented in Table 8.4. The stability at the deck is measured by the location of the zero moment point (ZMP) at the starting time (for ingress) and final time (for egress). Even though the value of the metric for the most stable case is 10, the final value is subtracted from 10 in order to match the value to other metrics as explained earlier in Section 4.3.3. Therefore, when the number is larger (closer to 10), it indicates instability of the avatar and hence potential danger of falling.

The second attribute is about the discomfort. When, for some of the joints like the shoulder or spine, the joint angle reaches near its limits, the discomfort values are obtained by the penalty function as discussed in Section 7.2. Those penalties are normalized and presented as maximum penalties among the joints that reach their limits. Therefore, the closer the joint reaches to the limits, the more penalties the joint gets; 10 is the highest magnitude a joint can reach. Overall, the neutral angle difference is the integral of normalized deviation from the neutral angle over time. 10 indicates the most uncomfortable magnitude that the operator feels.

The last attribute is related to accessibility. This attribute estimates the ease of getting in and out of the cab when the operator passes through the door and the seat area. First of all, we assumed that normal walking speed is the most comfortable gait. The best design would allow the operator to walk in and out of the cab easily. The maximum knee and hip angle in bending direction from the normal walking speed are selected as metrics to estimate this attribute. Then, the deviation is presented only if the obtained knee and hip angles are larger than those for walking. When the angle is larger, it means the operator starts to raise his/her leg to pass the seat area, avoiding the seat corner. The accessibility to the door from the ladder is presented as normalized maximum trunk rotation. The higher the number is, the harder the access to the door from the ladder.

Table 8.4 Values of metrics for ingress (NK: neck joint; KN: knee joint)

## (a) Current model (point 2 of every case)

Metric	Tall-Heavy	Medium	Short-Lean
Overall torque	5.7	5.7	5.8
Maximum torque	7.7NK	7.0NK	6.9KN
Stability at the deck	9.1	5.0	4.3
Discomfort-penalty	5.0	5.0	5.0
Overall neutral angle difference	1.1	1.1	1.1
Accessibility: door to seat	0	0	0
Accessibility: ladder to door	2	1	1

## (b) Point 1 of case 1

Metric	Tall-Heavy	Medium	Short-Lean
Overall torque	5.7	5.6	5.8
Maximum torque	7.2NK	7.0NK	7.1NK
Stability at the deck	9.6	5.6	5.8
Discomfort-penalty	5.0	5.0	5.0
Overall neutral angle difference	1.2	1.2	1.3
Accessibility: door to seat	0	0	0
Accessibility: ladder to door	2	2	2

## (c) Point 3 of case 1

Metric	Tall-Heavy	Medium	Short-Lean
Overall torque	5.7	5.7	5.8
Maximum torque	6.5NK	6.9NK	6.8NK-KN
Stability at the deck	9.8	6.9	8.8
Discomfort-penalty	5.0	5.0	5.0
Overall neutral angle difference	1.1	1.1	1.1
Accessibility: door to seat	0	0	0
Accessibility: ladder to door	2	1	1

## (d) Point 1 of case 2

Metric	Tall-Heavy	Medium	Short-Lean
Overall torque	5.7	5.7	5.8
Maximum torque	6.5NK	6.7NK	7.5NK
Stability at the deck	10.0	6.0	3.6
Discomfort-penalty	5.0	5.0	5.0
Overall neutral angle difference	1.3	1.3	1.9
Accessibility: door to seat	0	0	0
Accessibility: ladder to door	2	1	3

Table 8.4 continued

## (e) Point 3 of case 2

Metric	Tall-Heavy	Medium	Short-Lean
Overall torque	5.7	5.6	5.8
Maximum torque	6.5NK	6.6NK	6.9NK
Stability at the deck	8.8	5.5	2.1
Discomfort-penalty	5.0	5.0	5.0
Overall neutral angle difference	1.1	1.0	1.1
Accessibility: door to seat	0	0	0
Accessibility: ladder to door	2	1	1

## (f) Point 1 of case 3

Metric	Tall-Heavy	Medium	Short-Lean
Overall torque	5.7	5.7	5.8
Maximum torque	6.9NK	6.9NK	6.9KN
Stability at the deck	9.3	5.1	3.3
Discomfort-penalty	5.0	5.0	5.0
Overall neutral angle difference	1.1	1.0	1.2
Accessibility: door to seat	0	0	0
Accessibility: ladder to door	2	1	2

## (g) Point 3 of case 3

Metric	Tall-Heavy	Medium	Short-Lean
Overall torque	5.7	5.7	5.8
Maximum torque	6.2KN	6.7KN	6.8KN
Stability at the deck	9.8	5.2	6.7
Discomfort-penalty	5.0	5.0	5.0
Overall neutral angle difference	1.2	1.2	1.2
Accessibility: door to seat	0	0	0
Accessibility: ladder to door	2	1	2

## 8.3.1 Results for Ingress

To analyze details, the current design case – Table 8.4a – is selected from among seven different design cases. The overall result is that there is not much difference due to different anthropometry. Maximum torque was exerted at either the knee joint or the neck joint as shown in Table 8.4a. Maximum torque on the neck is slightly increased for the tall-heavy avatar; it can be seen as the effect of the height. Instead of the maximum torque on the neck, the short-lean avatar exerted maximum torque at the knee joint. It was

obtained during the single support phase just before the sitting position. In the single support phase, all the body weight is moved to the supporting leg. Therefore the torque on the knee is high as shown in Figure 8.5. Preparation to sit occurs at the last single support (on the left foot). In real life, the operator jumps up to the seat in a short time to avoid higher torque on his/her knee, because the operator is aware of the existence of the seat. However, since cognitive function is not modeled and time is not used as a design parameter in this study, the avatar has to follow a particular timeline and does not recognize the existence of the seat until it has to sit down; therefore the maximum torque was obtained at the knee while preparing to sit down.

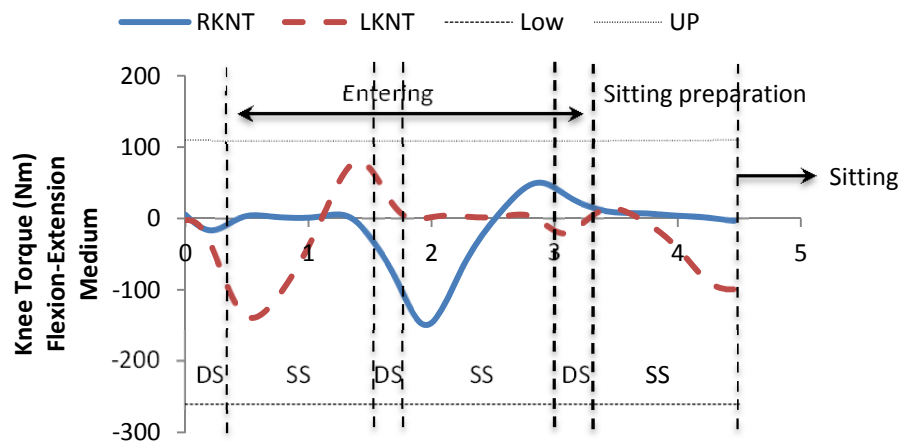


Figure 8.5 Knee torque for ingress with medium avatar

Calculated ZMP position is shown in Figure 8.6 for ingress in the current model. Most of the ZMP positions are biased to the left side. In the current formulation, ZMP position is not controlled; instead, whether ZMP is in the foot support region (FSR) or not is considered as a constraint. Therefore, since this is still in the FSR, the avatar does not

fall. However, the most stable position can be defined as the center of the FSR polygon. When compared, the most stable position ZMP in Figure 8.6 is less stable for the tall-heavy avatar than for the other two avatars.

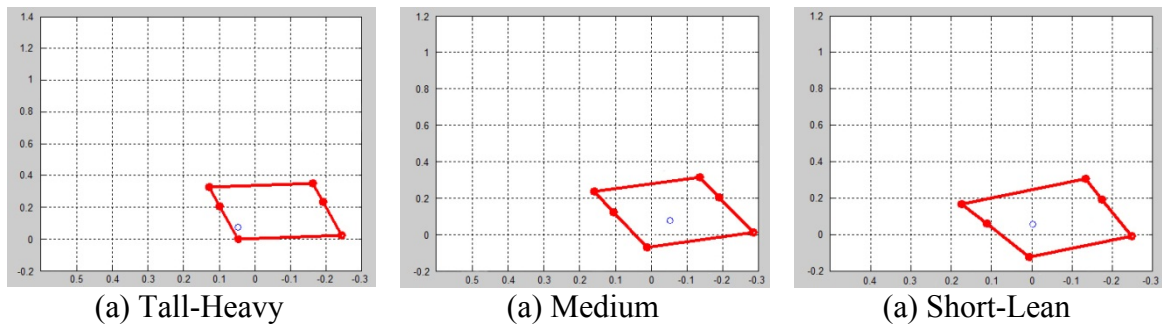


Figure 8.6 ZMP positions for Table 8.4a by different digital human models

For the accessibility attribute, since ladder location has not been designed in this study, the simulation is planned to start and end in front of the door on the deck area. Therefore, the magnitude of trunk rotation is small. Another metric for accessibility from door to seat is calculated only when the knee and hip bending values are greater than those for normal walking. Therefore the magnitude zero means that the angles for knee and hip bending are smaller than those for normal walking. There is enough space to walk into or out of the pathway. In other words, the operator does not feel discomfort walking by the corner of the seat.

There was not much variance in the overall neutral angle values in Table 8.4a due to anthropometric changes. This means the movement (joint angle history) follows similar patterns for different anthropometries. While there is not much difference among the avatars, there is a slight difference among the design cases. However, when we consider all the design cases, the overall neutral angle difference from point 1 in the case 2 model is higher than that in the other cases, as shown in Figure 8.7. This may be caused by the fixed number of steps or improper hand position. The operator has to reach the



control panel in the second step. Since the location of the control panel is too far to reach from the second step, this may cause more discomfort. If the operator touches the backrest of the seat area (anything closer to the body) or if he/she takes more steps to reach the control panel, it would solve this problem. Therefore, without any changes in the assumptions, the closer the seat is located to the door, the less discomfort the operator feels.

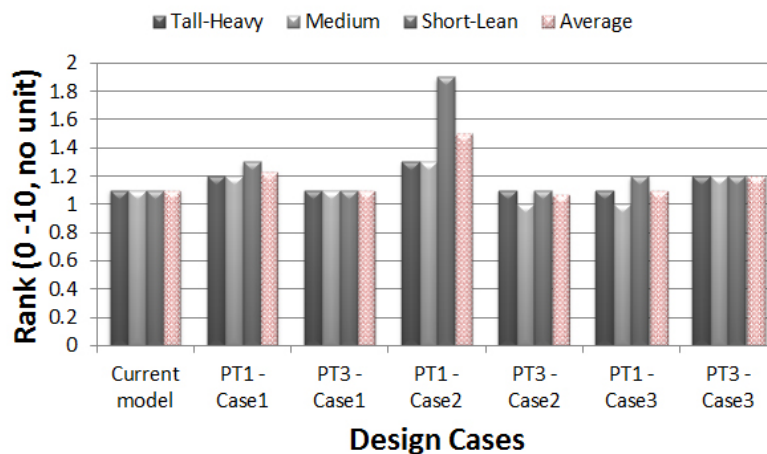


Figure 8.7 Overall neutral angle difference ranking for ingress

Since our goal is to compare different cab designs for each anthropometry, all the metrics are averaged for each avatar after obtaining the individual magnitude of each metric. All the metrics can be presented as one number per avatar. Figure 8.8 depicts the rank depending on the avatars.

Then, the ranks of the three different avatars are averaged again to make one number for each design case. Finally, we could reach a magnitude for each design case in Figure 8.9. Point 3 in case 2, where the seat is located closer to the door than in the current model, has the lowest rank among the seven design cases. In other words, point 3

in case 2 is a better design than the current model for different-sized operators from the points of view of injury, accessibility, and comfort.

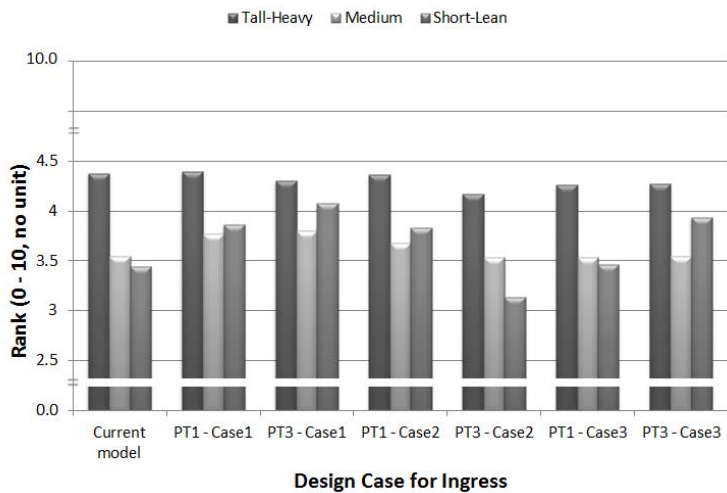


Figure 8.8 Avatar-wise cab design ranking for ingress

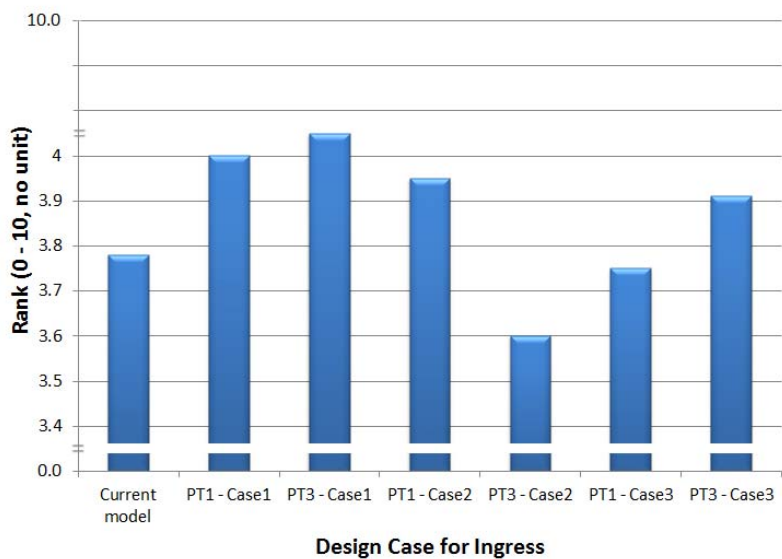


Figure 8.9 Overall cab design ranks for ingress

### 8.3.2 Results for egress

To analyze details, the current design case – Table 8.5a – is selected from among seven different design cases. In the same way as ingress, the overall torque results show that there is not much difference due to different anthropometries. To observe the instant at which the maximum torque is generated, the knee torque profile for the medium avatar is plotted in Figure 8.10. Similar to ingress, the movement from sitting to standing tends to cause maximum torque on the knee joint. Maximum torque at the knee joint is exerted between the time when the body is rising from the seat and when the right foot single support phase is occurring to move to the next step. Also, since the ZMP location was moved from the hip to the foot to stand up, it made a dramatic change in the torque compared to the torque while standing up around 2 seconds.

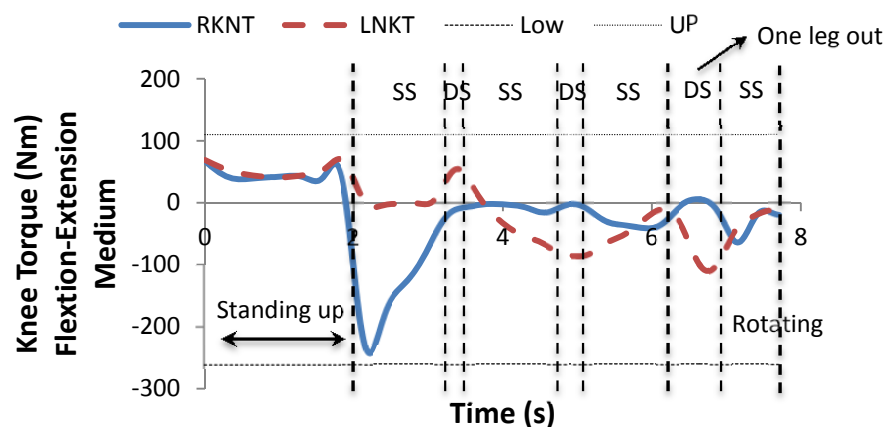


Figure 8.10 Knee torque for egress with medium avatar

The calculated ZMP position is shown in Figure 8.11 for egress using the current design. Most of the ZMP positions are biased. However, the ZMP constraints are satisfied, which indicates that none of the cases is unstable since the ZMP position is in the FSR.

However, it can be seen that, compared to the most stable position defined as the center of the FSR polygon, the ZMP locations in Figure 8.11 are less stable.

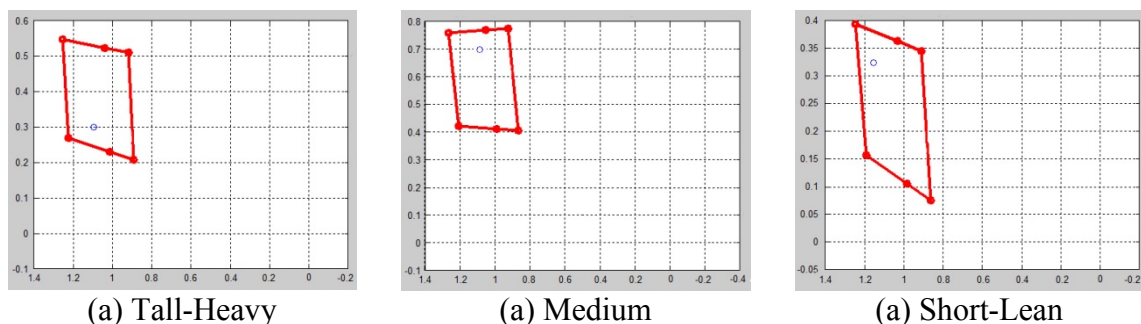


Figure 8.11 ZMP positions for Table 8.5a for different digital human models

The accessibility attribute for egress is excluded from Table 8.5. The operator motion is very close to forward walking during ingress. However, for egress, the default motion is closer to sideways walking. Since the egress task is not designed to follow the walk forward pattern, the metric – measuring the knee and hip joint angle in the bending direction – is not applicable for egress. The same reasoning is true for the metric for accessibility from the seat to the ladder that we applied for ingress. Using the same metric, in almost all cases, calculating the average trunk rotation for an egress task gives the same result (a value very close to zero). However, this does not mean that the current design being evaluated is a good design from an egress point of view. Therefore, using this metric may mislead a designer, and thus the accessibility attribute has been excluded for egress.

There was small variance by anthropometric difference in the overall neutral angle values in Table 8.5a. The maximum normalized penalties are calculated for each joint and averaged. The results are presented in Figure 8.12. It shows that the tall-heavy avatar obtained a penalty more frequently than others. This may cause a higher overall neutral angle difference.

Table 8.5 Values of metrics for egress (HP : hip joint)

## (a) Current model (point 2 of every case)

Metric	Tall-Heavy	Medium	Short-Lean
Overall torque	5.7	5.7	5.7
Maximum torque	8.4KN	7.5KN	6.9NK
Stability at the deck	7.7	7.6	7.7
Discomfort-penalty	5.0	5.0	5.0
Overall neutral angle difference	2.2	1.9	1.8

## (b) Point 1 of case 1

Metric	Tall-Heavy	Medium	Short-Lean
Overall torque	5.7	5.6	5.7
Maximum torque	7.8KN	8.6KN	6.7NK
Stability at the deck	3.4	8.3	6.7
Discomfort-penalty	5.0	5.0	5.0
Overall neutral angle difference	1.6	2.7	1.3

## (c) Point 3 of case 1

Metric	Tall-Heavy	Medium.	Short-Lean
Overall torque	5.7	5.7	5.7
Maximum torque	7.6KN	7.5KN	7.9HP
Stability at the deck	9.1	8.9	9.0
Discomfort-penalty	5.0	5.0	5.0
Overall neutral angle difference	1.6	1.4	2.7

## (d) Point 3 of case 2

Metric	Tall-Heavy	Medium	Short-Lean
Overall torque	5.7	5.6	5.6
Maximum torque	6.9NK	6.8NK	6.1NK
Stability at the deck	6.4	6.7	6.9
Discomfort-penalty	5.0	5.0	5.0
Overall neutral angle difference	1.1	1.0	1.3

## (e) Point 1 of case 3

Metric	Tall-Heavy	Medium	Short-Lean
Overall torque	5.7	5.7	5.7
Maximum torque	7.2KN	7.1KN	6.6NK
Stability at the deck	6.4	7.9	7.1
Discomfort-penalty	5.0	5.0	5.0
Overall neutral angle difference	1.0	1.7	1.8

Table 8.5 continued

(f) Point 3 of case 3

Metric	Tall-Heavy	Medium	Short-Lean
Overall torque	5.8	5.7	5.7
Maximum torque	9.8KN	9.0HP	5.3KN
Stability at the deck	9.2	8.9	9.1
Discomfort-penalty	5.0	5.0	5.0
Overall neutral angle difference	2.8	2.7	2.3

The simulation result for point 1 of case 2 has not been presented. Since simulation results have not obtained a feasible solution, we could not get the results of the metrics. The reason could be that the hands may not reach the objects while the avatar is exiting with the current foot positions. In order to avoid this problem, either proper hand locations or more steps need to be provided.

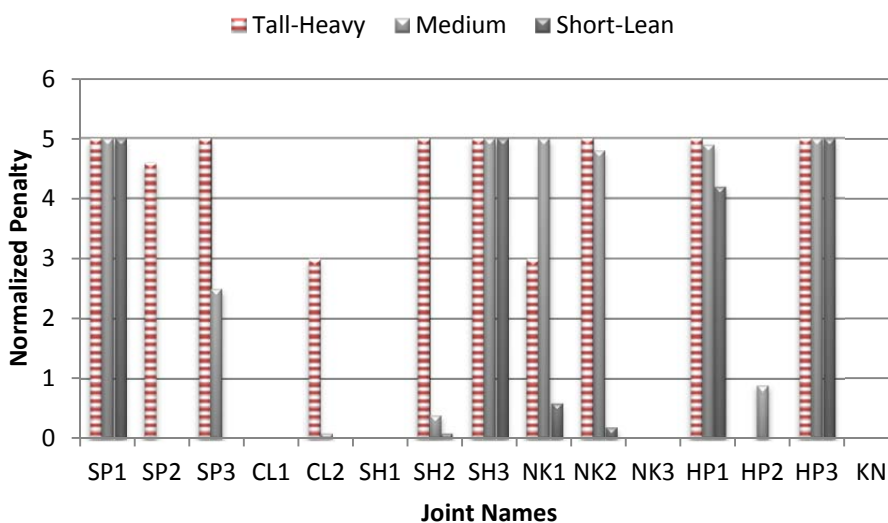


Figure 8.12 Normalized penalty for each joint in Table 8.5a.

Since our goal is to compare different cab designs for each anthropometry, all the metrics are averaged for each avatar after obtaining the individual magnitude of each

metric. All the metrics can be presented as one number per one avatar. Figure 8.13 depicts the rank depending on the avatars.

Then, the ranks of the three different avatars are averaged again to make a one number for each design case. Finally, we could reach to a magnitude for each design case in the Figure 8.14. Point 3 of case 2, where the seat is located closer to the door than in the current design, has the lowest rank among the six design cases. In other words, point 3 of case 2 is a better design than the current model for different-sized operators from the points of view of injury, accessibility, and comfort.

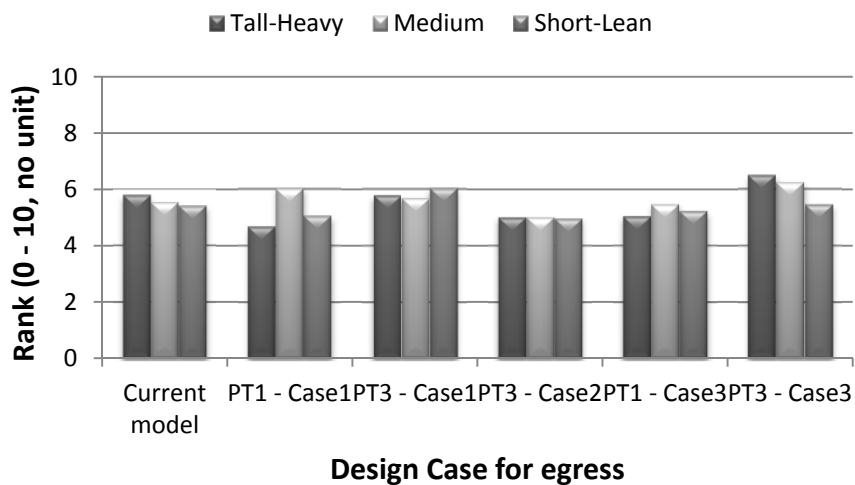


Figure 8.13 Subject-wise cab design ranking for egress

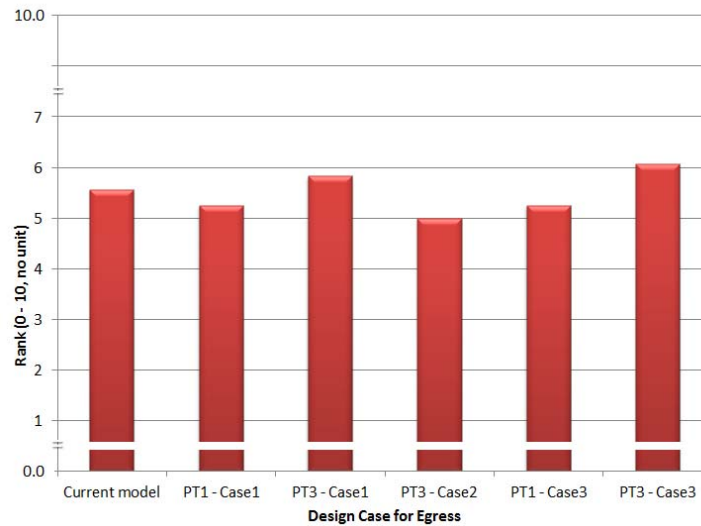


Figure 8.14 Overall cab design ranks for egress

#### 8.4 Conclusions

In this chapter, several different heavy earthmoving equipment cab designs were presented to study the effect of layout on human ingress and egress motions. Two more digital human models are introduced to study the effect of anthropometric changes. We obtained simulation results and evaluated metrics for cab design evaluation as described in Chapter 7. All the metrics are averaged for each avatar after obtaining the individual magnitude of each metric. Then, the ranks of the three different avatars are averaged again to make a one number for each design case. Therefore we could have the results in Figure 8.9 for ingress and Figure 8.14 for egress. However, cab design has to be identical for both ingress and egress. We cannot choose two different cab designs as one for the ingress and one for the egress. For this reason, point 1 in case 2 has been dropped due to the unavailable egress motion. Therefore, by averaging ranks from Figure 8.9 and Figure 8.14 (ingress and egress), we could finally reach one magnitude for each design case for both ingress and egress motion (Figure 8.9).



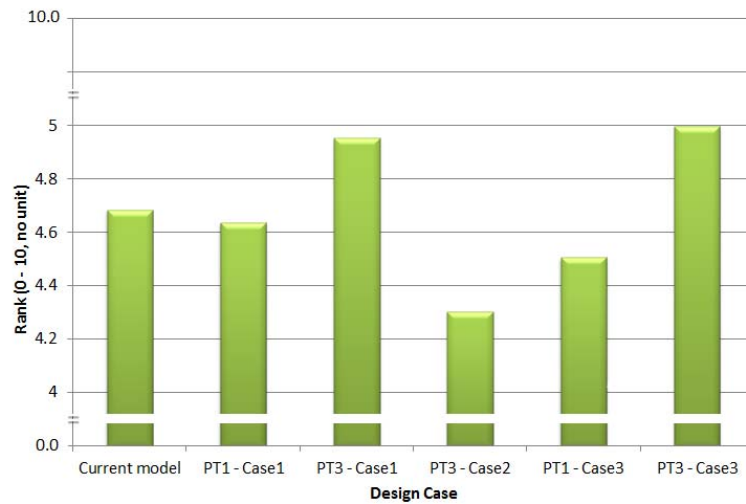


Figure 8.15 Overall cab design ranks for ingress and egress

Additional metrics for the cab design evaluation can be developed by designers. However, with the presented design metrics, Figure 8.15 shows that point 3 of case 2 has been marked as the lowest rank. Therefore, we could suggest a guideline to the designer to place the seat position close to the door like the design case (point 3 of case 2). This will make a better design than the current model for different-sized operators for both ingress and egress from the points of view of injury, accessibility, and comfort.

## CHAPTER 9

### CONCLUSIONS AND FUTURE RESEARCH

#### 9.1 Conclusions

In this dissertation, a model is developed to perform ingress/egress motion for heavy equipment to study the response of the operator for different cab designs. The ingress/egress task in the heavy equipment environments was defined and a couple of safety factors based on guidelines from the equipment manufacturers were introduced. Through the video analysis of ingress/egress motion, key components and input parameters were identified. Inputs were categorized as hand position and cab geometry. A simplified prop model that includes a door frame, ceiling, seat, and steering wheel was created based on the key components.

Simulation results were presented with single objective function (dynamic effort) optimization problems. However, there were limitations to performing the ingress/egress motions, which meant dynamic effort was not always the most appropriate. Therefore, several problems with the current formulation were discussed and updated. In this process, different performance measures were suggested and were used with predictive dynamics to study human performance. The goal of multiple-objective optimization was to find the true performance measure behind the human motion so that predictive dynamics could produce more natural human motions. Using multiple performance measures, artificial constraints such as task-specific joint limits were eliminated. Thus, the full range of motion for all 55 DOF were considered. With unrestricted range of motion, the ingress/egress tasks could take all the different inputs and increase the variations of cab designs and anthropometry types that the optimization problem could handle.

In order to evaluate different cab designs, several design metrics, which become a crucial source of information for decision-making, were proposed: propensity to get

injured, comfort, and accessibility. The resulting values of the metrics from virtual experiments enhance designers' ability to make decisions and plan further design changes.

Several different heavy earthmoving equipment cab designs were presented to study the effect of layout on human ingress and egress motions. Two more digital human models were introduced to study the effect of anthropometry. Then the virtual experiments were performed for all the cases with different input parameters employing the multi-objective optimization approach. Simulation results based on the presented metrics were presented as one magnitude for each design. Finally, we could conclude that the design where seat location is close to the door is better than the current design for different-sized operators for both ingress and egress from the points of view of injury, accessibility, and comfort.

While substantial benefits can be gained by implementing the tool presented in this study, a few limitations should be kept in mind while making decisions. There is wide variance in ingress and egress strategies among operators. In order to simplify the problem, several assumptions were described in Section 3.4. Since number of steps is fixed to a minimum of three, it may limit the operator's strategy. Moreover, the objects to avoid were also simplified during the motion; this may cause unrealistic motion at some point. Therefore, an understanding of ingress and egress strategies is needed.

In Chapter 7, seven design metrics are set up to evaluate cab designs. However, seven design metrics cannot represent all of the designers' purposes. Since we assumed that all the metrics are equally important, a simple average of each metric is taken. However, designers can give priority by their choices; they can give more weight to evaluate cab designs. More design metrics can be set up based on the designers' purposes; this can create an improved design metrics set.

Even though there are several limitations, the results obtained from this study are promising and allow a user to perform comparative virtual studies of ingress/egress motions for different cab layouts and subsequently analyze the kinematics and kinetics

results. This, in turn, helps in designing better cab interiors for drivers without having to build expensive prototypes. This study is helpful in gathering information about the critical effect of joint actuation requirements under different loading conditions, which helps designers create better layouts to prevent and reduce injuries and increase comfort for operators. By investigating changes in cab geometry during ingress and egress, working conditions for different sizes of operators can be improved. Such a capability will help with better design of in-cab environments of heavy vehicles and could be a useful tool in reducing injuries to operators.

## 9.2 Future research

The cab design analysis tool developed in the current work provides benefits to the designers of heavy equipment cabs and could reduce the number of physical prototypes and experimental studies needed before finalizing the design for production. However, some additional work could definitely increase the usability and accuracy of the predictions as well as cab analysis. Below are some of the areas where additional research and software tool enhancements could help designer in making this tool even more useful.

### 9.2.1 Different Populations

In this research, three different digital human models have been used in the ingress and egress motion simulations. An identical set of joint torque limits and angle limits are applied. However, each person exerts different joint torques and moves in a diverse range of motion, especially the injured, arthritic, or obese person. These disabilities may reduce the range of motion and the torques they can produce. Thus, we can expand this research to different populations to study how it affects the motion and how design should be changed to accommodate these subjects.

### 9.2.2 Different Performance Measures

In Chapter 6, we investigated two objective functions: dynamic effort and joint discomfort. However, we cannot conclude that only these two functions drive the entire human motion. In reality, human motion is governed by multiple objectives such as stability, energy, and fatigue. In addition, possible performance measures should be investigated further, and the Pareto optimum surface may need to be generated to find the true optimal solution. This research will provide a clue for the true performance measure behind the human motion so that the predictive dynamics can predict more natural human motions.

### 9.2.3 Reaction Forces as Design Variables

Ingress and egress motion requires a large amount of interaction between the operator and the environment (cab). Hence, the reaction forces applied by the cab on the operator are a very important element of the task and cab design evaluation. In the current simulation, reaction forces are applied as inputs so that the user can impose the reaction forces. Since not only the magnitude of reaction force is changing, but also the direction of the reaction force over time, it is hard to get the information from the experiment. The reaction force magnitude and direction also changes with changes in hand and foot contact locations, which in turn depend on the cab designs. Hence, unless we get reaction forces for each design by performing experiments, these assumptions would introduce some error in our analysis. Also, if we get reaction forces for each design, the advantages of using this tool are no longer valid. Therefore, changing the formulation to include the reaction forces as design variables will enhance the accuracy of analysis.

### 9.2.4. Design of Ladder

In this dissertation, ladder climbing has not considered. We assumed that the operator had already climbed the ladder and was standing on the platform just at the end

of ladder where the ingress task starts and the egress task ends. However, as discussed in the literature search, ladder climbing, especially the first flexible step, plays a major role in the injuries observed in the field. In addition, considering the ladder climbing as a part of the ingress and egress process would provide more accurate information to the designers. Including ladder climbing in simulations would also require adding more metrics corresponding to the ladder-climbing task.

## REFERENCES

- Anderson, F.C. and Pandy, M.G. "Dynamic optimization of human walking", *Journal of Biomechanical Engineering*, vol. 123(5), pp. 381-390, 2001.
- Andreoni, G., Rabuffetti, M. and Pedotti, A., "Kinematics of head-trunk movements while entering and exiting a car", *Ergonomics*, vol. 47(3), pp. 343-59, Feb. 2004.
- Causse, J., Chateauroux, E., Monnier, G. and Wang, X., "Dynamic analysis of car ingress/egress movement: an experimental protocol and preliminary results", *SAE International Journal of Passenger Cars- Mechanical Systems*, vol. 2 (1), pp.1633-1640, Oct. 2009.
- Causse, J., Wang, X. and Denninger, L., "Effects of roof height on car ingress/egress movement", 1<sup>st</sup> International Symposium on Digital Human Modeling, Paper ID 2231, 2011.
- Cherednichenko, A., Assmann, E. and Bubb, H., "Computational approach for entry simulation", *SAE International*, Technical Paper 2006-01-2358, Jan. 2006.
- Dufour, F. and Wang, X., "Discomfort Assessment of Car Ingress/Egress Motions using the Concept of Neutral Movement", *SAE International*, Technical Paper 2005-01-2706, Jan. 2005.
- Fathallah, F.A and Cotnam, J.P., "Maximum forces sustained during various methods of exiting commercial tractors, trailers and trucks", *Applied Ergonomics*, vol. 31(1), pp 25-33, Feb. 2000.
- Flatow, S., "Safety in the trucking industry: non-driving incidents", *Professional Safety*, vol. 45(11), pp.25-30, 2000.
- Gavan, G.R., Strassel, D.P and Johnson, D., "The development of improved ingress/egress systems for large haulage trucks", *SAE International*, 800680, Apr.1980.
- Giacomin, J. and Quattrocchio, S., "An analysis of human comfort when entering and exiting the rear seat of an automobile", *Applied Ergonomics*, vol. 28(5-6), pp. 397-406, 1997.
- Giguère, D. and Marchand, D., "Perceived safety and biomechanical stress to the lower limbs when stepping down from fire fighting vehicles", *Applied Ergonomics*, vol. 36(1), pp 107-119, Jan. 2005.
- Kaner, C. and Bond, W.P., "Software engineering metrics: what do they measure and how do we know?", *In Proceedings of the 10th International Software Metrics Symposium*, IEEE CS Press, 2004.
- Kwon, H., Hariri, M., Bhatt, R., Arora, J. and Abdel-Malek, K., "Simulating ingress motion for heavy earthmoving equipment", *HCI International*, vol. 6777, pp. 109-118, Jul. 2011.
- Lestrelin, D. and Trasbot, J., "The REAL MAN project: objectives, results, and possible follow-up", *SAE International*, Technical Paper 2005-01-2682, Jan. 2005.

- Lin, L.J., Cohen, H.H., “Accidents in the trucking industry”, *International Journal of Industrial Ergonomics*, vol.20, pp.287-300, 1997.
- Marler, R.T. and Arora, J.S., “Function-transformation methods for multi-objective optimization”, *Engineering optimization*, vol.37 (6), pp. 551 - 570, 2005.
- Monnier, G., Chateauroux, E., Wang, X., “Inverse Dynamic Reconstruction of Truck Cabin Ingress/Egress Motions”, *SAE Int. Journal of Passenger Cars- Mechanical Systems*, vol. 2(1) , pp. 1593-1599, Oct. 2009.
- Moore, S.M., Porter, W.L. and Dempsey, P.G., “Fall from equipment injuries in U.S. mining: Identification of specific research areas for future investigation”, *Journal of Safety Research*, vol. 40(6), pp. 455-460, Dec. 2009.
- Pudio, P., Lempereur, M. and Lepoutre, F.-X., and Gorce, P., “Prediction of the car entering motion”, *SAE International*, Technical Paper 2006-01-2357, Jan.2006.
- Reed, M.P., “Simulating Crew Ingress and Egress for Ground Vehicles”, *Proceedings of the Ground vehicle systems engineering and technology symposium*, 2009.
- Reed, M.P., Ebert, SM., Hoffman, SG., “Modeling foot trajectories for heavy truck ingress simulation” *Proceedings of the Applied Human Factors and Ergonomics Conference*, 2010.
- Reed, M.P. and Huang, S., “Modeling vehicle ingress and egress using the human motion simulation framework”, *SAE International*, Technical Paper 2008-01-1896, 2008.
- Reed, M.P., Ebert-Hamilton, S.M. and Hoffman, S.G., “Hand positions and forces during truck ingress”, *Proceedings of the Human Factors and Ergonomics Society Annual Meeting*, vol. 54(15), pp.1097-1100, Sep. 2010
- Riley, P.O., Schenkman, M.L., Mann, R.W. and Hodge W.A., “Mechanics of a constrained chair-rise”, *Journal of Biomechanics*, vol. 24(1), pp. 77-85, 1991.
- Schiehlen, W., “Multibody system dynamics: roots and perspectives”, *Multibody System Dynamics*, vol.1, pp. 149-1888, 1997.
- Schultz, A.B., Alexander, N.B. and Ashton-Miller, J.A., “Biomedical analyses of rising from a chair”, *Journal of Biomechanics*, vol. 25(12), pp. 1383-1391, 1992.
- Thelen, D.G., Anderson, F.C. and Delp, S.L., “Generating dynamic simulations of movement using computed muscle control”, *Journal of Biomechanics*. vol. 36, pp. 321-328, 2003.
- Roebroek, M.E., Doorenbosch, C.A.M., Harlaar, J., Jacobs, R. and Lankhorst , G.J.,” Biomechanics and muscular activity during sit-to-stand transfer”, *Clinical Biomechanics*, vol. 9(4), pp.235-244, Jul. 1994.
- Xiang, Y., Arora, J.S., Rahmatalla, S. and Abdel-Malek, K., “Optimization-based dynamic human walking prediction: One step formulation”, *International Journal for Numerical Methods in Engineering*, vol. 79(6), pp. 667–695, Aug. 2009.



- Xiang, Y., Chung, HJ., Mathai, A., Rahmatalla, S., Kim., J, Marler, T., Beck S, Yang, J., Arora, J.S., Abdel-Malek, K. and Obuseck, J., "Optimization-based dynamic human walking prediction.", *Digital Human Modeling for Design and Engineering Symposium*, 2007.
- Yang, J., Marler, R.T., Kim, H., Arora, J. and Abdel-Malek, K., "Multi-objective optimization for upper body posture prediction", *10th AIAA/ISSMO Multidisciplinary Analysis and Optimisation Conference*, Aug. 2004.